2021

Tailoring Thermoresponsive Poly(N-Isopropylacrylamide) Toward Sensing Perfluoroalkyl Acids

Dustin Thomas Savage
University of Kentucky, dustin.savage@uky.edu
Author ORCID Identifier:
https://orcid.org/0000-0001-6330-099X
Digital Object Identifier: https://doi.org/10.13023/etd.2021.003

STUDENT AGREEMENT:

I represent that my thesis or dissertation and abstract are my original work. Proper attribution has been given to all outside sources. I understand that I am solely responsible for obtaining any needed copyright permissions. I have obtained needed written permission statement(s) from the owner(s) of each third-party copyrighted matter to be included in my work, allowing electronic distribution (if such use is not permitted by the fair use doctrine) which will be submitted to UKnowledge as Additional File.

I hereby grant to The University of Kentucky and its agents the irrevocable, non-exclusive, and royalty-free license to archive and make accessible my work in whole or in part in all forms of media, now or hereafter known. I agree that the document mentioned above may be made available immediately for worldwide access unless an embargo applies.

I retain all other ownership rights to the copyright of my work. I also retain the right to use in future works (such as articles or books) all or part of my work. I understand that I am free to register the copyright to my work.

REVIEW, APPROVAL AND ACCEPTANCE

The document mentioned above has been reviewed and accepted by the student's advisor, on behalf of the advisory committee, and by the Director of Graduate Studies (DGS), on behalf of the program; we verify that this is the final, approved version of the student's thesis including all changes required by the advisory committee. The undersigned agree to abide by the statements above.

Dustin Thomas Savage, Student

Dr. Thomas D. Dziubla, Major Professor

Dr. Stephen E. Rankin, Director of Graduate Studies

TAILORING THERMORESPONSIVE POLY(N-ISOPROPYLACRYLAMIDE) TOWARD SENSING PERFLUOROALKYL ACIDS

DISSERTATION

A dissertation submitted in partial fulfillment of the
requirements for the degree of Doctor of Philosophy in the
College of Engineering
at the University of Kentucky

By

Dustin Thomas Savage
Lexington, Kentucky

Director: Dr. Thomas D. Dziubla, Professor of Chemical Engineering
Lexington, Kentucky
2020

https://orcid.org/0000-0001-6330-099X

ABSTRACT OF DISSERTATION

TAILORING THERMORESPONSIVE POLY(N-ISOPROPYLACRYLAMIDE) TOWARD SENSING PERFLUOROALKYL ACIDS

Widespread distribution of poly- and perfluoroalkyl substances (PFAS) in the environment combined with concerns for their potentially negative health effects has motivated regulators to establish strict standards for their surveillance. The United States Environmental Protection Agency issued a cumulative domestic threshold of 70 ppt for water supplies, and this bar is even lower in some local districts and other countries. Monitoring PFAS consequently requires sensitive analytical equipment to meet regulatory specifications, and liquid chromatography with tandem mass spectroscopy (LC/MS/MS) is the most common technique used to satisfy these requirements. Though extremely sensitive, the instrument is often burdened by pretreatment regimens, sedentation, and user proficiency barriers that encumber or limit its effectiveness. As an alternative, polymeric strategies for detecting PFAS are promising candidates for funneling recognition, transduction, and receptor elements into a single sensing platform to overcome some of the hurdles affecting LC/MS/MS. Toward this end, poly(*N*-isopropylacrylamide) (PNIPAM), an extensively studied thermoresponsive polymer, is a hydrogel with tailorable swelling properties dependent upon its polymeric composition and surrounding media. This polymer holds a lower critical solution temperature (LCST) around 32 °C that marks its transition from a relatively hydrophilic, swollen state to a hydrophobic, collapsed state once heated, and prior research indicates that surfactants such as sodium dodecyl sulfate can heavily influence the temperature at which this transition occurs and the ultimate swelling ratio for crosslinked hydrogels. Two particularly concerning fluorosurfactants, perfluorooctanoic acid (PFOA) and perfluorooctane sulfonate (PFOS), were hypothesized to act similarly to their non-fluorinated analogs by augmenting the swelling of PNIPAM in a dose-dependent manner. The effect of these fluoropollutants on PNIPAM was therefore studied to identify 1) if PFOS and PFOA would have an appreciable effect on the swelling behavior of varying PNIPAM morphologies, 2) if the swelling response could be enhanced by adding functional comonomers into the PNIPAM backbone, and 3) if the swelling behavior could be outfitted with Förster resonance energy transfer (FRET)-compatible dyes to signal the contaminants' concentration. As such, crosslinked PNIPAM hydrogels were functionalized with fluorinated comonomers to induce fluorine-fluorine attraction amongst the polymers and their analytes to strengthen their recognition capability and microgels were equipped with FRET-capable dyes to achieve a fluorescent transduction motif indicative of the contaminants' presence. Results indicated that PFOS augments the swelling of PNIPAM hydrogels significantly while PFOA causes microgels to collapse at temperatures below their innate LCST. FRET primarily replicated swelling observations as expected for the distance-mediated fluorescent phenomenon. Though the fluoropollutants generated appreciable swelling perturbations at concentrations within the

micromolar range, additional functionalization is necessary to exploit the molecular-level interactions between PNIPAM and target fluorosurfactants to yield detection limits within the range needed for environmental applications.

KEYWORDS: Poly- and perfluoroalkyl substances (PFAS), poly(*N*-isopropylacrylamide (PNIPAM), environmental remediation, Förster resonance energy transfer (FRET), hydrogels, polymeric sensors

Dustin Thomas Savage

12/28/2020

TAILORING THERMORESPONSIVE POLY(N-ISOPROPYLACRYLAMIDE) TOWARD SENSING PERFLUOROALKYL ACIDS

By

Dustin Thomas Savage

Dr. Thomas D. Dziubla
Director of Dissertation

Dr. Stephen E. Rankin
Director of Graduate Studies

12/28/2020

ACKNOWLEDGMENTS

Without the tireless aid of my primary advisor, Dr. Thomas D. Dziubla, and my co-advisor, Dr. J. Zach Hilt, the work presented herein would not have come to fruition. Their feedback, wisdom, and insights were instrumental in directing the success of the research conducted throughout my graduate career. Additionally, my committee members, Dr. Lindell Ormsbee and Dr. Chris Richards, provided bountiful critiques that sharpened both my understanding of the principles at play and the resultant material presented herein. Finally, Dr. Marcelo I. Guzman's timely contribution as my outside examiner proved critical for assessing the dissertation.

The Electron Microscopy Center at the University of Kentucky supplied characterization equipment used in this work, and access to their facilities, even in difficult times, is greatly appreciated. Training and data collection by Dr. Dali Qian and Dr. Nicolas Briot were instrumental in interpreting the processes studied.

This work was supported by NIEHS/NIH grant P42ES007380. The content is solely the responsibility of the authors and does not necessarily represent the official views of the NIH.

TABLE OF CONTENTS

LIST OF TABLES

LIST OF FIGURES

CHAPTER 1. INTRODUCTION

As a broad group of anthropogenic chemicals produced since the mid-20th century, poly- and perfluoroalkyl substances (PFAS) have attracted attention due to their potential toxicity, ubiquity, and persistence.[1-5] Substances under the PFAS umbrella serve predominately as flame retardants, polymerization aids, and stain-resistant coatings owing to their ability to lower the surface tension of water below that of comparable hydrocarbon surfactants and the high stability of their carbon-fluorine (C-F) bonds.[6] The latter property makes them particularly concerning with regard to their environmental burden; the C-F bond is routinely cited as the strongest in organic chemistry with a bond dissociation energy of 105.4 kcal mol^{-1},[7] inhibiting their degradation under ordinary conditions. With global emission estimates exceeding hundreds of metric tons annually despite long-chain fluorocarbon production phase-out in many developed economies,[6, 8, 9] PFAS are found in nearly all environments and biota.[10-15]

Two alarming species under the PFAS umbrella, perfluorooctanoic acid (PFOA) and perfluorooctane sulfonate (PFOS), represent the most studied perfluoroalkyl acids (PFAAs) available and have biological half-lives extending to 3.8 and 5.4 years,[16] respectively. Adding to their ubiquity,[17, 18] annual emission estimates for C_4-C_{14} perfluorocarboxylic acids (PFCAs), a subset of PFAAs of which PFOA is included, ranged between about 55 tonnes/yr and 520 tonnes/yr from 2003 to 2015 with substantial variability across time.[8] From the onset of PFAS production in 1951 to 2015, the total level of PFCA emissions spans 2,610 tonnes to 21,400 tonnes with another 20 tonnes to 6,420 tonnes projected for 2016 to 2030.[8] Combined with another 4,481 tonnes of PFOS produced by 2000 and 96,000 tonnes of perfluorooctane sulfonyl fluoride in use by 2017,[19] the staggering number of PFAAs in circulation has helped inflate the growing list of at least 4,730 chemicals documented under the PFAS umbrella.[20] Attempts to substitute frequently used fluorosurfactants with alternatives combined with atmospheric oxidation of fluorotelomer alcohols[21-23] exacerbate this load further.

Intake via food, water, and ambient air has led to detectable PFAS accumulation in most humans.[18, 24-29] Excessive exposure to these substances has been associated with numerous unsavory health outcomes[30] including carcinogenesis,[31] endocrine disruption,[32]

reproductive toxicity,[33, 34] hepatotoxicity,[35] and immunotoxicity,[36] leading regulatory agencies like the United States Environmental Protection Agency (EPA) to set health advisory limits for their consumption.[37, 38] Taking the estimates for PFAS production as measures of environmental burden or stockpiles with the potential for release, ingenuitive monitoring efforts are essential to identify contaminated areas and supplies as a means to combat exposure risks for susceptible populations and alleviate their environmental burden.[39]

CHAPTER 2. BACKGROUND

2.1 Introduction

In the field of environmental analytics, liquid chromatography coupled with tandem mass spectroscopy (LC/MS/MS) stands as the most frequented technique used for trace fluoropollutant detection. This is due to its reliability, extreme sensitivity, and ability to differentiate chemical species within complex matrices. The instrument is often prescribed by regulatory agencies to satisfy monitoring criteria, receiving standardized protocols from national organizations like the EPA.[40] As part of any detection method's success in determining analyte concentrations, there are three distinct components integral to its operation: 1) a recognition element that discriminates between chemicals, which, in this case, is a column embedded with an affinity agent capable of separating species, 2) a signal transduction element such as an ionizer, and 3) a reporter element like a mass analyzer. Together, these elements regulate the system's response to a wide range of analytes by selecting for specific chemicals via recognition zones in the instrument's column and translate their presence into an observable output with a mass spectrometer. Notably, to achieve serviceable reproducibility and protect the instrument's valuable hardware, pretreatment is often required that, when combined with the investment of retrieving samples from their source, can generate considerable lag between initial sample collection and final signal processing as shown in Figure 2.1. Though accessibility to LC/MS/MS has grown, skilled operators are still required to produce reliable results, and the cumbersome process of transporting samples from the field to sedentary laboratory equipment imposes potential sources of error that may hinder even artisan users. These issues leave the instrument with several concerns that are difficult to reconcile collectively.

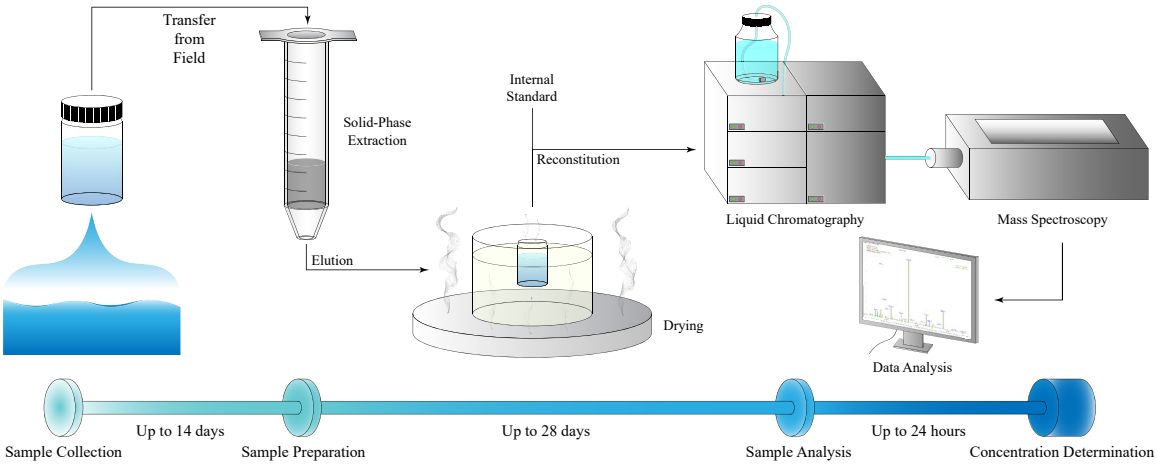

Figure 2.1. Depiction of the steps and timescales described by EPA Method 537.1 for analyzing PFAS with LC/MS/MS.[40] Note that the durations shown represent the upper extremes for sample storage coupled with preparation at each step; the actual time required for each phase could be much lower than those shown.

As an alternative, polymeric systems for evaluating complex matrices have emerged due to their capability to incorporate two or three of the sensing elements simultaneously into a discrete sensor while competing with the rigorous analytical standards prompted by LC/MS/MS. Depending on the polymer and transduction scheme applied, polymers can house highly specific recognition sites for target molecules, offer a platform for inducing a signal representative of an analyte's presence, and, with or without the aid of attached signal processing units, convert the signal into a comprehendible format indicating the concentration of the system's target. The robustness of this format has led to a myriad of different sensing strategies aimed at detecting PFAS in aqueous samples. Recent reviews have covered current analytical practices for determining PFAS levels,[41-44] focused primarily on enhancing chromatographic techniques through improved contaminant isolation as part of pretreatment protocols. Numerous studies take this process a step further by coupling polymeric recognition agents to transduction motifs, circumventing the need for large analytical apparatuses. Polymeric approaches for confronting the daunting task of meeting current regulatory thresholds for PFAS detection, set domestically at 70 ppt by the EPA[39] with even more stringent standards across individual states and other countries, are surveyed here to canvas the strides already made toward solving the monitoring issue.

Confronting this analytical challenge in the context mentioned above, literature to date has emphasized methods to detect both PFOA and PFOS, but, to adequately characterize the attention expended by various researchers to tackle the swath of PFAS pollution as a whole, sensors paying diligence to other forms of PFAS are also described here. Within this scope, polymers utilizing biologically-derived components, synthetic analogs, or non-biological materials coupled to attractive moieties for their targets are first discussed in a broad overview of their general classifications and secondly as specific examples of the various polymeric schemes seeking to sense PFAS. Although not specifically detailed, transduction motifs complementing each polymer are elucidated when appropriate for continuity.

2.2 General Polymeric Sensing Approaches

In the following sections, brief descriptions of relevant methods utilizing polymers as a primary component of their sensing capability are provided with select references to reviews and primary literature that detail each subject in detail. These are not comprehensive overviews of the subject area but are simple breakdowns of the general operating principles undergirding each approach that will aid understanding of the articles presented in later sections. Additionally, the references used as descriptors are not relegated solely to the field of environmental remediation and offer pathways into complementary areas that might further comprehension of the methods and their usages as a whole.

2.2.1 Biological or Biomimetic Polymers

Biosensors employ strong analyte-receptor binding interactions to pinpoint specific targets amongst complex matrices. Numerous sensing elements lie under the broad umbrella of biological sensing techniques, but those utilizing discrete polymeric systems are primarily limited to peptides, antibodies, enzymes, and aptamers.[45] Whole cell and bacteriophage biosensors use secondary (e.g., enzymatic) or ensemble polymeric queues, but their implementation nonetheless necessitates cellular chaperones that fall outside of the scope discussed here. Reviews for these schemes by Gu et al.,[46] Gui et al.,[47] and Singh et al.[48] summarize their application succinctly for those interested.

Regarding standalone biopolymers, interactions exploiting amino acids capitalize mostly on individually weak binding events such as aromaticity, hydrogen bonding, and van der Waals forces to form strong tandem complexes.[49] Especially in antibody and enzymatic associations, structural complementarity and electrostatics also play a role in building niche pockets for harboring specific targets. When targeting nucleic acids, careful sequencing of nucleotides along the polymer backbone facilitates Watson-Crick base pairing to further enhance efficacy.[50] The robustness of biopolymers to incorporate multiple of these strategies in unison makes them tailorable for a vast array of small molecule analytes, prompting their usage as the tool of choice for many assay-based detection formats.

Peptides represent relatively short-chained sequences of amino acids stemming from 20 constituents in the standard genetic code or libraries of synthetic components.[51] Varying in their functionality, the ordering of residues throughout their chain can drastically modify the peptide's association with substrates. Their fidelity marks them as the building blocks for proteins that, in part, elicit the multitude of highly specific interactions found throughout biological systems. Immobilization upon a surface via direct anchoring of the peptide's C- or N-terminus or intermediate derivatization sets a responsive layer for the analyte of interest which, when coupled to electrochemical (amperometric, impedimetric, potentiometric), optical (luminescent, colorimetric), mechanical (acoustic, magnetoelastic), or thermal transducers,[52] forms a matrix for reporting the presence of a range of potential toxins. Typically, peptides create strong associations with their target by combining the weak mechanisms mentioned earlier into a recognition site suited only for a particular analyte. The complexity of the analyte could impart additional complexity for the peptide; small molecules with limited functional groups may favor only a few select residues, whereas large contaminants (e.g., bacteria) could necessitate an intricate suite of amino acids artistically positioned to either isolate a single component of the target's overall structure or multiple components in tandem. Appropriate residue selection is, therefore, primarily attained through either combinatorial chemistry, protein structural decomposition, phage display,[53] or *in silico* design[54] with paired knowledge of the target binding sequence or functionality. Once optimized, artificial peptides are routinely synthesized with solid-phase approaches to

avoid relying on surrogate organisms, making their production feasible at scale.[52] Their adaptability to a host of threatening agents has led to their use as biosensors for volatile organic compounds,[53] drugs,[55] and pathogens.[56]

Antibodies function as the immune system's elaboration of peptide specificity. Whereas peptides constitute discrete binding domains for contaminants, antibodies take the full form of proteins containing the recognition element and machinery for the intruder's dispatchment. The enormity of information regarding antibody types, functionality, immobilization strategies, transducing schemes, and assay formats extends far beyond the short description presented here; excellent reviews by Conroy et al.[57] and Sharma et al.[58] provide copious instruction on the topic. Summarily, antibodies are Y-shaped proteins composed of four distinct regions, namely two heavy and two light chain sections. The heavy chain components have three constant regions and one variable region; the light chain components have one constant region and one variable region. The heavy chain constant region sequence varies between five categories, IgA, IgD, IgE, IgG, and IgM, and directs the mode of removal once the antibody binds to its target. The variable chain segments impart target specificity and are together known as the complementarity-determining region. Targets can be further broken down into two subclasses: those that elicit a host immune response, an antigen, and those that are non-immunogenic and require coupling to a carrier protein, haptens.[59-61] When either invokes an adaptive immune response from its host, polyclonal antibodies that bind to not only the target but also secondary epitopes are produced. From a sensing perspective, these antibodies complicate measurements by lacking selectivity and potentially generating false positives.[56] Monoclonal antibodies are typically created by fusion of an immunized host cell with a myeloma cell into a hybridoma which gives an antibody with a binding pocket selective for the target. Recombinant antibodies are expressed as fragments from a bacterial host infused with a synthetic vector coded for the linked variable regions of monoclonal antibodies.[58] Other variants such as camelid and shark antibodies and nanobodies are also investigated to improve the sensing element's durability and reproducibility.[56] Once acquired, antibodies are immobilized on the surface of sensors by physisorption predominately regulated by van der Waals and hydrophobic forces or chemisorption via electrostatics or covalent bonds. Surfaces like nitrocellulose, poly-L-

lysine, agarose, silica, or styrene often serve as solid supports; metallic layers modified with chemical functionalities act as sites for chemisorption.[62] Deposited antibodies can form either a direct, non-competitive assay by binding their target and transmitting a signal with (e.g., sandwich assay) or without (e.g., electrochemistry) the aid of a secondary labeling agent[63] or an indirect, competitive assay by measuring the residual concentration of a labeled antigen or competitor.[64] Alternative formats can capitalize on antibody binding to an immobilized antigen (e.g., mechanical). Signal transduction follows many of the same strategies mentioned for peptides packaged into immunoassay kits such as the western blot.

Enzymes take the specificity of antibodies a step further by incorporating catalytic sites into their domains that form the basis for life-sustaining metabolism. Like antibodies, the wealth of research surrounding enzymes will only be summarized here in brief, and readers seeking additional insight into the subject are encouraged to visit reviews by Robinson[65] and Pinyou et al.[66] for the fundamental and electrochemical biosensor applications of these biomolecules, respectively. LeLand C. Clark initially spurred broader investigation of enzymatic biosensors with his and Lyon's development of a blood glucose monitor in 1962 following Clark's discovery of a catalytic platinum electrode for measuring ambient oxygen in 1956.[67-69] Investment has since led to the modern availability of small, discrete glucose monitors used for the treatment of diabetes and a myriad of other small molecule sensing regimes implementing the same or similar general design principles.[69] Enzymes used in this capacity mostly follow Michaelis-Menten kinetics with regard to their substrate conversion capacity, trending from a first-order (i.e., linear) profile at low substrate concentrations towards zero-order at saturation.[68] Notable exceptions, such as allosteric enzymes, may instead display a sigmoidal response, but these examples are rare.[65] Over the course of catalysis, the substrate is consumed to release both a chemical product and a local electrical response. Methods for capitalizing on these products for sensing are broken into several subcategories, namely: using a catalytic surface to produce an electric signal from the enzymatic byproduct (e.g., the case of the "Clark electrode"), exploiting chemical mediators to activate the byproduct with respect to a transducer, and direct measurement of the enzyme's electrochemical response via fixation on a transduction element.[69] To

these ends, numerous biosensors for environmental contaminants have emerged, including acetylcholinesterase, butyrylcholinesterase, and phosphatases for organophosphorus compounds,[45, 59, 60, 70, 71] NADH-dependent dehydrogenases for formaldehyde,[60] sulfite oxidase for SO_x,[60] nitrate reductase for NO_x,[69] and numerous enzymes for heavy metals.[69] Typically, pollutant sensors follow an inhibition model for their analysis by recording the loss of enzymatic activity as a function of contaminant concentration, whereby the analyte, or inhibitor, smothers the active site in nondestructive, competitive inhibition or deforms the active site in destructive, non-competitive inhibition.[69] The latter instance can occur when the inhibitor either covalently binds to the active site or complexes with the enzyme-substrate complex to impede activity. Signals accrued from these assays are primarily transmitted via fluorimetry (in the case of unbound enzymes) or electrochemically (for immobilized enzymes) like peptides and antibodies discussed earlier with amperometry serving as the primary route.[72, 73] Like antibodies, enzymes are haunted by instability, and immobilization strategies in the form of adsorption, chemisorption, entrapment, and ion exchange are frequently used to mitigate denaturation.[68, 69, 71, 73-75] Genetic modification is also studied as a means for both improving stability and aiding in purification.[71, 75] Once acquired and stabilized, enzymes find their way into a variety of applications, ranging from diagnostic contact lenses to, with the help of antibody recognition sites, commercial enzyme-linked immunosorbent assay (ELISA) kits.[73]

Aptamers represent oligonucleotides that constitute the sensing elements of nucleic acid-based biosensors. Due to their sensitivity, tailorability, and reproducibility, aptamers have received tremendous attention as therapeutics and biosensing agents, and their sensing applications are well summarized by Song et al.[76] and Munzar et al.[77] Apart from the bioreceptors discussed earlier, aptamers traditionally arise from natural series of sugars, ribose in the case of ribonucleic acids (RNA) and deoxyribose for deoxyribonucleic acids (DNA), phosphate groups, and nucleobases, divided amongst adenine, guanine, cytosine, uracil (for RNA), and thymine (for DNA).[78] Their sugar-phosphate backbone interspersed by functional bases imparts hydrophilicity and, when combined with the array of binding interactions resulting from their structural and chemical cues, selectivity for targets ranging in size from small molecules to proteins,

albeit at the cost of the hydrophobicity and binding site diversity available for amino acid complexes.[79] Also, unlike the immunogenic requirement for antibodies and the host-production aspect of enzymes, aptamers are usually isolated from an initial library of roughly 10^{13} to 10^{16} prospective oligonucleotides[80, 81] containing a 30 to 40 mer random interior sequence regions flanked by primer annealing sites.[78, 80, 82] Selection of optimally binding sequences is obtained through systematic evolution of ligands by exponential enrichment (SELEX) whereby the pool of aptamers is exposed to the target ligand and binding sequences are extracted and amplified via polymerase chain reaction (PCR). The new pool is again exposed to the target, washed, and amplified, often for between 8 to 16 cycles.[78] Numerous strategies have surfaced to reduce the number of cycles required, enhance the potency of the final pool, eliminate residual conflicting primer regions, and reconcile difficulties in target immobilization for binding complex purification. These methodologies are expansive and have been reviewed extensively elsewhere.[78, 80, 82] Complementing efforts to improve SELEX, synthetic nucleotides and polymerases are sought to advance aptamer sensitivity and allow PCR incorporation of unnatural monomers, respectively.[81, 83] Once a suitable aptamer pool has been developed, efficacious oligonucleotides are fashioned into surface-bound or solution-based sensing configurations. Optical approaches frequent fluorescent quenching- or colorimetric nanoparticle (e.g., gold)-based assays[84] while electrochemical methods employ redox labels (e.g., ferrocene, methylene blue) to elicit a detectable response to the ligand's presence.[85] Similar to peptides, mass-based transducers such as surface acoustic wave (SAW), quartz crystal microbalance (QCM), and static or dynamic microcantilevers are also used.[85] Signals accrue from these techniques as a consequence of structural reorientation upon target binding or interruption of Watson-Crick base pairing to release a signaling or impeding probe. The flexibility of this design has led to a myriad of creative complexation schemes encompassing hairpins, duplexes, clusters, and cocktails to customize aptamers for particular targets.[79, 85]

Although each bioreceptor posts advantages mainly toward sensitivity or producibility, their reliance primarily on aggregate weak binding interactions often makes their effectiveness environmentally susceptible. Aptamers, for example, utilize their three-dimensional conformation as a contributor to their overall binding proficiency, and

slight variations in physical and thermal conditions from selection can alter either their structural integrity or residue binding capacity.[79] Amino acid complexes likewise suffer from conditional limitations to their use, potentially resulting even in denaturation of antibodies and enzymes that render them dysfunctional.[56] These constraints are, however, combatted by stabilization efforts for each sensing element and, when administered appropriately, do not outweigh their capability to distinguish analytes in extremely dilute samples. Biosensors consequently retain a strong foothold in sensing research expenditure as reliable methods for contaminant detection.

2.2.2 Molecularly Imprinted Polymers (MIPs)

Molecularly imprinted polymers (MIPs) are synthetic analogs to the selective biological binding motifs of antibodies, employing "template" molecules in their synthesis to implant vacancies within the resulting polymer that generate sensitivity and selectivity toward the desired target. Typically, the template used during synthesis is the analyte of choice, but substitutes are utilized when the target may negatively impact the polymerization. For example, if the template binds sufficiently strongly to the network such that subsequent purification is impeded, a structural analog to the analyte can be used that mimics the space occupied by the molecule of interest without incurring the bonds formed by the template's binding moiety. Additionally, if the target is difficult to acquire in quantities sufficient for templating or poses toxicity concerns, a substitute may also be used.[86] When selecting appropriate monomeric units for targeting a specific analyte, three binding motifs are commonly employed: covalent, semi-covalent, and non-covalent. The covalent approach exploits functional moieties on the target molecule to either attach the molecule to a polymerizable modifier prior to polymerization[87] or dock a cleavable monomer with a target residue in the resulting polymer. After polymerization, the template is cleaved from the backbone and washed away to provide a binding site suitable for covalent assembly or non-covalent self-assembly by the target.[88] In the latter case, template reattachment by relatively weak bonds (i.e., hydrogen, ionic, van der Waals, π-π) classifies the strategy as semi-covalent.[89, 90] In a more robust approach that does not necessitate functional groups on the template, non-covalent MIPs are synthesized with weakly binding monomers and the target simultaneously. During

polymerization, the analyte loosely associates with the fledgling network to generate architecturally distinct zones that remain after removing the template with a suitable solvent. Due to its ease of execution and translatability among analytes, the non-covalent method is the most routinely used procedure and dominates analytical approaches utilizing molecularly imprinted technology (MIT).[90, 91]

Unlike their biological counterparts in proteins, MIPs are not limited to amino acid chains to hone their target, but, rather, a host of monomers and crosslinkers with varying functionalities. For non-covalent MIPs, methacrylic acid (MAA) represents the most commonly employed monomer due to its ability to both accept and donate hydrogen bonds, and ethylene glycol dimethacrylate (EGDMA) acts as its complementary crosslinker.[89, 91] Alternative combinations are occasionally tailored to suit a particular target, such as *N*-methacryloylamido-(L)-phenylalanine methyl ester and 2-hydroxyethyl methacrylate with EGDMA for cholesterol[92] and 1*H*,1*H*,2*H*,2*H*-perfluorodecyltriethoxysilane with tetraethylorthosilicate (TEOS) for perfluorinated compounds (PFCs),[93] leading to expansive lists of monomer-crosslinker duos.[89-91] Equally important to the selection of monomers for the formulation of an efficacious MIP is the choice of porogen, or solvent, for synthesis. The porogen serves to dissolve the various monomers and template, ensure ample interaction between them, and distribute pores within the resulting polymer. Solvent polarity can dramatically impact complexation of the template and receptor[94-96] by interfering with or inhibiting bond formation. Typically, for systems utilizing MAA as a receptor, non-polar (e.g., dichloromethane, toluene, chloroform) or moderately polar, aprotic (e.g., acetone, acetonitrile, tetrahydrofuran, *N*,*N*-dimethylformamide) solvents are recommended to maximize bond energies for templating.[91] The selected solvent's ability to distribute pores throughout the network also determine the final porosity, pore volume, and available surface area for binding, making the porogen a critical component to the polymer's ultimate imprinting efficiency.

The synthesized MIP can take on a range of sizes and structures depending upon the applied procedure, ranging from stable nanoparticles to bulk coatings and gels. Methods to directly generate imprinted particles in the nano- to microscale domain include precipitation, emulsion, seed, and suspension polymerization while bulk free-

radical or living polymerization accompanied by milling offers an indirect avenue for producing microgels.[86, 89-91, 97] The latter provides the simplest means of execution from an experimental standpoint, with living polymerization approaches delivering greater control over the polymer's structure than conventional free-radical polymerization. Applying the same chain growth phenomena to a smaller scale, precipitation involves the production of uniform spheres from a dilute solution whereby chain growth gradually results in, as its name suggests, precipitation. Emulsion encapsulates the polymeric chains inside a surfactant-stabilized droplet, usually in a traditional oil-in-water dispersion; suspension uses high mixing speeds to homogenize the oil and water phases into discrete droplets without the aid of a surfactant. Seed, or swelling, polymerization utilizes swollen particles as vessels to mold the size of resulting gels. The polydispersity of each method varies significantly; suspension and milling can yield particles with diameters from single to hundreds of microns while precipitation, emulsion, and seed return monodisperse gels in the upper nanoscale to lower microscale range. Alternatively, rather than filling the entire network with imprints, surface imprinting alleviates diffusion limitation concerns by allocating imprints solely on the surface of the polymer to enhance binding kinetics and minimize template consumption.[98]

Once synthesized, MIPs are combined with secondary signaling motifs, whether electrochemical, spectroscopic, or piezoelectric, to deliver a readily measured response when in contact with their target. The numerous methods underlying each signaling class' subcategories have their own unique advantages of autonomy, precision, miniaturization, or translatability, but their respective descriptions are outside the scope of this survey and have already been detailed extensively by Chen et al.[89] Regardless of the signal transduction technique employed, the primary measure of the imprint's effectiveness is the magnitude of its imprinting factor (IF), which is simply the imprinted polymer's output value from its signaling strategy or uptake measure compared to a polymer synthesized under identical conditions without a template. A high IF indicates successful integration of recognition sites or enhanced uptake by the network, distinguishing the MIP as an improvement for sensing over its non-imprinted counterpart. With the straightforwardness of producing MIPs demonstrating respectable imprinting

capabilities, MIT has found its way into diverse applications of analytical chemistry including food,[90, 97] environmental,[86] and pharmacological[99] analyses.

2.2.3 Other Polymeric Recognition Elements

Outside of the broad classifications presented in the previous two subsections, two additional sensing approaches are worthy of note: chemiresistive and adsorptive polymeric materials. The former class utilizes conductive polymers (e.g., polyaniline, polypyrrole) stationed between two electrodes to relate the change in resistivity through the polymer to an analyte's concentration.[100, 101] Intricate matrices employing multiple polymers and embedded catalytic components can be used to tease targets from complex samples. Sophisticated post hoc analysis permits species discrimination via multicomponent arrays, making the system suitable for a variety of targets.[102] The latter category encompasses a generic approach for concentrating analytes for subsequent chromatographic analysis or aiding in elution differentiation as part of the same instrumentation. Typically, these polymers focus on either strong (e.g., electrostatic) or weak (e.g., hydophobic) associations or combinations of the two to tailor their capture-release functionality to the needs of the backend analysis method. Although efforts to apply this strategy are plentiful in the literature, these studies are omitted to include only sensing systems offering direct analysis of contaminated samples. Methods using adsorptive materials for PFAS have been reviewed extensively already[41, 44, 103] and need not reiteration here.

The polymeric sensing schemes mentioned herein do not constitute an exclusive listing of all technologies; rather, those described are the pertinent approaches investigated in the literature for sensing PFAS thus far. Other methodologies, such as polymeric chemosensors,[104] are interesting avenues for future exploration that are outside the scope of this survey.

2.3 Polymeric PFAS Sensors

Polymeric methods for detecting PFAS are hereafter listed according to their responsive element and transduction motif. The former constitutes the primary

organizational structure for the upcoming sections with the latter an implicit scheme consistent within each subsection.

2.3.1 Biological and MIP PFAS Sensors

The lack of PFAS immunogenicity has, unfortunately, limited biosensor applications to only a few examples by Zhang et al.,[105] Zhang et al.,[106] and Cennamo et al.[107] The first application used a two-step assay procedure to initially competitively bind peroxisomal proliferator-activated receptor-alpha (PPARα)-retinoid X receptor-alpha (RXRα) conjugates to either free-in-solution or immobilized PFOS in a well plate. PPARα-RXRα-PFOS complexes formed from free PFOS in the supernatant were then transferred to a well containing PPARα antibodies, and complementary biotin-tagged DNA probes specific for the PPARα-RXRα heterodimer binding sequence were added as a biotin-streptavidin anchor. Finally, streptavidin-modified quantum dots (QD-SA) were inserted to bind to the immobilized DNA-biotin receptor and emit a fluorescent signal indicative of the original solution's PFOS concentration. This somewhat complicated procedure yields an impressive limit of detection (LOD) of 2.5 ppt, competing closely with conventional LC/MS/MS detection limits. Its linear range between 2.5 and 75 ppt also grants room for surveying the anticipated window of environmentally relevant samples. The study did not, however, test performance in the presence of other competing analytes or PFCs, leaving the possibility of interference from other PPARα-binding moieties open.

The second biosensor by Zhang et al.[106] monitored PFOS inhibition of an enzymatic biofuel cell (BFC) equipped with either glutamate dehydrogenase (GDH) or bilirubin oxidase (BOD) atop multi-walled carbon nanohorns (MWNHs)-modified glassy carbon electrodes (GCEs). Working electrodes were formed by immobilizing MWNHs with *N*-hydroxysuccinimide and 1-ethyl-3-(3-dimethylaminopropyl)carbodiimide followed by physical deposition of GDH for the bioanode and BOD for the biocathode. Immersion of both cathodes in a solution containing glutamate and nicotinamide adenine dinucleotide catalytically converted both molecules to α-ketoglutarate, ammonium, and a nascent proton at the bioanode which supposedly fueled reduction of diatomic oxygen at the biocathode. Despite not supplementing bilirubin, the authors claim that the BOD

coating on their biocathode aided in generating an electrocatalytic current through their electrode, but they did not include cyclic voltammograms comparing the current response of both BOD- and non-BOD-MWNH-GCEs under oxygen rich and poor conditions to confirm. Inclusion of the enzyme might add a binding layer to the electrode that ultimately raises the open circuit voltage (V_{oc}) differential between the electrodes when exposed to PFOS, but the exact mechanism underlying its use is unclear. Nonetheless, the BFC demonstrated remarkable selectivity toward PFOS with a maximal interferent normalized V_{oc} of approximately 2% for perfluorononanoic acid (PFNA) relative to 26% for PFOS. Though they did not test complex matrices, the linear range for their system from 5 to 500 nM with a LOD of 1.6 nM (about 861 ppt) approaches the magnitude desired for environmental sensing applications and may breach the threshold with further improvement.

In the lattermost biosensing example by Cennamo et al.,[107] they developed a "mono-specific antibody" for PFOA by exposing rabbits to a bovine serum albumin (BSA)-PFOA hapten containing approximately five PFOA molecules per protein complex. These polyclonal antibodies were immobilized on a self-assembled monolayer of α-lipoic acid atop a planar gold surface in contact with a plastic optical fiber to form a surface plasmon resonance (SPR)-based sensing platform. PFOA binding to the bioreceptor causes a shift in the refractive index of the surface, leading to a colorimetric response capable of sensing the contaminant at sub-ppb levels. Similar results were obtained for PFOS, indicating that the biosensor is specific for linear fluorinated subspecies rather than individual residues. Testing only two PFAS does, however, leave the responsiveness of the system to variable chain lengths or non-linear species in question.

The same authors in a series of publications explored using MIPs derived from (vinylbenzyl)trimethylammonium chloride, 1*H*,1*H*,2*H*,2*H*-perfluorodecyl acrylate, and EGDMA with an ammonium perfluorooctanoate template as an alternative for biological sensing elements.[108-110] Their studies employing the same SPR signaling motif used earlier led to a LOD as low as 0.13 ppb, demonstrating the potency of MIT to replicate and potentially surpass the sensing capabilities of their biological counterparts. Interestingly, despite including a quaternary comonomer in their MIP mixture, their

results reported nearly identical responses from a range of 11 different linear PFAS with different head group functionalities and chain lengths.[109] This peculiarity would appear to highlight size complementarity from imprinting as the primary response mediator, but they also claim indiscriminate results for C_4 to C_{12} PFAS. Their entries do not display parsed analyses of individual species, so evaluation of the contributing factors to their observed binding phenomena is difficult.

Other methods to exploit MIT with optical transduction have also surfaced with a spectrum of response ranges between differing configurations. Feng et al.[111] anchored 3-aminopropyltriethoxysilane (APTES)-fluorescein 6-isothiocyanate (FITC) conjugates to silicon dioxide (SiO_2) nanoparticles using TEOS with PFOS as a template. Within their matrix, excess APTES acted as a free primary amine suitable for acid-base pairing and/or hydrogen bonding with their target. PFOS binding to receptor sites resulted in charge-transfer quenching of FITC, leading to a linear reduction in fluorescence intensity across an analyte concentration of 5.57 to 48.54 ppb. The quenching constants (K_{sv}), or slopes, of their Stern-Volmer plots for PFOS were heavily pH dependent, decreasing from 16.83 at pH 3.5 down to 8.31 at pH 7.4 due to inhibited amine protonation, and their IF follows a similar trend. The constants for analogous analytes (PFOA, perfluorohexane sulfonate (PFHxS), perfluorohexanoic acid (PFHxA), phenol, and sodium dodecylbenzenesulphonate (SDBS)) were lower than that of PFOS but, nonetheless, still within the same order of magnitude and up to approximately 60% that of PFOS in the case of PFOA. Co-added species did little to impact PFOS detection in mixed matrices, noting the high binding capacity of their system for their target of interest over other potentially interfering contaminants. Altogether, their system showed promise for utilizing MIT as a platform for identifying select PFAS in environmental samples albeit at concentrations above desired thresholds, giving a premise for later efforts to improve on the technology as a means for fabricating highly sensitive MIPs.

Jiao et al.[112] thereafter employed epichlorohydrin to link chitosan powder and carbon quantum dots (CQDs) together with templated PFOS to capitalize on the amino groups of chitosan in much the same manner as Feng et al.[111] In this design, PFOS complexation was reported to enhance nitrogenous defects amongst CQDs which resulted in higher photoluminescence intensity. The constants describing their intensity dose-

response curves were similarly subject to somewhat high values for structurally analogous substances, rising to about 33% of their PFOS value for perfluorooctanesulfonyl fluoride and PFOA, but they did not test individually mixed matrices to check potential interference. Rather, supplementing PFOS into serum and urine samples offered 81% to 98% recovery, which, unfortunately, does not resolve inference mechanisms. Ions and metabolic additives showed roughly 8% to 20% reduction in intensity, possibly accounting for the losses in recovery. Unlike the earlier report by Feng et al.,[111] this design even showed a negative slope for SDBS and sodium dodecyl sulfate (SDS), possibly indicating differences in binding pathways or structural memory between the MIPs. Their claim of a linear range from 0.02 to 0.2 ppt with a 0.66 ppq LOD in serum and 0.85 ppq LOD in urine is, to say the least, astounding and stands as the lowest detection limits found for any of the polymeric sensors described here.

In another example of quantum dots (QDs) acting as the signal transducer, Zheng et al.[113] capped thioglycolic acid-modified CdTe@CdS QDs with a PFOA-imprinted APTES/TEOS shell to preserve the optical properties of their imbedded QDs while featuring aminated sites for their target. PFOA binding demonstrated a Stern-Volmer response whereby PFOA showed an approximately 50% increase in K_{sv} over non-imprinted controls while other analytes (PFOS, SDS, SDBS) did not offer a significant change. These results were recorded at a pH of 3.8 to balance potential silica dissolution under more acidic conditions and electrostatic impairment in a more basic setting. Though they did not test discrete mixed matrices, spiked water samples reported serviceable recoveries between 91% and 107%, and their linear range between 0.25 and 15 μM with a LOD of 25 nM approaches the levels needed for environmental monitoring while boasting minimal investment and avoidance of sample preconcentration. Leveraging these aspects with slightly greater precision would bridge the sensing requirements for a competitive polymeric sensor, and their results offer a base for improving optically-based MIT to reach these goals.

As a segue between optical and electrochemical transducers, Chen et al.[114] demonstrated an interesting use of electrochemiluminescence (ECL) by encasing ultrathin graphitic-based carbon nitride (utg-C_3N_4) in a PFOA-imprinted polypyrrole shield. In their design, sulfate radicals ($SO_4^{\cdot -}$) generated from the photolysis of

peroxydisulfate ($S_2O_8^{2-}$) function to excite utg-C_3N_4 nanosheets, and decay of these sheets to their ground state yields a luminescent signature. PFOA, being susceptible to oxidation by $SO_4^{\cdot-}$, consumes the system's fuel and, consequently, lowers the observed ECL. Although the sensor is highly dependent upon pH, showing a maximum ECL offset at a pH of 6.0, a myriad of coadded PFAS had insignificant effects on the signal output for PFOA. The system holds two linear ranges from 0.02 to 40 ppb and 50 to 400 ppb, but the origin of the discontinuity between these regimes is not mentioned. As upcoming articles will illustrate, dual linear ranges are not uncommon for electrochemical detection methods; the zones might occur due to local concentration gradients encumbering surface diffusion and limiting electron transfer, ultimately mitigating PFOA-receptor occupancy in this case. A LOD of 10 ppt positions this sensor for facing environmentally relevant contaminant concentrations and among the most sensitive covered here.

The electrochemical sensor produced by Karimian et al.[115] likewise reported two linear ranges for PFOS. In their approach, an electropolymerized poly(*o*-phenylenediamine) layer imprinted with PFOS atop a gold electrode allowed the analyte to block ferrocenecarboxylic acid (FcCOOH) contact with the electrode surface, reducing the observed voltammetric signal. The use of an electroactive redox probe, FcCOOH, is supplemented to overcome the lack of electroactivity for PFAS, a common theme that will be repeated for several upcoming electrochemical sensing schemes. Monitoring the peak current as a function of analyte concentration revealed a steep linear range between 0.1 and 4.9 nM and a shallow range from 9.5 to 1,500 nM. Like the aforementioned ECL sensor,[114] no direct explanation was provided for the presence of two distinct ranges. Further analysis of the dilute regime indicated a LOD of 0.04 nM, meeting the author's goal of sub-nanomolar detection to address the needs of environmental monitoring. Comparison of mixed matrices indicated that smaller analytes (i.e., heptafluorobutyric acid and perfluorobutane sulfonate (PFBS)) interfered significantly with the normalized response to PFOS, leading to an approximate 20% increase or decrease in signal at a tenfold excess, which was attributed to binding site competition. Moro et al.[116] attempted to apply the same MIP to a gold screen-printed electrode (SPE) with the aim to translate the technology into a commercially viable platform. The sensor was, unfortunately,

unable to produce satisfactory detection results, encumbered by surface heterogeneity and template aggregation that left the device with substantial measurement error.

Kazemi et al.[117] later used a similar method to Karimian et al.[115] employing an *o*-phenylenediamine (OPD) PFOS-templated layer electropolymerized atop a GCE with FcCOOH again acting as the redox probe. This sensor's mechanism was effectively the same as for their predecessor, using the diffusion inhibition of analytes to mitigate FcCOOH electroactivity at the working electrode surface. When measuring the differential pulse voltammetry signal accrued with their MIP electrode, a platinum counter electrode, and a silver/silver chloride (Ag/AgCl) reference electrode, the peak current response to PFOS also exhibited two distinct linear ranges, one between 0.05 and 0.5 nM and another from 1 to 500 nM. The sharp slope accompanying the former range was attributed to excessive available binding sites in a dilute regime, but the discontinuous change to a leisurely slope in the latter region was not explained. Evaluation of association constants for various analytes indicated that non-fluorinated species had negligible affinity to the system relative to PFOS, but fluorinated analogs, PFOA and PFBS, had similar and even higher affinities for the MIP in the case of the shorter chained perfluorosulfonate. The heightened affinity for PFBS was reasoned to occur as a consequence of its shorter perfluorinated chain accessing binding sites while maintaining the same head group electroactivity as PFOS, seemingly discounting differences in hydrophilicity between the molecules. Their LOD down to 0.05 nM met the author's detection limit goals, but the inability of the sensor to operate in complex matrices was noted as a significant limitation that would require hefty cross-referencing for field implementation.

Rather than using a redox probe, Fang et al.[118] employed supporting electrolytes to detect PFOA, PFOS, and 1*H*,1*H*,2*H*,2*H*-perfluorooctanesulfonic acid (6:2FTS) with conventional pencil led as their working electrode. Seeking to mitigate production costs, they electropolymerized polypyrrole imprinted with PFOA onto a washed pencil lead substrate with copolymerized methylene blue as a cationic anchor for their anionic targets. Upon binding, targets generated a potentiometric shift, and the magnitude of this shift was registered as the sensor's signal intensity. Unlike any of the other MIPs discussed, their MIP was "conditioned" in a concentrated PFOA solution for 24 h prior to

potentiometric testing. This step was said to partly free PFOA cavities by establishing equilibrium between the initially bound template and conditioning solution which, by their analysis, enhanced the system's selectivity when exposed to analogous compounds. The improvement likely occurs due to residual PFOA leakage into their sample solution during cross-comparison. They also noted a lower LOD with reduced conditioning concentrations, probably resulting from additional vacancies in their polymer matrix. Ultimately, their optimized conditions led to a LOD of 0.1 μM for PFOA. MIPs were also generated with PFOS and SDS which, as expected, increased interference for their respective templates and even, in the case of the SDS-MIP, caused indiscernible differences among the responses for each analyte. The lack of complete fluorination for 6:2FTS lowered its signal compared to PFOA and PFOS when tested with the PFOA-MIP, and SDBS showed significant overlap with the response curve recorded for PFOA. Unfortunately, a non-imprinted polymer was not included in their analysis, preventing retrospection of their imprint's effectiveness and associated IF. Their detection range of 0.01 to 10 mM lies far above the practical range for non-preconditioned sensing applications, but their use of a non-traditional electrode aimed at cost-effectiveness was nonetheless fascinating.

Toward the development of a sensing strip for PFAS, a photoactive bismuth oxyiodide (BiOI)-based electrochemical sensing platform showcased by Gong et al.[119] for PFOA and later fashioned for perfluorooctane sulfonyl fluoride (PFOSF) by Li et al.[120] utilized acrylamide/EGDMA MIPs to tailor the response of each system for their desired contaminant. In the former entry, silver iodide nanoparticles (AgINPs) were implanted into BiOI nanoflakes under successive ionic layer adsorption and reaction (SILAR) atop fluorine-doped tin oxide (FTO) glass, and the preformed PFOA-MIP was cast thereafter. In this case, both the AgINPs and MIP were shown to enhance the photocurrent through the electrode due to the synergistic band gaps between the inorganic materials in the photoactive layer and the favorable conductivity of acrylamide. With triethanolamine (TEA) acting as an ambient electron donor, PFOA binding to the MIP blocked diffusion of TEA to the FTO surface and exhibited a marked reduction in measured photocurrent. This response was highly specific for PFOA, leaving a peak normalized photocurrent of about 24% for PFNA with lower false positives for other fluorinated and non-fluorinated

analogs of PFOA and less than 7% deviations for coadded interferents. The extension of this work by Li et al.[120] employed a SPE printed onto a polyethylene terephthalate film with a combination of carbon, silver, and silver chloride inks as a customizable replacement for FTO. The SPE was covered with BiOI nanoflakes with the SILAR approach used previously before capping with a preformed PFOSF-MIP layer. With this design, PFOSF binding to their MIP inhibited diffusion of tris(hydroxymethyl)aminomethane hydrochloride and AA (undefined) electrolytes and similarly reduced the photocurrent measured under visible light. Sensitivity analysis demonstrated a wide linear response range between 0.05 and 500 ppb, slightly narrower than the 0.02 to 1,000 ppb range reported for PFOA.[119] Analogous fluorinated interferants only caused a maximal response deviation of roughly 9%, close to that of their earlier model. Non-fluorinated competitors had negligible effects on the sensor response altogether. Granted the difficulty of detecting PFOSF with conventional analytical equipment such as LC/MS/MS and gas chromatography due to the pollutant's lack of chromophores and ionizable groups, their LOD of 0.01 ppb places their sensor as one of the most sensitive routes for detecting the contaminant available. Their LOD for PFOA hitting the same mark of 0.01 ppb likewise offers a precise method for identifying the contaminant, affirming this sensing platform as a noteworthy contribution to the field of polymeric molecular sensors.

Tran et al.[121] opted for a supporting electrolyte mixture of potassium chloride in a pH 7.0 phosphate-buffered saline buffer solution to achieve photoelectrochemical detection of PFOS with an acrylamide/EGDMA MIP. For their system, anodized titanium formed well-defined nanotube arrays that were modified with APTES and 3-methacryloxypropyl trimethoxysilane to serve as methacrylate anchors. Subsequent photopolymerization yielded an electrode interface with a low electron-hole recombination rate that favors high conversion efficiency and charge transfer. When exposed to PFOS, the captured analyte facilitates charge transfer and raises the measured photocurrent under a 100 mW cm^{-2} xenon lamp. Oddly, the response behavior showing positive association is the opposite of that observed for the compositionally similar MIPs of Gong et al.[119] and Li et al.[120] The origin of this discrepancy is unclear; Tran et al.[121] used an electrode configuration of a MIP-covered titanium dioxide working electrode,

platinum counter electrode, and saturated calomel reference electrode, Gong et al.[119] employed a MIP-shielded FTO working electrode, platinum auxiliary electrode, and Ag/AgCl reference electrode, and Li et al.[120] used a carbon-BiOI-MIP working electrode, carbon arch counter electrode, and Ag/AgCl reference electrode atop a silver conducting medium. Differences in these strategies could affect node crosstalk, but their influence on performance is not obvious. The reliance of each working electrode on ambient electron donors for their photochemical activity may also play a role, but these contributions are not easily retrieved from each manuscripts' proposed mechanisms. For the titanium nanotube array, cross comparison of fluorinated and electroactive non-fluorinated analogues revealed less than 6% PFOS response deviation for up to 20-fold excess interferent concentrations. Aromatic non-fluorinated analytes, possibly due to the resonance of their aryl rings trapping charge transfer, slightly reduce photocurrent in the absence of PFOS. A linear range from 0.5 to 10 μM and LOD of 86 ppb with possible use for outdoor water samples gives this method potential for applicability with further optimization.

2.3.2 Non-MIP Sensors

Outside of MIP-based approaches for sensing PFAS, Kejun Tan's group explored using fluorescent dyes and CQDs in a variety of configurations to accurately identify PFOS in solution. In their earliest contribution, Liang et al.[122] used a competitive binding assay between eosin Y and PFOS for polyethyleneimine (PEI) as a quantitative marker for the contaminant. With their method, negatively charged eosin Y forms a ground state complex with PEI that quenches its fluorescence; when mixed, the electronegative head group of PFOS displaces eosin Y and restores its signal. Conditional variations indicated that pH heavily affects the system by altering the protonation states of each species, and extraneous salts interfered with the measured intensity delta by shielding PEI from initially quenching eosin Y. Temperature likewise lowered the signal response by weakening binding above 35 °C. SDS was mentioned to significantly impact the system, likely via the same displacement mechanisms as PFOS, and an excess of barium (Ba^{2+}) was noted to form filterable SDS precipitates that would serve to eliminate the compound prior to registering the PFOS concentration. The level of residual Ba^{2+} and its effect on

measured PFOS was not fully elucidated to verify whether the purification would inadvertently impact the system's application, though Ba^{2+} alone was shown to have little influence over the method's innate intensity. The study did not test other PFAS outside of PFOA (which showed little disturbance) nor the effect of complex matrices. Recoveries between 97.4% and 105.1% do not, unfortunately, alleviate concerns for potential PFOS extraction from Ba^{2+} sample pretreatment. The approach's simplicity while still holding a LOD of 15 nM shows the strength of fluorescent assays as tools for environmental monitoring that, as other applications elucidate, can meet the sensitivity needs of investigative parties.

In two additional contributions from the same group by Chen et al.[123] and Cheng et al.,[124] CQDs formed from OPD and 3-aminopropyltrimethoxysilane (APTMS), respectively, acted as the reporter elements for signal-off or signal-on sensing regimes. As part of a schematically simple approach reminiscent of Liang et al.,[122] the former entry from Chen et al.[123] compared the fluorimetric, colorimetric, and resonance light scattering (RLS) responses of OPD-CQDs agglomerated by PFOS to propose an accurate triple-channel optical assay for quantifying contamination levels in water supplies. PFOS electrostatic binding to the nitrogenous groups of OPD-CQDs formed large precipitates with a ground state complex that statically quenched their luminescence, simultaneously lowering their fluorescence intensity and absorption while raising their RLS intensity. As before, ionic strength and temperature were both negatively corelated with the differential fluorescence between blank and PFOS samples, again due to Debye length suppression and binding disruption. Though the absolute difference in fluorescence intensity seemingly decreased linearly with pH, the quenching efficiency was calculated to peak at pH 5.4 resulting from balancing the protonation states of both the anionic sulfonate head group for PFOS and the cationic amines populating the OPD-CQDs. Extraneous ions had little effect on the emission intensity of CQDs exposed to PFOS with cadmium chloride showing the greatest absolute deviation of only 5.34%. Secondary fluorinated analytes displayed low false-positive rates with PFOA holding the highest signature of approximately 15%, but no sulfonate or sulfate analogs were examined and they did not test mixed matrices. The latter contribution from Cheng et al.[124] followed a similar approach to Chen et al.[123] by initially quenching their APTMS-CQDs with berberine

chloride hydrate (BCH) and using competitive association with PFOS to liberate BCH and restore the particles' fluorescence. In this assay, PFOS simultaneously heightened the emission intensity for then-unquenched CQDs at 448 nm and synergistically augmented the emission of BCH at 533 nm, offering two peaks by which to correlate the contaminant's concentration. Combining PFOS, BCH, and CQDs together provided a slightly wider linear detection range of 0.22 to 50 μM compared to BCH-PFOS alone (0.23 to 40 μM) and also eased visualization with a deep blue to yellow shift. This combination also improved selectivity relative to Chen et al.[123] by reducing the maximal coanalyte false-positive to about 3% for PFHxA and lowering the maximum absolute deviation from added salts to 5.0% for lead nitrate. The LOD for both systems remain close at 21.7 nM for Cheng et al.[124] and 18.3 nM for Chen et al.,[123] showing the similarity of these methods for detecting PFOS.

Lin et al.[125] followed a similar approach to Tan's group by using nitrogen-doped carbon dots (NCDs) to achieve a LOD two orders of magnitude lower than their predecessor. Therein, they exploited thermal precipitation of thiamine with triethylamine to yield carbon dots passivated by several nitrogenous defects, which, when exposed to PFOS, followed the same mechanism described for Jiao et al.[112] to enhance the amino groups' imperfections and, consequently, augment their emission intensity. The molecular phenomena attending the intensity increase was countered by quenching at higher PFOS concentrations due to agglomeration in the manner described by Chen et al.[123] Like the other CQD studies, NCD emission was pH dependent with a maximum at pH 6.1 and resistant to interferent disturbances like those of Cheng et al.[124] An analog to PFOS, 6:2 chlorinated polyfluorinated ether sulfonate (commercially F-53B), was mentioned to raise the emission intensity by approximately 16.7% that of PFOS, and mixed ionic matrices with PFOS further complicated the output by another 20%. Coadded PFAS were not studied to test whether preferential binding might lessen the burden of cocontaminants. The measured linear range between 0.3 and 160 nM does, however, grant this quantum dot approach a detection range near the threshold set by the EPA, giving this method the potential for use in environmental monitoring.

In a unique approach, Faiz et al.[126] coated the end of a single mode optical fiber with a mixture of polyvinylidene fluoride (PVDF) and polyvinyl butyral to capitalize on

the ferroelectric properties of PVDF by forming an attractive polarized surface for their target that also functions as a Fabry-Perot interferometer. With this design, light traveling through the optical fiber is reflected at the foreplane and backplane of the PVDF coating, and the thickness and refractive index of these parallel planes influenced by analyte binding alter the optical path length between the reflected light and, consequently, produce a phase difference. This difference yields an interferogram that translates the path length into an analyte's concentration. The scheme was, however, limited to relatively high PFOA concentrations, noting a LOD of 5 ppm. The sensor was also susceptible to very slight changes in temperature due to thermal relaxation of the polymer modifying its optical properties, necessitating the use of complementary temperature sensors to generate a self-sufficient system.

Away from optical sensing schemes, Philippe Bühlmann's group demonstrated two electrochemical approaches for detecting perfluoroalkyl acids utilizing anion-exchanger membranes. In their earliest example by Boswell et al.,[127] polytetrafluoroethylene (PTFE) filter disks were impregnated by a fluorophilic phosphonium methyl sulfate ion-exchanger salt and a fluorophilic electrolyte salt to provide a cationic anchoring site for their targets and to reduce the membrane's electrical resistance, respectively. This membrane was packaged into a poly(chlorotrifluoroethylene) electrode containing an inner filling solution of potassium chloride separated from an outer filling solution of the target anion (i.e., PFOS, PFOA) by a glass wool plug. With the membrane operating as the interface between the sample and internal electrolyte matrix, the potential difference between the bias placed on a AgCl-coated Ag wire within the electrode and an external reference electrode followed a linear reduction through the logarithm of the sample anion's concentration. This Nernstian response was found across 100 nM to 100 μM for PFOS, and the electrode proved selective by at least four orders of magnitude for PFOA and six orders of magnitude for PFOS over other ambient ions. Despite these accomplishments, the ion-exchanger salt was notably susceptible to decomposition by hydroxide ions, leading to subsequent work to develop stable fluorophilic salts that resulted in the sensor detailed by Chen et al.[128] Therein, not only did they employ fluorophilic salts with tetraalkylphosphonium and bis(phosphoranylidene)ammonium groups, they also took

advantage of a three-dimensionally ordered macroporous carbon monolith attached to their electrode and PTFE support disk to replace the inner filling solution described earlier and further improve sensitivity. Combining these alterations with optimizing measurement conditions afforded detection limits down to 0.86 nM for PFOS and 0.17 nM for PFOA, hitting the threshold set for sampling precisely without the need for preconcentration. Their analysis also concluded only minor expected perturbations from shorter chain homologues due to disparate hydrophobicity, reducing the threat of environmentally common analogues from confounding their sensor.

2.4 Conclusions

As Figure 2.2 indicates, the direct polymeric sensing approaches present in literature are primarily split amongst fluorimetric and electrochemical transduction methods with MIT holding a strong contingent of the response schemes employed. Both transduction platforms have a wide detection limit; fluorimetric sensors span sub-ppq levels with the CQD contribution from Jiao et al.[112] up to roughly 10 ppb for the carbon dots from Cheng et al.[124] while the MIP electrodes for Gong et al.,[119] Chen et al.,[114] and Li et al.[120] are positioned at 10 ppt and the sensor from Tran et al.[121] lies at 86 ppb. Each transducer has unique advantages in attempting to overcome the hurdles present for sensing PFAS, namely their lack of innate immunogenicity, electroactivity, or luminosity. The ingenuity of the various designs seeking to surmount these limitations is remarkable, encompassing complex protein binding cascades to responsive waveguides aimed at revealing the concentration of concerning fluorinated organics in complex samples

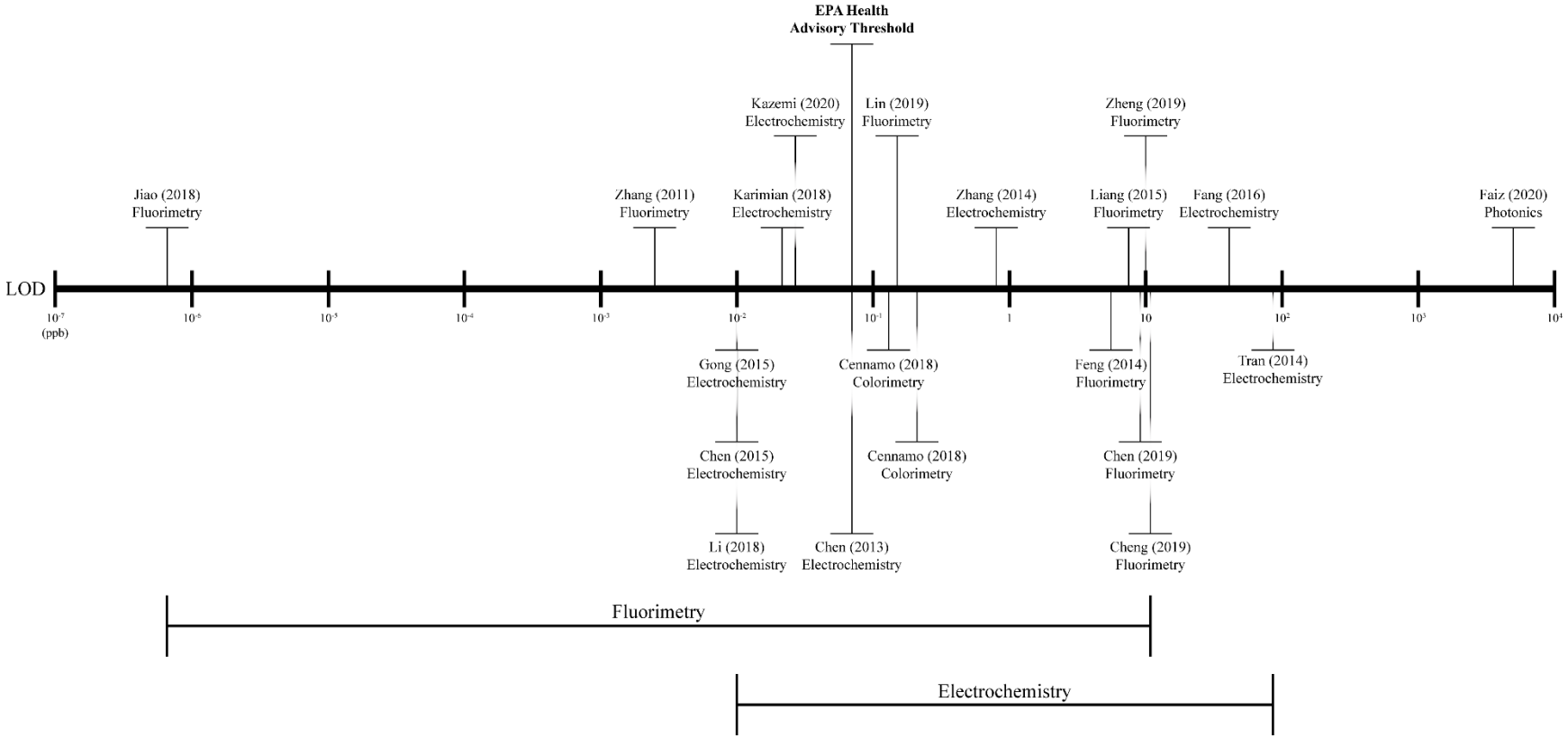

Figure 2.2. Limit of detection (LOD) scale for each polymeric sensor reviewed. Ranges for their primary transduction methods (fluorimetric and electrochemical) are depicted below the scalebar.

Though numerous monomers have seen use for uncovering PFAS, some are represented more commonly than others. Acrylamide, with its excellent electrical conductivity and an available amino binding site for perfluoroalkyl acids, acts as a staple for electrochemical MIPs. The rigidity, robustness, and crosslinking capabilities of EGDMA make it an ideal stabilizer for MIPs locking in specific target void volumes for both electrochemical and colorimetric applications. OPD, as a versatile monomer containing both amino and aromatic groups, can insulate electrodes for turn-off electrochemical sensors or utilize the binding potential of its nitrogenous moieties to quench its polymer's luminescence in the presence of contaminants. Finally, APTES functions as a relatively inert, hydrophilic constituent that can fill the role of a supporting substrate, modifiable shell, or shape-memory complex to facilitate MIT. Together, these four monomers form the basis for many of the polymeric sensing approaches reviewed here, but they are often bolstered by complementary monomers to finely tune the response of a polymer to the particular contaminant of interest sought by a given design. The flexibility of polymers to interact with and report the presence of individual chemical species in solution grants this class of materials the functionality to quickly and resolutely identify the concentration of concerning fluorinated contaminants in a manner that meets or surpasses the detection standards put forth by regulators without the complications of sample pretreatment or preconcentration attending LC/MS/MS.

2.5 Prospectus

Despite the strides already apparent in the literature to date, several pitfalls remain for the use of polymeric sensors targeting PFAS. MIT remains susceptible to significant interference from shorter-chained homologues than their template. Receptors utilizing cationic moieties may fall prey to slight variations in pH or ionic strength. Attraction via fluorinated groups relies on relatively weak intermolecular forces. Bioreceptors must overcome the limitation of deficient immunogenicity by PFAS. Electrochemical schemes require secondary probes to conquer their target's lack of electroactivity. Furthermore, the reliance on two primary transduction motifs, luminescence and electrochemistry, have inbuilt constraints in the extent to which each technique can reliably distinguish signal from noise. Disregarding the outlier from Jiao et al.,[112] fluorimetric approaches have a

lower observed range spanning three orders of magnitude compared to the four-order range for electrochemical transducers. Only four sensors, one fluorimetric[105] and the others electrochemical,[114, 119, 120] met or breached the 10 ppt detection threshold, leaving considerable room for improvement with upcoming sensors. Mechanical transducers, such as QCM, SAW, and resonators, have been unattended by polymeric sensing approaches, offering an avenue for continued exploration into even more precise designs for pinpointing PFAS.

With these considerations in mind, the advances already put forth by the environmental sensing community have etched away at the established sensitivity thresholds and provided convenient alternatives to the LC/MS/MS standard. The list of efforts to address simple and field-ready approaches for locating contaminated sites is promising for the potential of polymers to furnish solutions to the detection goals set by regulatory agencies. Nonetheless, with sensors becoming evermore keen, the criteria for their sensitivity will inevitably become more stringent, supplying continued impetus to further sensitivity for polymeric sensors past the limits of their predecessors.

2.6 Motivation

Having defined the advances set forth by polymeric sensors for detecting dilute PFAS, the project described herein will henceforth seek to meet the following goal: developing a synthetic polymeric sensor capable of detecting PFAS at environmentally relevant concentrations (i.e., cumulative 70 ppt) in complex matrices without pretreatment nor the use of molecular imprinting. The need to produce a system capable of detecting PFAS in environmental matrices will facilitate usage of the sensor for in-field detection. Utilizing a synthetic polymeric exempt from imprinting approach will avoid the tedium of executing a biological sensing approach for the non-immunogenic substances, strengthen the stability of the final sensing element, aid in producing the sensor at scale, and prevent the use of PFAS or closely related structural analogs in the synthesis of the polymeric sensing material.

It is worthy of note that the goals set forth in the preceding paragraph are ideal outcomes for the project that may not be achieved during the exploratory window of the research presented and may not be attainable by the methods heretofore employed.

Should either of these conditions hold true, shortcomings and caveats to the approach presented will be summarized at the conclusion of the work to assist future endeavors pursuing similar goals.

CHAPTER 3. RESEARCH APPROACH

Though the assortment of available polymeric sensors is already capable of detecting PFAS below the standard 70 ppt threshold, only eight sensors, including one significant outlier, managed to surpass this mark. Six of these sensors were based on molecular imprinting, another on a bioassay, and the last on a clever ion-exchange process. The dominant technology at play, molecularly imprinted technology (MIT), relies primarily on shape-memory to recognize target molecules in solution, which, though highly sensitive and selective, does little to capitalize on the innate interactions of the applied polymer and the functional species at play. Two notable examples, acrylamide and OPD, contain amino groups capable of weak electrostatic interactions with anionic fluorosurfactants like PFOA and PFOS, but this capacity is narrow with respect to the range of forces available for capturing and signaling the presence of the polymer's target. Non-electrostatic examples include using fluorous moieties to again apply singular facets for binding fluorinated contaminants. Individually, these components combined with imprinting are sufficient to reach the concentration thresholds currently set by regulators, but, in the search for even more resolute sensing regimes, tandem complexes utilizing more elaborate binding domains are necessary to truly realize the potential of polymeric sensors pursuant of the sensitivity extremes set forth by natural multiplex biorecognition elements.

With this condition in mind, a non-molecularly imprinted platform for exploring the extent of standalone polymeric interactions with perfluoroalkyl acid targets was proposed herein to take advantage of three binding pathways simultaneously with a single functional polymer. To that end, a highly studied thermoresponsive polymer, poly(*N*-isopropylacrylamide) (PNIPAM), was copolymerized with fluorous moieties to exploit electrostatics amongst its secondary amine groups with anionic analytes, favorable fluorine-fluorine attraction between comonomers and fluorosurfactant tail groups, and the tunable hydrophilicity and hydrophobicity surrounding the polymer's phase transition as a complex array for maximizing the polymer's sensitivity toward its targets. The switchable phase behavior of the polymer not only serves to possibly regulate analyte

binding by playing on fluorosurfactants' slight phase preference[129] but also to act as a crude indicator of the contaminant's concentration.

PNIPAM hydrogels have been shown to significantly alter their swelling behavior in surfactant solutions approaching the surfactant's critical micelle concentration (CMC).[130] Association between surfactants, particularly those with strongly anionic head groups like SDS, and PNIPAM is believed to form a string-of-pearls populated by polymer chains and bound micelles. These micelles contribute ionization within cross-linked networks which establish an osmotic pressure gradient that ultimately enhances the polymer's observed swelling.[130, 131] The origin of this phenomenon occurs at concentrations below the surfactant's CMC at a point known as the critical aggregation concentration (CAC). The CAC corresponds to the lowest surfactant concentration with detectable alterations in the polymer's behavior, typically arising at one or two orders of magnitude below the surfactant's CMC. Deviation in the CAC for polymer-surfactant complexes carrying copolymerized fluorine groups versus non-fluorinated polymers consequently offers a measure of the system's potential for interacting with fluorosurfactants of interest.

The phase behavior of PNIPAM follows a hydrophilic (swollen) profile at lower temperatures with a sharp transition to a relatively hydrophobic (collapsed) state at higher temperatures. The transition point bridging these two solvation states is termed its lower critical solution temperature (LCST). The LCST's position corresponds to the entropically driven disruption of hydrogen bonding between the monomer's amide constituent and the surrounding solvent together with destabilization of the solvent molecule's clathrate-esque ordering around the residue's isopropyl moiety. Surfactants that swell PNIPAM hydrogels also raise the polymer's LCST by impeding precipitation through the mechanisms mentioned earlier. The sensitivity of this parameter, affected simultaneously by the polymer's functionality and added solutes, therefore constitutes another metric by which to gauge the polymer's responsiveness toward PFAS.

Taking the thermodynamic cues of PNIPAM together with fluorous functionalization to enhance its receptivity to perfluorosurfactants, four distinct tests are necessary to weigh the capacity of this polymeric scheme to act as a sensing motif: 1) initial quantification of fluorosurfactant impact on the swelling and thermodynamic behavior of bulk PNIPAM hydrogels, 2) analysis of the influence fluorinated comonomers hold over

the innate and PFAS-modified thermodynamic properties for copolymerized hydrogels, 3) evaluation of bulk versus microgel morphology as a strategy to augment thermodynamic fluctuations in response to PFAS, and 4) investigation of the potential for modifying gels with Förster resonance energy transfer (FRET) compatible dyes to provide a quantifiable visual signal for the contaminants' presence. Assessment in this manner will explore four primary hypotheses: 1) fluorosurfactants, particularly those with strongly anionic head groups, will greatly increase PNIPAM network swelling similarly to SDS, 2) functionalization of PNIPAM with fluorous comonomers will promote fluorocontaminant attraction to the networks and accentuate the differential swelling response afforded by PFAS, 3) reducing gels from their bulk to microgel forms will sharpen the thermodynamic response of the microgels to lower contaminant concentrations, and 4) implanting gels with dyes, in addition to the receptivity enhancements provided by fluorination and miniaturization, will offer a visual route for determining the concentration of PFAS in suspect samples. The methodology used to test these hypotheses will follow the aforementioned sequencing shown in Figure 3.1. Each element in the sequence is supported by considerations for contingencies should an individual step go awry. Implementation of contingencies at each stage could change the course of upcoming steps, leaving the flow chart as a prospective outline for the progression detailed herein.

With the flow in Figure 3.1 guiding the investigations reported, upcoming chapters will demonstrate the implementation of each premise and respective conclusions drawn that inspired decisions made in subsequent entries. All four hypotheses were tested through the three following chapters. The first two have dedicated chapters while the latter two are packaged together. Final retrospective conclusions are then presented regarding the entirety of the project, and possible extensions of the work are given in parting.

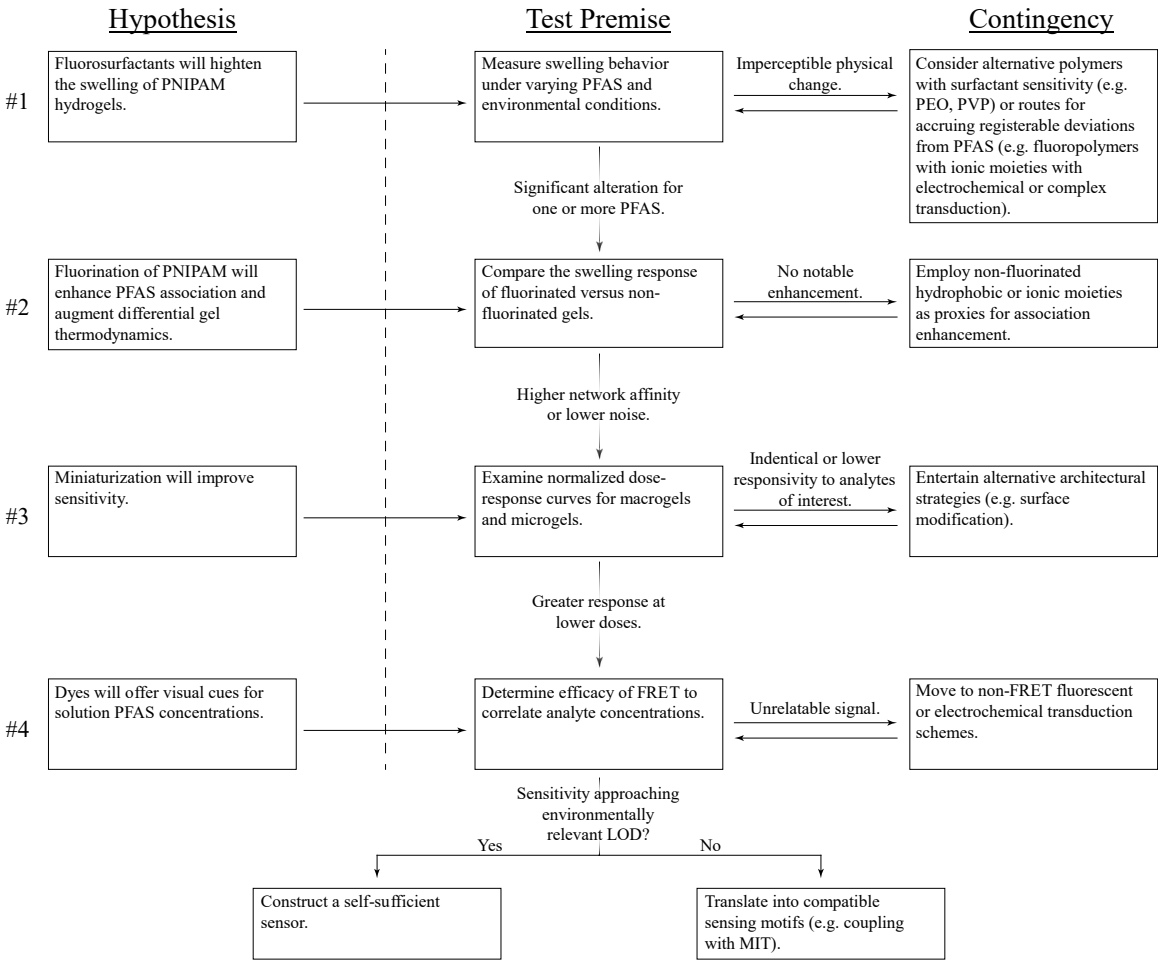

Figure 3.1. Prospective methodology for examining the potential of PNIPAM to act as a sensing material for PFAS.

CHAPTER 4. ON THE SWELLING BEHAVIOR OF POLY(*N*-ISOPROPYLACRYLAMIDE) HYDROGELS EXPOSED TO PERFLUOROALKYL ACIDS

The contents of this chapter are reproduced in part from a submission under the same name to the Journal of Polymer Science.

4.1 Introduction

Due to the flexibility of the PNIPAM's phase transition at its LCST near 32 °C, the polymer has seen use as a molecular sensor in numerous previous applications. Serpe's group[132-134] and others have experimented with detecting a suite of chemicals including biomolecules,[135-140] small molecules,[141-145] solvents,[146] and alkyl surfactants.[147] Supplementing the lattermost entry, the literature has explored the interaction of non-fluorinated surfactants with PNIPAM, indicating that the polymer swells and its LCST rises in solution with surfactants approaching their CMC.[148-153] The surfactant's influence on the phase behavior and physical properties of PNIPAM depends on its chemical characteristics (e.g., tail length and head group),[148, 150, 153] opening the floor for the unique attributes of fluorosurfactants, such as their simultaneous hydrophobicity and oleophobicity,[129] to offer an interesting contribution to the understanding of surfactant-polymer interplay. Probing the association of PFAS with PNIPAM and the physical changes that result can set the foundation for future detection schemes exploiting the phenomena. Notably, PFOS was observed to cause drastic increases in both the LCST and mass swelling ratio of PNIPAM hydrogels, and titration saw a decay on both fronts following the association progression expected for traditional alkyl surfactants.[131] Fluorimetric micropolarity studies showed aggregation below the limits discernable from bulk swelling data, leaving an opportunity for detection enhancement that will serve as the basis for forthcoming investigations.

4.2 Methods

4.2.1 Materials

Unless noted otherwise, all reagents were used as received without further purification. Syntheses were carried out using *N*-isopropylacrylamide (NIPAM, Sigma,

97%), *N*,*N'*-methylenebis(acrylamide) (MBA, Sigma, 99%), and 2-hydroxy-4'-(2-hydroxyethoxy)-2-methylpropiophenone (I2959, TCI, 98%) as monomer, crosslinker, and ultraviolet (UV) free radical photoinitiator, respectively. Phenol (Ph, Fluka, 99%), octanoic acid (OA, Alfa, 98%), methanol (MeOH, Pharmco, HPLC-UV grade), sodium dodecyl sulfate (SDS, VWR Chemicals, biotechnology grade), sodium octyl sulfonate (SOS, TCI, 98%), perfluorooctanoic acid (PFOA, TCI, 98%), and tetraethylammonium perfluorooctane sulfonate (TPFOS, BeanTown Chemical, 98%) were used as analytes for swelling tests. Nile red (NR, Sigma, technical grade) was employed for fluorimetric studies. Dimethyl sulfoxide (DMSO, Pharmco, reagent ACS grade) and deionized (DI) water (1 MΩ) were used as solvents in their respective experiments. Both DMSO and MeOH were stored over 3 Å molecular sieves to minimize residual water. Structures for each synthesis and test chemical are included in Figure 4.1.

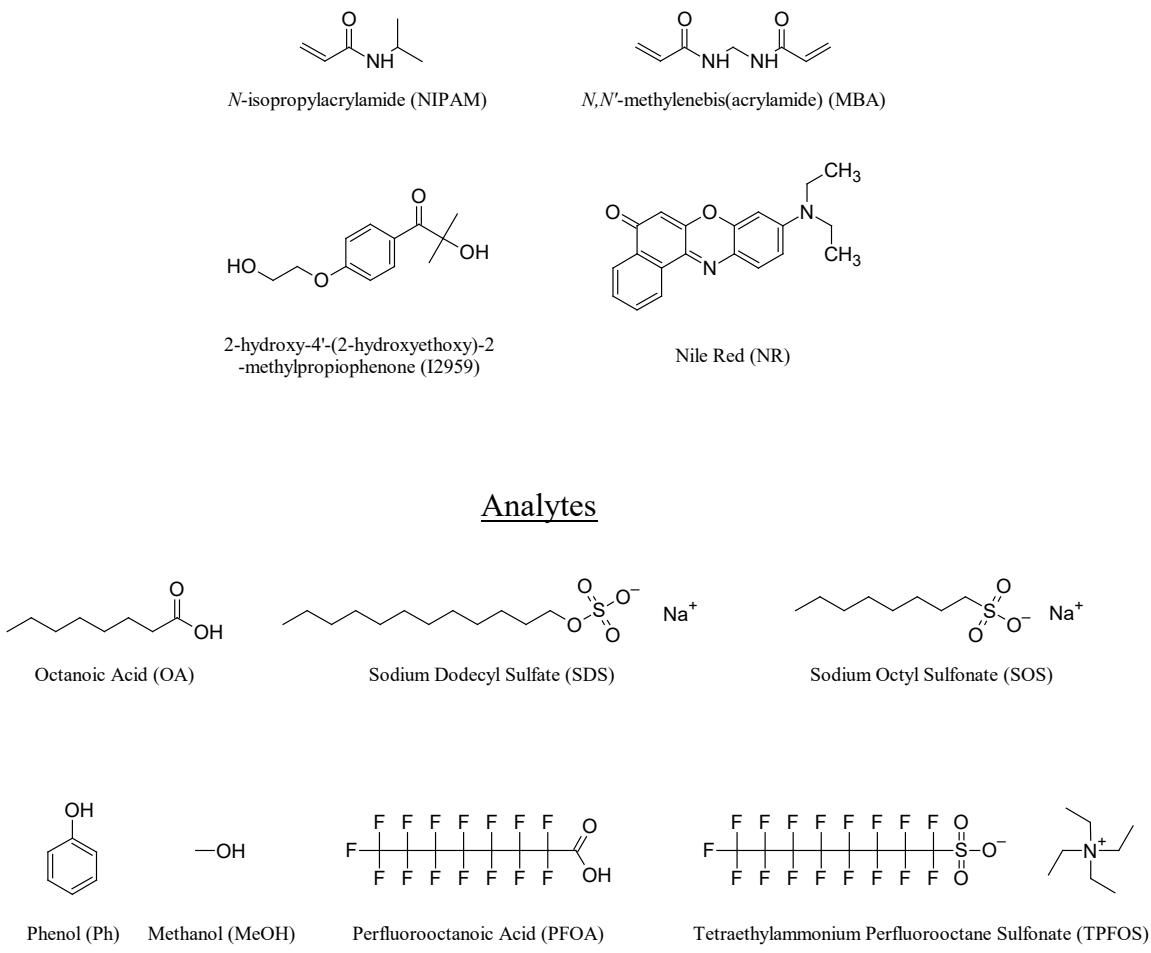

Figure 4.1. Chemical structures for each chemical used for hydrogel synthesis (NIPAM, MBA, and I2959) and swelling investigations (Ph, MeOH, OA, SDS, SOS, PFOA, TPFOS, and NR).

4.2.2 Hydrogel Synthesis

All hydrogels used in this work were synthesized via UV-initiated free radical photopolymerization with the initiator I2959. For a base gel (BG) fabricated with a feed concentration of 97.54 mol% NIPAM and 2.46 mol% MBA, 0.427 g (3.776 mmol) of NIPAM was first added to a 20 mL scintillation vial followed by 1.662 mL of anhydrous DMSO. Thereafter, 0.746 mL (0.015 g, 0.095 mmol) from a stock solution of 19.681 mg mL^{-1} MBA was added to the vial and mixed thoroughly. Another 0.174 mL (0.008 g,

0.037 mmol) from a 47.951 mg mL^{-1} stock solution of I2959 was then added and again mixed, bringing the total monomer concentration (TMC) to 1.290 M. The prepared pre-polymer solution was transferred to the gap between two glass slides provided by a 0.51 mm thick polypropylene spacer secured with binder clips. The mold containing the pre-polymer was then placed into a UV curing box (LESCO Exposure Lamp System FEM1011 powered by a PCM Solid State SEM1040) set to 5.00 mW cm^{-2} for 1 h. The cured hydrogel was freed from its mold and gently deposited into a capped jar containing 200 mL DI water and rotated atop an orbital shaker (SCILOGEX SCI-0180-E) at 50 rpm for 2 h. After soaking, the water was replaced with fresh water and the washing continued four times for a total of five cycles. Once fully washed, the swollen gel was laid on a piece of weigh paper and cut into individual disks with a long drive pin punch (6.95 mm inner diameter). The disks were then flash frozen in liquid nitrogen and lyophilized. Dry gels were used for subsequent swelling studies. Syntheses were performed in triplicate, and one sample from each synthesis was used for triplicate analysis (i.e., $n = 3$) of swelling and fluorimetry.

4.2.3 Characterization

Fourier-transform infrared spectroscopy (FTIR) was utilized to check the monomer conversion of the synthesized hydrogels. Attenuated total reflectance (ATR)-FTIR spectra were collected with a Varian 7000e FT-IR Spectrometer using Varian Resolutions Pro 4.0 software. The resolution was set to 8 cm^{-1} co-added over 32 scans at a speed of 5 kHz between 700 cm^{-1} and 4,000 cm^{-1}.

4.2.4 Swelling Studies

All solutions were housed in 20 mL borosilicate glass scintillation vials with cork-backed aluminum foil lined urea caps, and temperature regulation was achieved by immersion in an LKB Bromma 2219 Multitemp II Thermostatic Circulator. For each trial, an appropriate mass (SDS, SOS, TPFOS) or volume (OA, MeOH, Ph) of analyte was added to 20 mL DI water before inserting a dry gel disk. Analyte solution concentrations were maintained at 1 mM for all species except for MeOH which was introduced at 10 mM. In the case of PFOA, 12.7 µL from a 1.576 M stock solution of

PFOA in MeOH was injected to result in a 1 mM PFOA and 10 mM MeOH co-analyte solution. All samples were initially equilibrated at 5 °C for 72 h prior to taking their first mass measurement, and subsequent measurements were recorded every 24 h after raising the bath temperature by 2.5 °C. Titration measurements were performed following 16 h initial equilibration. Swelling ratios (Q) were calculated from the initial dry disk mass (m_i) and the swollen mass (m_s) at a specific temperature following $Q = m_s/m_i$.

4.2.5 Fluorimetric Studies

Fluorescence intensity measurements for gels mixed with NR were recorded with a Synergy Mx Microplate Reader (BioTek). Solutions with NR were produced by injecting 60.2 μL from a 250 μM stock solution of NR in DMSO into a 20 mL scintillation vial containing 15 mL of a solution containing an appropriate concentration of TPFOS and a BG, bringing the NR concentration to 1 μM with 56.3 mM of residual DMSO. Controls were generated by eliminating either the addition of the BG or NR, but DMSO was not supplemented in cases subtracting NR. Once mixed, solutions containing NR were wrapped in aluminum foil, and all solutions were left at room temperature for more than 96 h before measurement.

Upon equilibration, 250 μL of each solution was transferred to a well of a black 96-well polystyrene assay plate with a clear bottom (Corning). Swollen gels were deposited on the bottom of their respective wells by cutting the gels with the same pin punch employed during synthesis and carefully slipping the resulting disk through its solution. Air bubbles between the disks and flat bottoms of their wells were removed by gently rocking the top side of each disk with tweezers. The plate cover was replaced after situating all solutions and disks in their respective wells to minimize evaporation during incubation. Wells were read from their bottom at excitation/emission wavelengths of 590/660 nm, 579/651 nm, 578/641 nm, and 570/635 nm with a 9.0 nm slit to record the intensities at the maxima for 1 μM NR in water, in 10 mM TPFOS, in a BG alone, and in a BG incubated with 1 mM TPFOS, respectively (see Figure 4.2). The gain was kept at 100, and the read speed was held at normal. After performing the first read at room temperature, the incubator was set to 50 °C and maintained for 2 h prior to executing the second read.

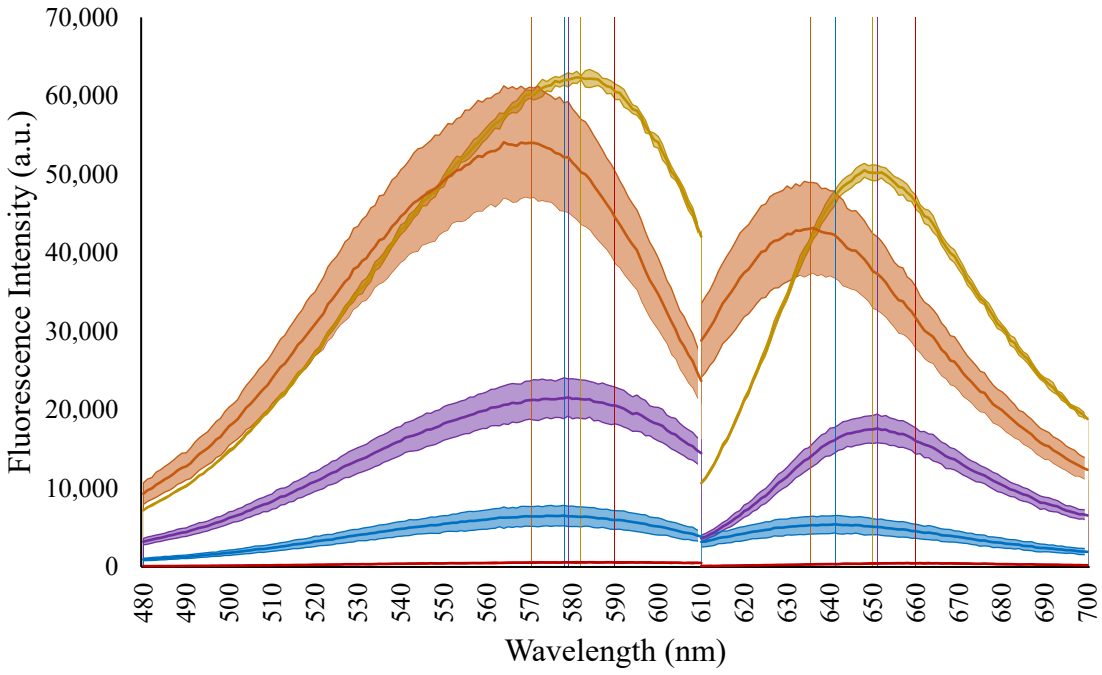

Figure 4.2. Spectral scans for 1 μM NR in water (red), in 10 mM SDS (gold), in 10 mM TPFOS (purple), in a BG (blue), and in a BG with 1 mM TPFOS (orange). Lines are meant to guide the eye toward excitation (left) and emission (right) peaks for each system. Shaded regions represent one standard deviation (n = 3) from the average marked by a central line.

4.2.6 Electron Microscopy

BG soaked in a 1 mM TPFOS solution was imaged and characterized by scanning electron microscopy (SEM, Quanta 250 SEM from FEI, Hillsboro, OR, USA) and energy dispersive X-ray spectroscopy (EDS, X-Max detector from Oxford Instruments, Abingdon, UK). Prior to imaging, the hydrogel, still in solution, was rapidly transferred and frozen at the surface of an SEM holder (aluminum stub attached on top of a large block of brass) by immersion in liquid nitrogen. The sample was then split using a carbon steel blade to expose fresh, frozen cross-section faces (see Figure 4.3). The holder was then rapidly transferred in the SEM, and the sample was characterized while still frozen. Imaging was performed at low accelerating voltage (2 keV electrons energy)

to minimize charging effects (since no conductive coating was deposited on the sample). Elemental analysis with EDS was conducted using an accelerating voltage of 10 kV.

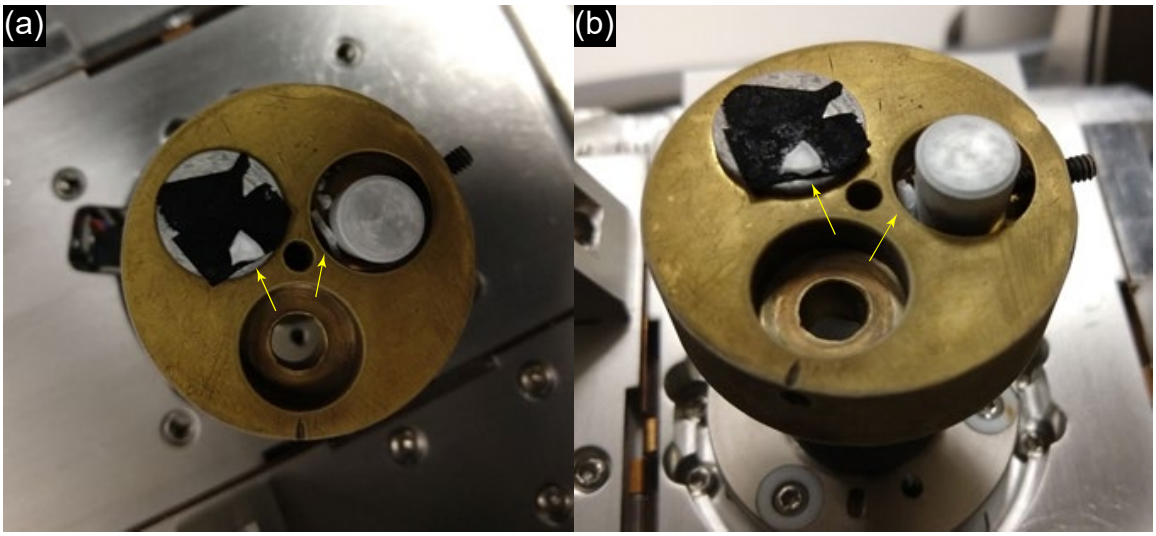

Figure 4.3. Electron microscopy setup of flash frozen gels atop aluminum stubs housed in a brass fixture. Samples are shown from (a) overhead and (b) frontal. Frozen BG samples are indicated with yellow arrows.

4.3 Results

4.3.1 Synthesis & Characterization

Synthesized hydrogels had an opaque appearance and were cut into discs with approximately 5.64 mm diameters and 0.52 mm thicknesses in their dry state. The gels' FTIR spectrum (from Figure 4.4) demonstrates a characteristic amide I band at 1,639 cm^{-1} associated with C=O stretching vibrations and an amide II band at 1,539 cm^{-1} corresponding primarily to N-H bending.[154] The fingerprint region peak at 1,458 cm^{-1} indicates CH_3 asymmetric deformation, and peaks at 1,389 cm^{-1} and 1,369 cm^{-1} follow $C(CH_3)_2$ symmetric deformation. Additional absorption at 1,173 cm^{-1} and 1,130 cm^{-1} points to CH_3 vibrations. Higher energy peaks at 3,426 cm^{-1}, 3,310 cm^{-1}, and 3,059 cm^{-1} mark N-H stretching while those at 2,970 cm^{-1}, 2,936 cm^{-1}, and 2,874 cm^{-1} represent C-H asymmetric and symmetric stretching.[155] Notably, the $CH=CH_2$ stretching, twisting, and wagging peaks at 1,620 cm^{-1}, 988 cm^{-1}, and 964 cm^{-1} for NIPAM and 1,624 cm^{-1}, 991 cm^{-1}, and 964 cm^{-1} for MBA, respectively, are absent from the polymer's spectrum.[156]

The shallow polymer peak at 980 cm^{-1} could suggest C=C bending, but the signal is below the range typically attributed to monosubstituted alkenes and is too low to decisively distinguish from noise. Altogether, the spectra provide evidence of polymerization incorporating NIPAM and MBA accompanied by appropriate washing to remove residual monomer.

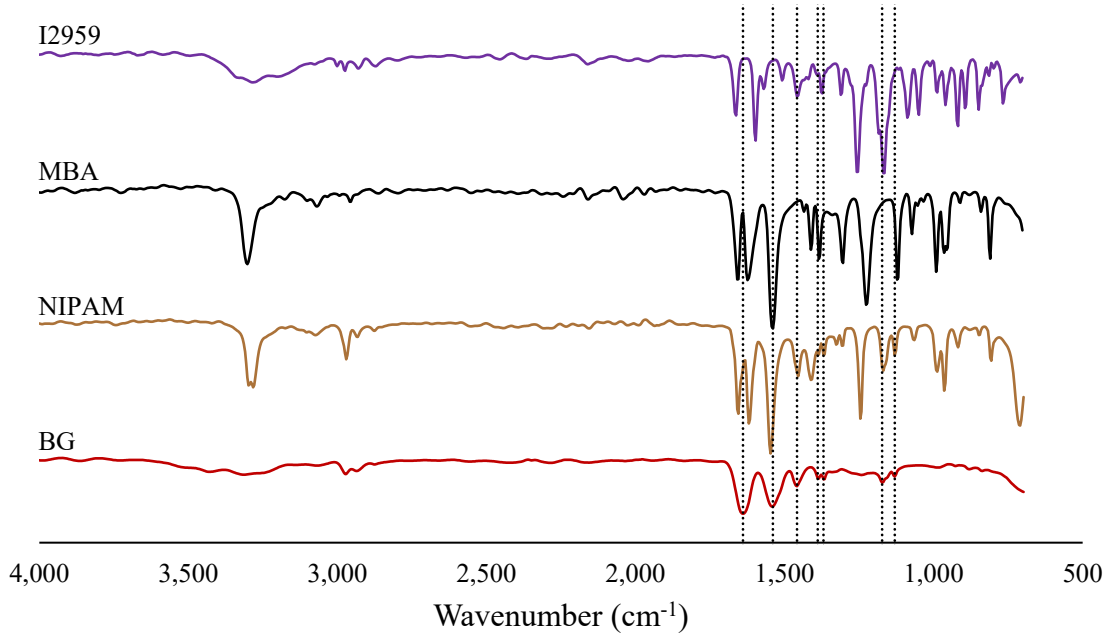

Figure 4.4. FTIR spectra for the photoinitiator (I2959), crosslinker (MBA), bulk monomer (NIPAM), and resulting gel (BG) scanned from 700 cm^{-1} to 4,000 cm^{-1}. Dotted lines correspond to pertinent polymer peaks at 1,639 cm^{-1} (C=O), 1,539 cm^{-1} (CH_3), 1,458 cm^{-1} (CH_3), 1,389 cm^{-1} ($C(CH_3)_2$), 1,369 cm^{-1} ($C(CH_3)_2$), 1,173 cm^{-1} (CH_3), and 1,130 cm^{-1} (CH_3) (from left to right).

4.3.2 Swelling Analysis

Evaluating the impact of hydrotropes (i.e., substances that aid solubilization of hydrophobic compounds by mechanisms other than micellization) and surfactants with known alterations to the LCST of PNIPAM[130] from Figure 4.5, Ph, OA, SOS, and SDS held at a constant 1 mM concentration display negligible changes to the swelling of hydrogels. Likewise, MeOH at an order of magnitude higher concentration does not appear to shift either the swelling or LCST of the system due to variations in solvent

quality. The carboxylic fluorosurfactant PFOA combined with MeOH similarly offers an insignificant swelling deviation. The tetraethylammonium salt of PFOS, TPFOS, on the other hand, exhibits a substantial increase in swelling of up to 65.5 ± 8.8 on a mass basis at 15 °C, far above the 19.3 ± 2.1 swelling ratio for BG in DI water alone. As an estimate of the polymer's LCST in each solution, the temperature at half maximum (THM) from linear interpolation designates PFOA with the lowest value (23.8 ± 0.2 °C) while SDS (24.0 ± 0.3 °C), OA (24.1 ± 0.0 °C), Ph (24.1 ± 0.3 °C), SOS (24.5 ± 0.2 °C), MeOH (24.5 ± 0.3 °C), and water (24.9 ± 0.2 °C) follow closely behind. TPFOS shows a markedly higher THM (40.2 ± 0.8 °C) than other species, but its broad transition from 15 °C to 47.5 °C with a seemingly logistic decay burdens pinpointing the transition's apex. The THM increase for TPFOS in relation to the water baseline (16.2 ± 0.7 °C) demonstrates the capacity of TPFOS to alter the network's swelling and transition behavior more so even than a hydrocarbon surfactant (SDS) with a longer chain length (12 carbons versus 8), more electronegative head group (sulfate versus sulfonate), and similar CMC (8.18 mM[157] versus 0.9-7.5 mM[129, 158, 159]).

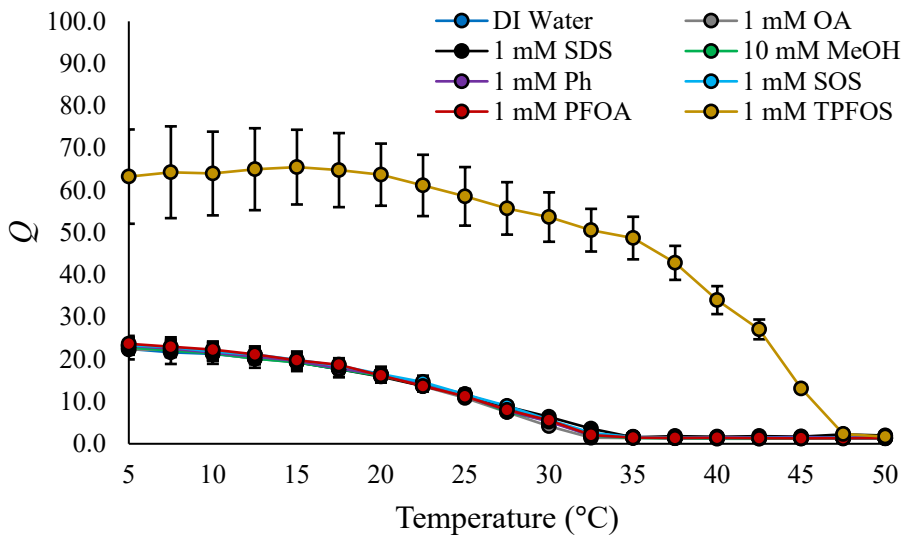

Figure 4.5. The swelling ratio (Q) as a function of temperature for BG in solutions of water (blue), 1 mM OA (gray), 1 mM SDS (black), 10 mM MeOH (green), 1 mM Ph (purple), 1 mM SOS (light blue), 1 mM PFOA with 10 mM MeOH (red), and 1 mM TPFOS (gold). Error bars correspond to a single standard deviation (n = 3).

4.3.3 Fluorimetry

To monitor the local environment of the gels associated with TPFOS, a solvachromatic dye, NR, was introduced to gel and fluorosurfactant mixtures as shown in Figure 4.6. In a relatively polar solvent (e.g., water), the spectra of NR shifts toward a longer wavelength (i.e., red) with a low fluorescence intensity, whereas in a non-polar solvent (e.g., n-heptane) the spectra shifts toward a shorter wavelength (i.e., blue) and its intensity increases dramatically.[160] As a probe, shifts in the peak wavelengths and intensity of the dye provide useful information regarding the behavior of surrounding chemical species in solution. Subject to a BG, the peak emission of NR shows a significant blue shift of 19 nm with a complementary increase in intensity (813 ± 64%), as would be expected for NR deposition along network chains. Together with a BG and TPFOS, the peak intensity further blue shifts by 25 nm relative to NR alone and demonstrates a heightened intensity of 3,261 ± 741%, 468 ± 69%, and 5,068 ± 603% compared to NR with TPFOS, a BG, or alone, respectively. The effects do not appear additive since the cumulative contributions of each component subtracted from the

aggregate intensity of all three components still yields 35,566 a.u., indicating a 79% intensity increase with all three components in solution concurrently. Assuming TPFOS saturates the network, the charge distribution originating from the amide component of NIPAM[151] would be effectively neutralized to meet or be in the proximity of the charge neutralization concentration (CNC), which defines the point of saturation for a polyelectrolyte exposed to surfactant where the net charge of the system is neutralized. Deprived of its charge, the confines of the gel would become more hydrophobic, reducing the network polarity and facilitating the blue shift for NR. Additionally, if surfactant association with the network minimizes the charge delocalization around individual TPFOS molecules caused by the electron withdrawing effect of fluorine atoms[161, 162] and lessens their tails' polarity, then the hydrophobic structure generated as a result of their interaction with the polymer would be reasonably less polar than their micelles formed in solution. Consequently, the gel-fluorosurfactant system would generate a larger blue shift (by 16 nm), as evidenced by the spectral scans in Figure 4.2. The synergism between the fluorosurfactant and polymer to produce hydrophobic zones with lower polarity than their constituents agrees with literature observations for non-crosslinked PNIPAM-SDS systems.[130]

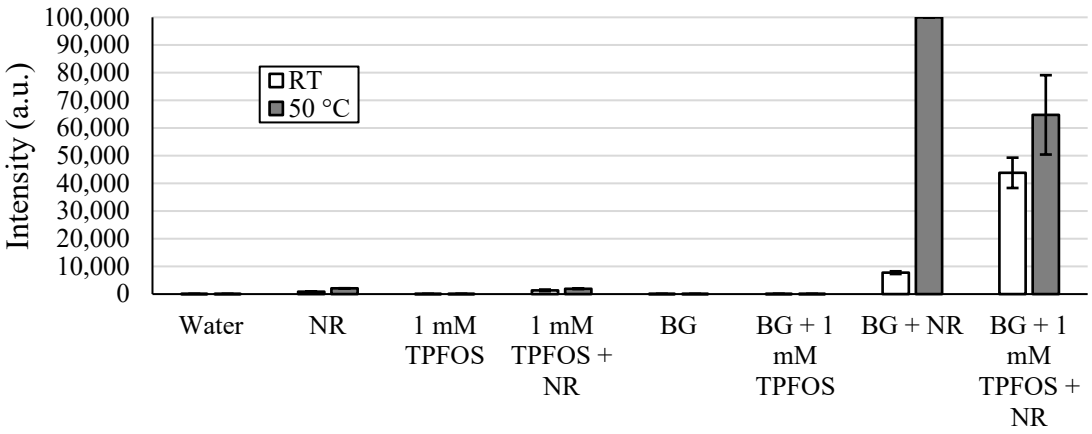

Figure 4.6. Fluorimetry of a BG, 1 μM NR, and 1 mM TPFOS mixtures at room temperature (RT) or 50 °C. Wavelengths for the excitation and emission of water and NR (590/660), 1 mM TPFOS with NR (579/651), a BG with NR and TPFOS without NR (578/641), and a BG with NR and TPFOS (570/635) correspond to the spectral peaks recorded for each fluorescing system in isolation (see Figure 4.2). Error bars represent one standard deviation from the mean (n = 3).

Raising the system's temperature above the LCST for pure and fluorosurfactant-swollen hydrogels compromises hydrophobic hydration for the BG samples,[163] providing a non-polar, dehydrated microenvironment that elevates the intensity of NR above the instrument's detection limit. The slight intensity increase for NR alone (144 ± 12%) is likely due to the reduction in dielectric constant, and, consequently, polarity, for water as a function of temperature, which may also partly contribute to the intensities for each NR system. Gels buffered by TPFOS, however, experience a signal increase relative to room temperature (49 ± 33%) that falls below the rise for the isolated polymer. The shallow increase nonetheless indicates continued association of TPFOS with the polymer above its transition temperature. Previous work by Murase et al.[152] reported lowered adsorption of ionic surfactants above the polymer's LCST with a simultaneous shift toward hydrophobic interactions, partly explaining the intensity increase relative to room temperature by owing partial dissociation of TPFOS from the network that permits greater mediation of the polymer's innate impact on NR. Concurrently, residual bound TPFOS, potentially due to a mix of ionic and hydrophobic interactions, diminishes the

resulting signal compared to BG with NR by preventing unhindered interplay between NR and partially collapsed network chains.

4.3.4 TPFOS Titration Assessment

Surveying the aggregation behavior of TPFOS within the network and the gel's responsiveness as a function of TPFOS concentration, the analyte was titrated, and the polymer's performance was recorded in terms of swelling and NR fluorescence intensity at comparable temperatures. From Figure 4.7 (a), the normalized swelling response at 20 °C shows a significant drop from 1.0 mM TPFOS (4.3 ± 0.4) to 0.5 mM (1.4 ± 0.0) and quickly falls to baseline (1.0 ± 0.1) by 0.25 mM. The intensity measure at room temperature, by contrast, demonstrates a relatively linear response between 0.01 mM (0.9 ± 0.2) and 0.5 mM (4.3 ± 0.2) with an attenuated rise to 1.0 mM (4.9 ± 0.6). Notably, the NR normalization indicates significant association that modifies the microenvironment sufficiently to change local polarization as low as 0.05 mM, possibly indicating the genesis of the CAC, or the point of accumulation at which surfactant-surfactant interplay occurs, for the polymer-fluorosurfactant system. The linear response in the range of 0.05 mM to 0.5 mM might also point to the range for the CAC to CNC transition whereby TPFOS progressively accumulates throughout the network until saturation. Plateauing of the normalized intensity beyond 0.5 mM combined with the drastic increase in normalized swelling ratio over the same concentration could mark the onset of multilayering past the CNC (sketched in Figure 4.8). Interlacing of fluorosurfactant tails within this range might expose the sulfonate head groups of secondary layers to one another along network chains, providing electrostatic repulsion between exterior layers that complements chain rigidification from the initial monolayer. These combined effects would serve to progressively expand the gel as additional TPFOS coalesces with the network, offering little observable change in micropolarity amongst multilayers while enhancing swelling. Altogether, sequencing of the aggregation cascade for TPFOS to the gels presents vital information for the association breakpoints that found the system's sensitivity.

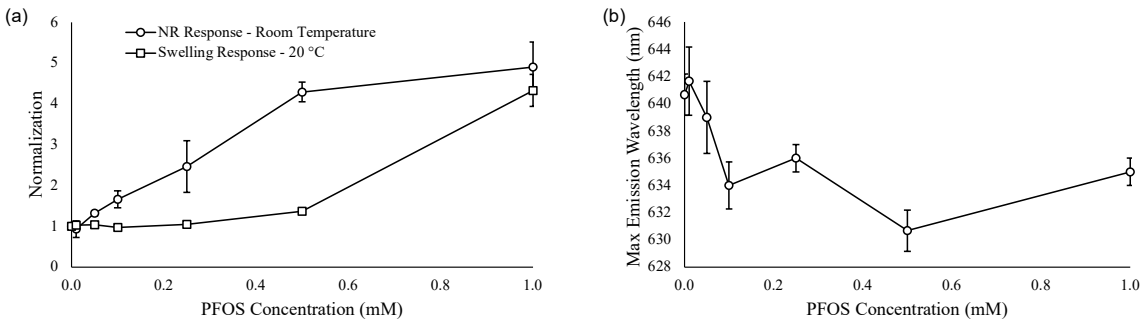

Figure 4.7. (a) Normalized data for the fluorescence intensity of NR in BG at room temperature (circles) compared to the swelling ratios for the same gels at 20 °C (squares) with concentrations of TPFOS between 0 and 1 mM. (b) The peak emission wavelengths for NR in BG excited at 570 nm between the same TPFOS concentrations. Error bars show one standard deviation (n = 3).

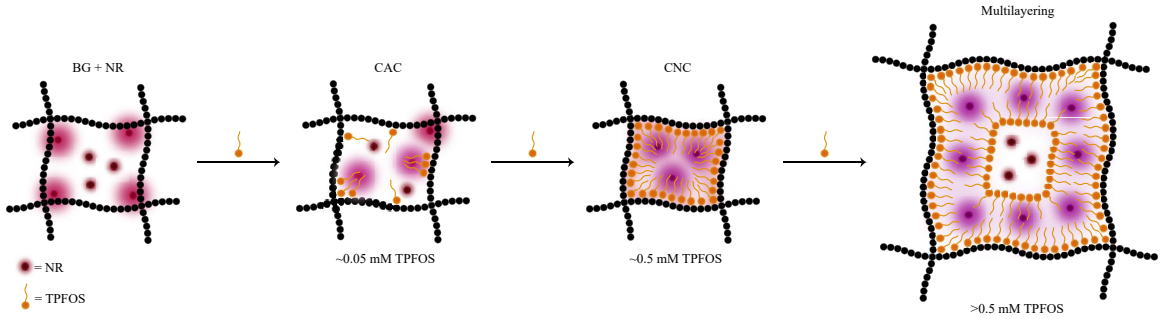

Figure 4.8. Cartoon of NR behavior in contact with polymer chains and TPFOS aggregates. In water, the peak emission of NR red shifts with low intensity; near a chain or fluorosurfactant, the wavelength blue shifts and emits at a higher intensity. The net of these effects defines the dye's observed spectrum.

The peak emission wavelength for the titrated gels excited at 570 nm in Figure 4.7 (b) follows the trend of microenvironmental polarity shifts exhibited by the normalized fluorescence intensity. Although the data contains considerable noise, the maxima downshift from 640.7 ± 1.5 nm to around 636.0 ± 1.0 nm between 0 mM TPFOS to 0.25 mM, similar to the range for the normalized intensity increase in Figure 4.7 (a). Later peaks fluctuate between 630.7 ± 1.5 nm for 0.5 mM and 635.0 ± 1.0 nm for 1.0 mM, possibly an artifact of the measure's imprecision. Nonetheless, the plateau from 0.25 mM to 1.0 mM agrees in large with the general trajectory afforded by the intensity data. The gradual decline in wavelength maxima relates lowered polarity as a result of TPFOS

accumulation within the network; assuming binding or positioning of TPFOS along the polymer backbone depolarizes or shields the amide groups, the linear response of the gel up to saturation, or the CNC, suggests monolayer deposition along network chains in the intermediate aggregation range. Thereafter, assuming NR adjacent to monolayer fluorosurfactant tails experience similar micropolarity to those sandwiched between interlaced multilayers, the spectra of NR would stagnate above the CNC, as evidenced by the leveling of the wavelength pattern. Residual NR left in solvent-rich zones formed by electrostatic repulsion between layers would presumably exhibit similar spectral properties to those outside fluorinated monolayers in the CAC to CNC range, contributing little to the overall intensity observed for the system. Altogether, the peak emission wavelength as a function of TPFOS concentration agrees with the behavior established by the normalized intensity, detailing further the aggregation windows for this polymer-surfactant system.

4.3.5 Electron Microscopy

Imaging the confines of BG samples immersed in a 1 mM TPFOS solution offers a route to observe morphological changes to the gel potentially induced by fluorosurfactant layering or microstructuring within the network. As shown in Figure 4.9, the gel has a lattice structure with a porosity gradient expanding through the sample's depth. Approximately 200 μm below the swollen gel's surface, the pore radius increases from approximately 4 μm to 15 μm to between 10 μm and 40 μm throughout the remainder of the gel's interior. Elemental analysis of these pores from Figure 4.9 (e) appears to map all elemental signatures (S, F, C, O, N) homogeneously without distinguishable aggregation. The lack of clustering from spectral linescans (see Figure 4.10) makes determination of fluorosurfactant binding patterns within the network difficult; the anticipated size scale for TPFOS microstructures is expected to fall in the low nanometer range as shown by Knoblich et al.,[159] which is significantly lower than the resolution used here. Parsing the atomic compositions from EDS, the contributions of sulfur (0.6 ± 0.1%) and fluorine (14.8 ± 0.2%) to the maps estimate PFOS ion to be within 6% to 9% of the species present when balanced against NIPAM and MBA. Consequently, at a 1 mM concentration, each PFOS molecule occupies between 10 and 16 acrylamide

residues. This suggests that, rather than columnated ordering perpendicular to network chains that would follow the string-of-pearls or tubular packing conformation found for SDS[131, 164, 165] and the threadlike micelle structure of TPFOS free in solution,[159, 166, 167] PFOS orients itself acutely to the polymer chains. Alignment in this fashion might partially expose the sulfonate head group to electrostatic repulsion from surrounding deposited PFOS, lending to the significant swelling observed at higher concentrations.

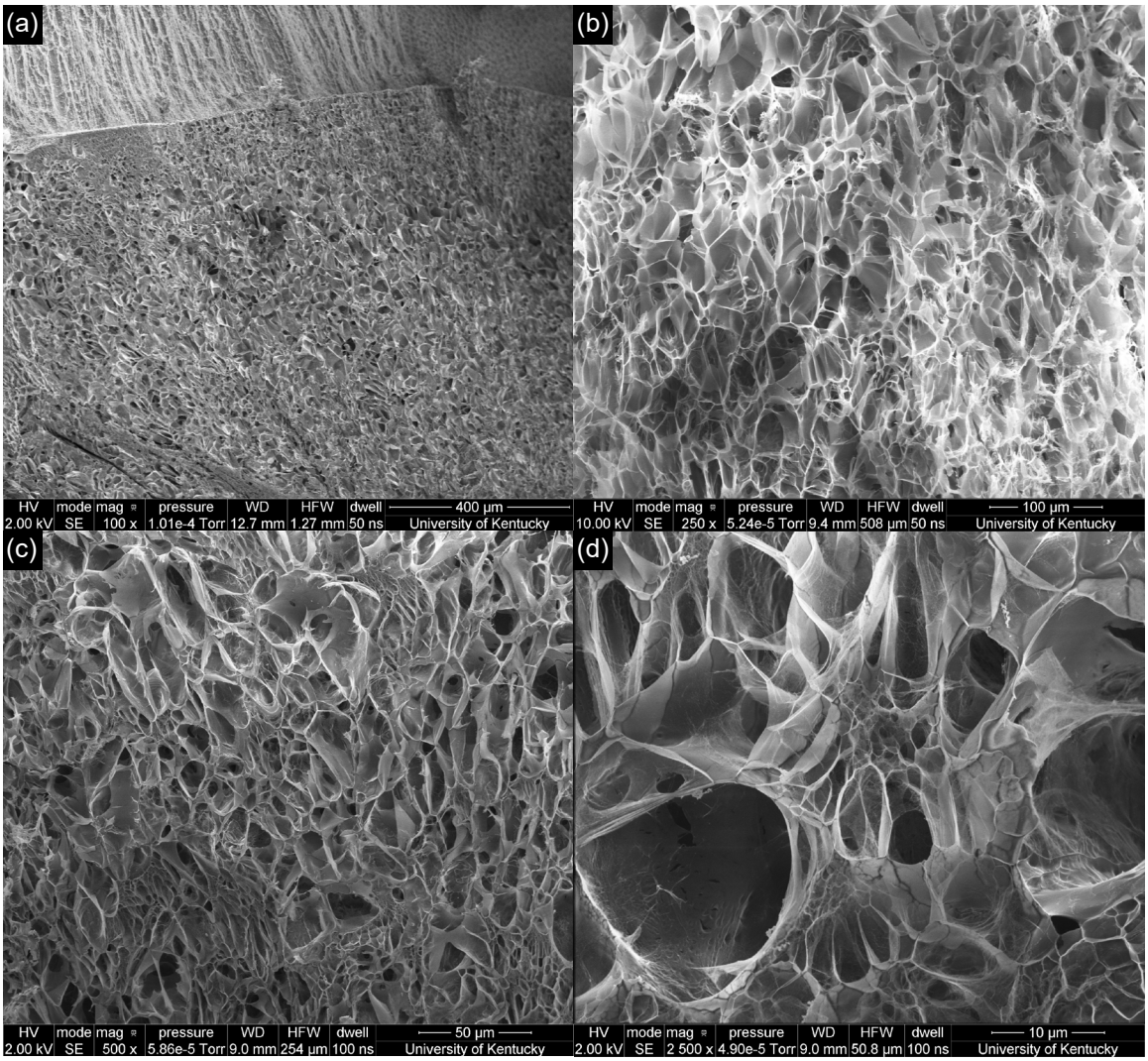
(a)
HV mode mag pressure WD HFW dwell 400 µm
2.00 kV SE 100 x 1.01e-4 Torr 12.7 mm 1.27 mm 50 ns University of Kentucky
(b)
HV mode mag pressure WD HFW dwell 100 µm
10.00 kV SE 250 x 5.24e-5 Torr 9.4 mm 508 µm 50 ns University of Kentucky
(c)
HV mode mag pressure WD HFW dwell 50 µm
2.00 kV SE 500 x 5.86e-5 Torr 9.0 mm 254 µm 100 ns University of Kentucky
(d)
HV mode mag pressure WD HFW dwell 10 µm
2.00 kV SE 2 500 x 4.90e-5 Torr 9.0 mm 50.8 µm 100 ns University of Kentucky

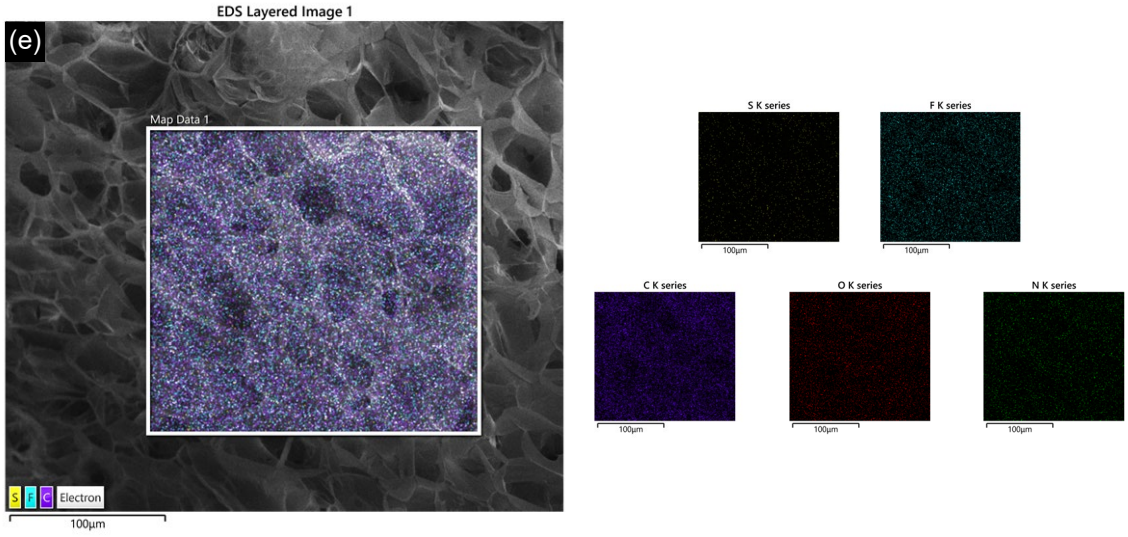
EDS Layered Image 1
(e)
Map Data 1
S F C Electron
100µm
S K series
F K series
C K series
O K series
N K series
100µm

Figure 4.9. SEM and EDS of a BG interior after soaking in 1 mM TPFOS. The upper quartile of (a) shows the surface of a gel followed by pore expansion through its depth. Images (b), (c), and (d) focus on the pore morphology at varying scales. Scale bars for each image correspond to (a) 400 μm, (b) 100 μm, (c) 50 μm, and (d) 10 μm. The EDS map shown in (e) highlights S, F, and C; each elemental signature is shown independently to the right of the map.

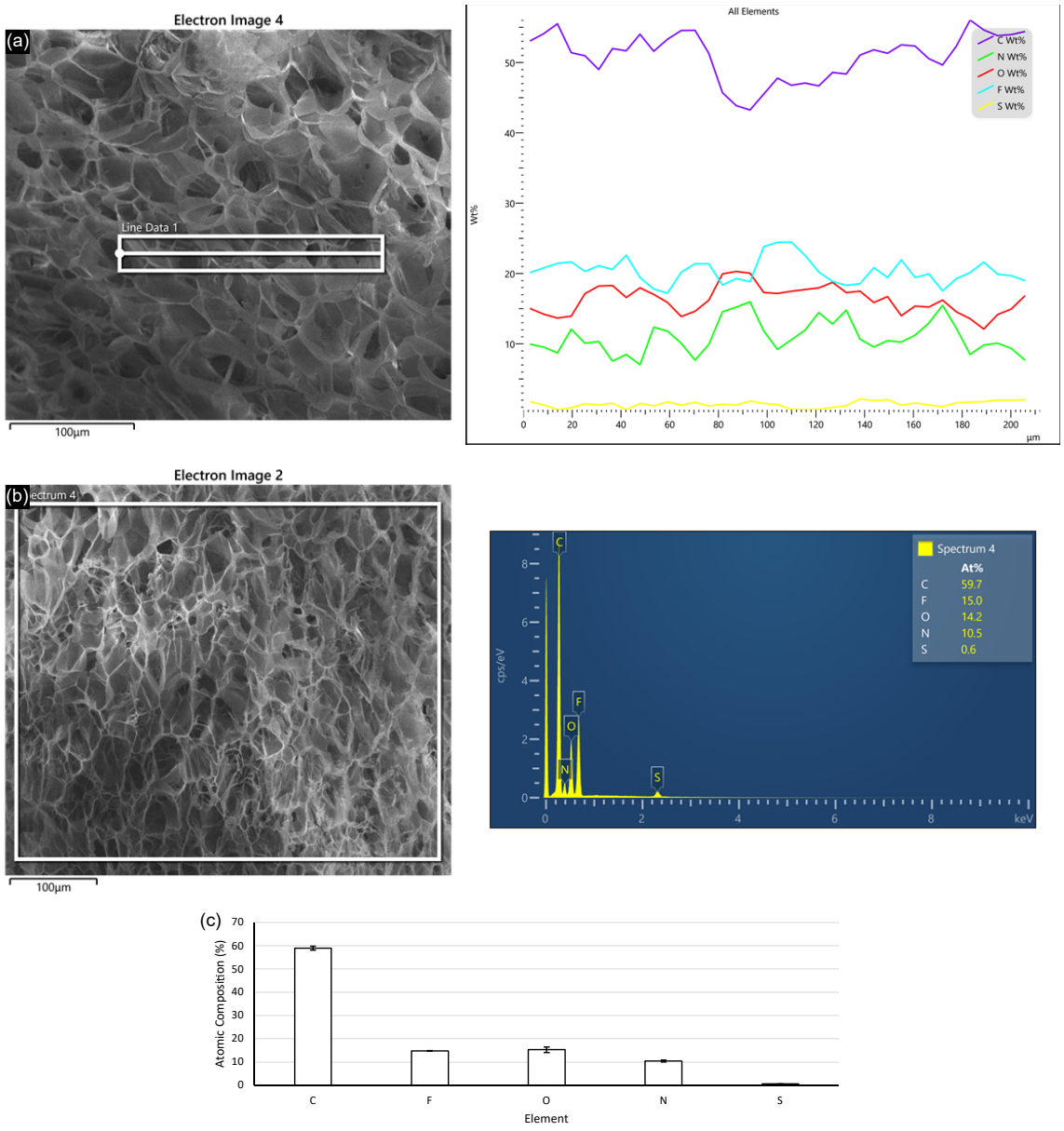

Figure 4.10. Elemental analysis with energy dispersive X-ray spectroscopy. Signal variation from the linescan in (a) does not reveal clustering, but rather a relatively homogeneous elemental distribution across the plane of the gel interior. An example of a spectral map is shown in (b); the average and standard deviation from five maps is displayed in (c). The plot in (a) was relayed with 16x binning.

4.4 Discussion

The remarkable capability of TPFOS to alter the swelling behavior and thermodynamic properties of PNIPAM observed in this study is interesting considering the phenomenon's existence for other non-fluorinated surfactants at higher concentrations. Substantial literature has reported the aggregation behavior of non-fluorinated surfactants with polyelectrolytes, captured succinctly in a recent review by Khan and Brettmann.[131] From their analysis, the accumulation of surfactants within a polymer passes through four distinct stages: direct association via hydrophobicity, electrostatics, or hydrogen bonding, depending upon the properties and charge of the polyelectrolyte and surfactant; buildup of surfactant moieties along the polymer backbone to the point of observable physiochemical change, known as the CAC; saturation of the backbone, or the CNC; and, finally, the stage at which unassociated surfactant forms micelles in the surrounding media, or the CMC. The middle sections of this progression are apparent from the TPFOS titration data presented here, but with stark differences between molecular-level interactions observed from fluorimetry and macroscale network expansion from swelling. SDS, the most extensively studied surfactant with a known impact on the swelling of PNIPAM, typically demonstrates an effect at concentrations nearing its CMC.[149-152] Linear perfluorosurfactants hold CMCs near non-fluorinated surfactants with approximately 1.5 times the number of carbon atoms,[129] suggesting that SDS and TPFOS should have similar responses at the concentrations studied herein. This condition is, however, not the case observed for TPFOS, leaving the source of its disparity in question.

Probing the component characteristics of surfactants, the head group has been shown to heavily influence the phase behavior of polymer-surfactant systems: Sakai et al.[150] previously documented the range of transition temperatures observed for PNIPAM gels with C_{12} surfactant concentrations on the order of 0.1 M, noting that anionic surfactants, particularly those with sulfate heads, displayed the greatest increase in the gel LCST. Sulfonate groups still elevated the transition temperature, but to a lower degree than sulfates. Other head groups (e.g., carboxylic, amine, trimethylammonium, and neutral) had little to no effect on the LCST, and a phosphate head group even reduced the transition temperature at high surfactant concentrations. The study also reported that the

counterion did not play a significant role in the LCST's position. These results then propose that, in light of TPFOS meeting the 1.5 times tail length criterion mentioned earlier, SDS should be more effective at impacting the LCST for PNIPAM. With the opposite holding true in this study, the chemistry of the tail group consequently appears to be the dominant factor regulating the thermodynamic response of the system.

Fluorination of the tail group may enhance perturbation of the phase transition due to the preference for fluorinated groups to position themselves at the interface between oil and water phases: when polyfluoroalkyl surfactants, particularly those with long alkyl chains between a hydrophilic head group and a pendent CF_3, are introduced into solution alone or with a hydrocarbon surfactant above their CMC, the pendent fluorine groups reptate their tails in a manner that aligns the fluorine constituent of their tail at the interface between the hydrophobic portion of the molecule and the surrounding solvent barrier (i.e., adjacent to the head group).[129, 168] This partitioning, driven by interfacial tension rather than classic hydrophobicity, would improve fluorosurfactant association with the polymer hydrocarbon backbone below the LCST. Interaction therefore manifests at lower concentrations than those for alkyl surfactant analogs, as shown by the swelling response at 1 mM for TPFOS compared to SDS and SOS.

The thermodynamic ramifications of the fluorosurfactant on the thermoresponsive polymer are, however, not fully segregated from the surfactant's head group. The carboxylic C_8 perfluorosurfactant tested, PFOA, did not demonstrate considerable impact on the swelling or phase behavior of PNIPAM, potentially due to either weaker acidity (-0.5[169] versus -3.27[170]) or a higher CMC (between 8.7 mM and 10.5 mM)[129, 157, 171] than TPFOS. Regarding acidity, solutions tested were unbuffered, possibly allowing protonation of PFOA that would hamper electrostatic association with PNIPAM and dampen its response to the network. Salt was, however, ineffective at disturbing the swelling response of TPFOS at concentrations permitting solubilization (see Figure 4.11), indicating that suppressing the Debye length of counterions surrounding multilayered fluorosurfactants with hydrophilic head groups exposed[129] did not significantly impede swelling. The non-fluorinated analog to PFOA, OA, displayed greater depression in swelling at 30 °C (by -24 ± 6%, compared to 2 ± 11% for PFOA), but the dip is barely distinguishable from noise and falls far below the extremes presented by TPFOS.

Induction of electrons by the fluorinated tail[161, 162] may even further impede electrostatics between the head group of PFOA and the amide groups of NIPAM, reducing their interaction sufficiently to abolish a notable swelling response. The relatively high solubility of each surfactant apart from TPFOS and PFOA, lending to CMCs of around 80 mM with large variability for OA[157, 172-174] and 0.155 M to 0.162 M for SOS,[157] might also confer symptoms of their apparent inaction. Stable dissolution without impetus to aggregate reduces their association to the polymer network, which, when observing the response at a single concentration, falls outside the range necessary for the surfactants to adequately disrupt the hydrophobic hydration mediating PNIPAM's phase behavior.[163] The CAC for PFOA might nonetheless lie below the concentration used, but, as demonstrated for TPFOS, the impact on swelling from association below the CNC does not appear substantial. The driver for carboxylic surfactants to marginally deswell the network rather than swell as for sulfonate and sulfate surfactants is unclear, as electrostatic binding to the hydrophilic regions of PNIPAM would, initially, be expected to curtail hydrogen bonding to the surrounding solvent and precipitate the network. Evidence for swelling enhancement must consequently result from surfactant-surfactant microstructuring within the network that promotes electrostatic repulsion, as surmised from the fluorimetric and swelling data shown.

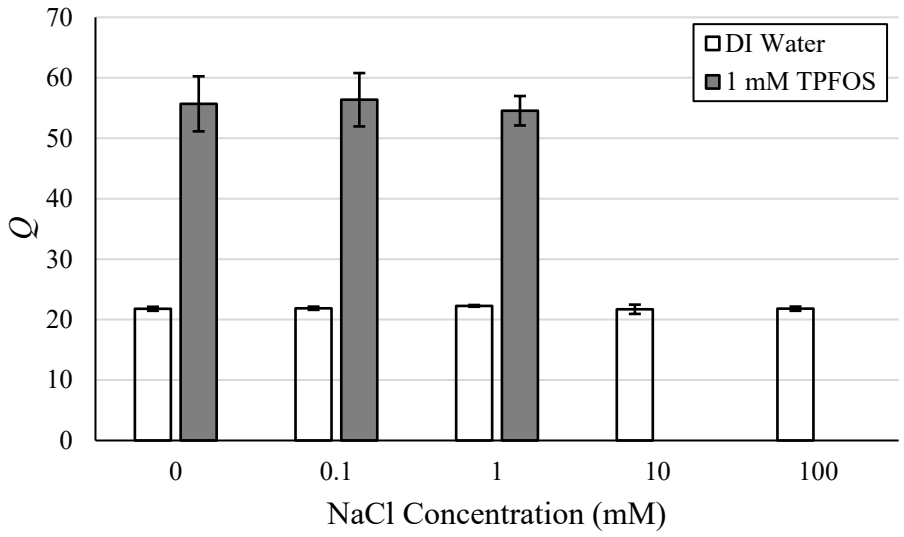

Figure 4.11. The swelling ratio of BG at varying salt concentrations with (gray) or without (transparent) 1 mM TPFOS. Error bars correspond to a single standard deviation ($n = 3$).

Notably, the CMC for perfluorinated sulfonates is heavily dependent on the counterion. Hydrophobic counterions (e.g., tetraethylammonium, the one used in this study) reduce the CMC and Krafft point (the temperature above which concentrated surfactants form micelles in solution rather than mixed crystalline phases) of PFOS significantly below that of hydrophilic counterions (e.g., sodium).[129] The counterion could encourage the molecule's partitioning toward the polymer (i.e., with a relatively hydrophobic counterion) or residence in the solution phase (i.e., with a hydrophilic counterion), but, as reported by the work of Sakai et al.,[150] it should have little overall impact on the polymer-surfactant phase transition. Rapid dissociation of the sulfonate perfluorosurfactant should permit uninterrupted electrostatic association to the network without temporary impediment from counterion neutralization. Once associated, the counterion shell[129] might attenuate further surfactant uptake and coalescence past the CNC (particularly in the case of a bulky counterion like tetraethylammonium), but that phenomenon is not readily discernable from this study.

The other known phase transition modifiers tested did not show significant changes in the swelling or thermoresponsiveness of PNIPAM at the concentrations used here. The hydrotrope examined (i.e., Ph) was likely too dilute to have an effect. In general,

hydrotropes are known to collapse PNIPAM by disrupting the hydration shell around NIPAM and interrupting hydrogen bonding to the surrounding solvent despite not having a CMC.[175] The minimum hydrotrope concentration acts in a similar manner to describe solubilization improvement beyond certain, usually high, concentrations, and the concentration applied herein was below that anticipated for solvation mechanisms and hydrotropy to begin based on those used for other studies.[176] Reduction in the LCST due to solvation (i.e., 10 mM MeOH)[163] was also unnoticed, again likely resulting from the low ($5.5 \cdot 10^{-5}$ mol%) concentration tested. Considering these observations together with its peculiarity from other comparable surfactants, TPFOS appears especially suited to alter the thermodynamics of PNIPAM in a manner suitable for detection.

4.5 Conclusions

From the analytes tested in this study, TPFOS shows significant potential to modify the physiochemical behavior of PNIPAM at a concentration two orders of magnitude below its hydrocarbon analogs. This behavior is unexpected with respect to its structure; hydrocarbons with longer chains (i.e., SDS, C_{12} versus C_8) and more electronegative head groups (sulfate versus sulfonate) show imperceptible changes in hydrogel swelling capacity at a 1 mM concentration when compared to TPFOS. Fluorination, consequently, imparts unique capabilities for fluorosurfactants to affect responsive polymers, potentially due to either relatively enhanced hydrophobicity, greater preference for interfacial separation, or charge delocalization. Homogeneity of fluorine distribution throughout the network once swollen by TPFOS indicates that the fluorosurfactant layers itself rather than coalescing into discrete micellar structures within the polymer matrix. Resolute descriptions of the layering regime and the mechanisms of aggregation remain unknown for this particular system. The focus of future studies will simultaneously attempt to probe the propensity of fluorosurfactant absorption and increase the polymer's receptivity toward its target by functionalizing with favorable comonomers. Emphasis on reducing the CAC for this polymer-fluorosurfactant system below the 0.05 mM threshold observed here constitutes the gateway for translating this system or variants thereof into a simplistic detection scheme for fluorosurfactant pollutants.

CHAPTER 5. LEVERAGING THE THERMORESPONSIVENESS OF FLUORINATED POLY(*N*-ISOPROPYLACRYLAMIDE) COPOLYMERS AS A SENSING TOOL FOR PERFLUOROOCTANE SULFONATE

5.1 Introduction

As a way to tune the PNIPAM's swelling to PFOS, the addition of fluorinated comonomers into the polymer network was hypothesized to result in fluorine-fluorine attraction and reduce interaction with non-fluorinated analytes. Together, these contributions along with the weak polyelectrolytic character of PNIPAM would augment the gels' swelling response by lowering the concentration at which fluorosurfactants associate with the network and, consequently, destabilize the hydration shell surrounding PNIPAM or accelerate multilayering with electrostatic repulsion. Perturbations resulting from these phenomena relative to non-fluorinated analogs potentially offer a route for lowering the detection limits of systems employing these gels. To test this hypothesis, three fluorinated comonomers representing different structural arrangements, a pendent trifluoro group (2,2,2-trifluoroethyl acrylate, TFEA), a C_7 fluorinated chain (1*H*,1*H*,7*H*-dodecafluoroheptyl acrylate, DFHA), and branching (1,1,1,3,3,3-hexafluoroisopropyl acrylate, HFIA), were selected for copolymerization. Assessing the incorporation of the fluorinated groups into the polymer backbone along with the swelling behavior of each copolymer provides the basis for identifying an optimal copolymer designed for fluorinated analytes that will constitute the groundwork for improving forthcoming polymeric strategies for addressing contamination from perfluorinated chemicals.

5.2 Methods

5.2.1 Materials

Unless noted otherwise, all reagents were used as received without further purification. Monomers used throughout the syntheses were *N*-isopropylacrylamide (NIPAM, Sigma, 97%), 2,2,2-trifluoroethyl acrylate (TFEA, TCI, 98%, stabilized with 4-methoxyphenol), 1*H*,1*H*,7*H*-dodecafluoroheptyl acrylate (DFHA, Alfa, 97%, stabilized with 50 ppm 4-methoxyphenol), and 1,1,1,3,3,3-hexafluoroisopropyl acrylate (HFIA, Matrix, 99%). Gels were crosslinked with *N*,*N'*-methylenebis(acrylamide) (MBA,

Sigma, 99%) and synthesized using the free radical photoinitiator 2-hydroxy-4'-(2-hydroxyethoxy)-2-methylpropiophenone (I2959, TCI, 98%). Phenol (Ph, Fluka, 99%), octanoic acid (OA, Alfa, 98%), methanol (MeOH, Pharmco, HPLC-UV grade), sodium dodecyl sulfate (SDS, VWR Chemicals, biotechnology grade), sodium octyl sulfonate (SOS, TCI, 98%), perfluorooctanoic acid (PFOA, TCI, 98%), tetraethylammonium perfluorooctane sulfonate (TPFOS, BeanTown Chemical, 98%), and potassium perfluorobutane-1-sulfonate (PFBS, Sigma, synthesis grade) were used as analytes for swelling tests. Dimethyl sulfoxide (DMSO, Pharmco, reagent ACS grade), acetone (Pharmco, reagent ACS/USP/NF grade), and deionized (DI) water (1 MΩ) were used as solvents in their respective experiments. Both DMSO and MeOH were stored over 3 Å molecular sieves to minimize residual water. Structures of the various chemicals used are provided in Figure 5.1.

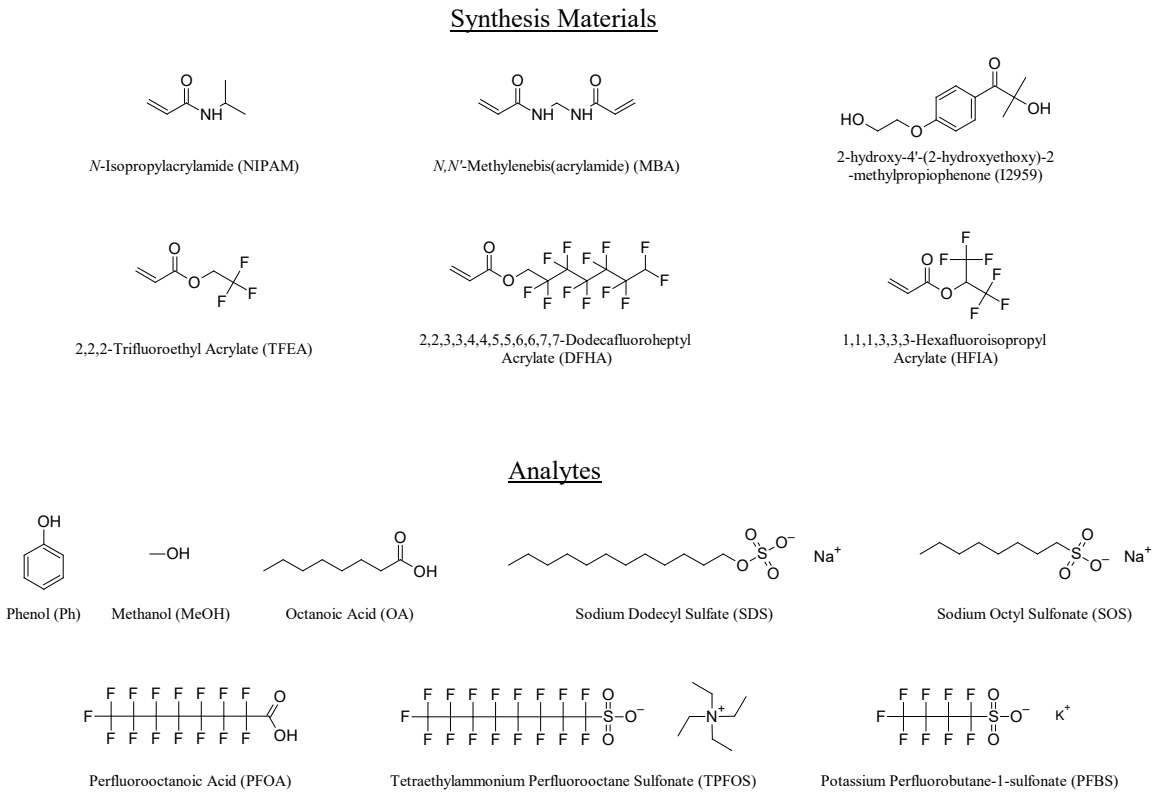

Figure 5.1. Materials used throughout the syntheses of fluorinated PNIPAM copolymers and accompanying swelling tests.

5.2.2 Hydrogel Synthesis

All syntheses were conducted in the manner described previously. Briefly, for a gel synthesized with 5 mol% DFHA, 0.752 mL (0.096 mmol) from a 19.681 mg/mL stock solution of MBA was added to a 20 mL scintillation vial containing 0.430 g (3.803 mmol) of NIPAM and 1.577 mL of anhydrous DMSO. Another 75.32 µL (0.195 mmol) of DFHA was injected followed by 0.175 mL (0.037 mmol) from a 47.951 mg/mL stock solution of I2959. The solution was mixed, inserted between glass sheets separated by a 0.51 mm thick polypropylene spacer, and cured with UV light at 5.00 mW/cm^2 for 1 h. The set gel was transferred to a jar holding 200 mL DI water and soaked for 2 h under 50 rpm shaking. The water was replaced with fresh water and the cycle repeated for a total of five washes. Washed hydrogels were portioned into disks with a 6.95 mm punch and lyophilized. Gels synthesized with ≥10 mol% TFEA were soaked in acetone for approximately 1 min before cutting and disks were air dried overnight prior lyophilizing.

Dry gel disks were then used for subsequent swelling analyses. Conditions used for each gel variant are provided in Table 5.1.

Table 5.1. Gel synthesis conditions and corresponding acronyms for each system. Title acronyms correspond to the component order (Comp.), total monomer concentration (TMC), and initiator concentration (I).

Acronym	Comp. 1	Comp. 2	Comp. 3	mol% 1	mol% 2	mol% 3	TMC (M)	I (mM)
BG	NIPAM	MBA	-	97.539	2.461	-	1.290	12.381
D5.0	NIPAM	MBA	DFHA	92.537	2.461	5.002	1.300	12.470
T2.5	NIPAM	MBA	TFEA	95.039	2.461	2.500	1.300	12.470
T5.0	NIPAM	MBA	TFEA	92.537	2.461	5.002	1.300	12.470
T10.0	NIPAM	MBA	TFEA	87.539	2.461	10.000	1.300	12.470
T12.5	NIPAM	MBA	TFEA	85.039	2.461	12.500	1.300	12.470
T15.0	NIPAM	MBA	TFEA	82.539	2.461	15.000	1.300	12.470
T20.0	NIPAM	MBA	TFEA	77.539	2.461	20.000	1.300	12.470
T35.0	NIPAM	MBA	TFEA	62.539	2.461	35.000	1.300	12.470
H5.0	NIPAM	MBA	HFIA	92.537	2.461	5.002	1.300	12.470

5.2.3 Characterization

FTIR and X-ray photoelectron spectroscopy (XPS) were utilized to check comonomer incorporation in the synthesized gels. ATR-FTIR spectra were collected with a Varian 7000e FT-IR Spectrometer set to a resolution of 8 cm^{-1} co-added over 32 scans at a speed of 5 kHz. Elemental analysis was performed on each gel with a K-Alpha XPS (Thermo Scientific) using a spot size of 400 μm for a binding energy survey from -10 to 1,350 eV with a pass energy of 200 eV. The energy step size was held at 1 eV across 10 scans with a 10 ms dwell time. Two spots on opposite ends of each sample were captured to monitor intrabatch heterogeneity, and data represents the average and standard deviation from the two points for each gel between three gels synthesized identically. Linescans were drawn along the central z-axis of split T35.0 samples with a spot size of 30 μm. Six spots were planted equidistant from one another along the length of the scan, permitting three reflected points for each disk spanning from the thickness's center. Parameters for surveys collected across the line scan were the same as those used for surface surveys.

5.2.4 Swelling Studies

Swelling assessments were conducted similarly to the method used previously. Solutions of 1 mM SDS, SOS, OA, and Ph, 10 mM MeOH, and 1 mM PFOA with 10 mM MeOH were kept at 5 °C in an LKB Bromma 2219 Multitemp II Thermostatic Circulator for 72 h prior to taking their first mass measurement, and subsequent measurements were recorded 24 h after incrementing the bath temperature by 2.5 °C. Gels incubated with TPFOS other than T20.0 were initially equilibrated for 1,128 h before their first measurement. T20.0 samples were held for 1,656 h (see Figure 5.2). TPFOS samples followed the same 24 h equilibration between temperature ramps as for the other analytes. Titration samples were initially held at 20 °C for 16 h before data collection, and 24 h was allotted before recording after ramping the temperature to 35 °C and 45 °C. Kinetic analyses were maintained at 5 °C throughout their duration.

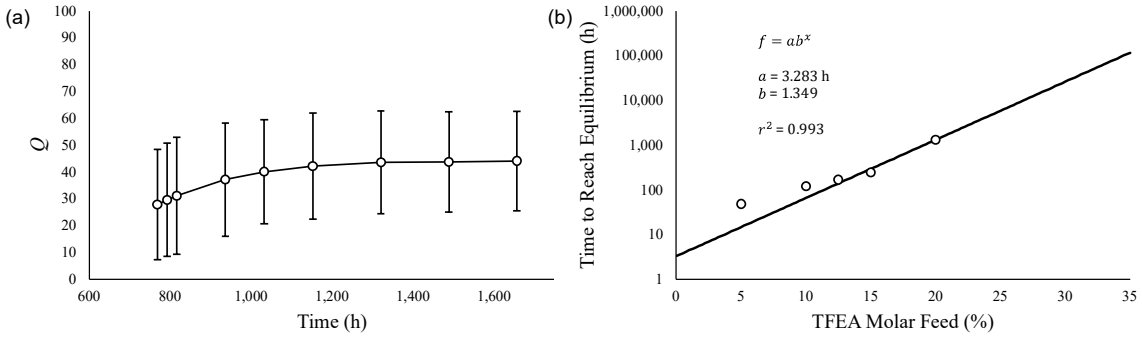

Figure 5.2. (a) Kinetic swelling analysis of T20.0 gels soaked in 1 mM tetraethylammonium perfluorooctane sulfonate. (b) Plotted equilibration times from (a) and Figure 3 (a) fit logarithmically. Swelling ratios in (a) represent a single standard deviation for n = 3 gels.

Swelling ratios (Q) were calculated from the initial dry disk mass (m_i) and the swollen mass (m_s) at a specific temperature following $Q = m_s/m_i$. The water-analyte swelling difference (σ) for a given gel was determined from the swelling ratio of the hydrogel exposed to a given concentration of analyte at a specified temperature (Q_A) compared to its swelling ratio in water at the same temperature (Q_W) with $\sigma = (Q_A - Q_W)/Q_W \cdot 100\%$. Normalized area under the curve (AUC) was computed using the trapezoidal rule for each point along the σ curve between 5 °C and 50 °C referenced

against the BG AUC. LCST estimates were drawn from linear interpolation of the temperature at which half the sum of the maximum and minimum swelling ratio lies.

5.3 Results

5.3.1 Synthesis & Characterization

Fluorinated comonomers were successfully incorporated into the backbone of PNIPAM hydrogels by formulating the syntheses in an organic solvent (DMSO) suitable for all monomers (NIPAM, MBA, DFHA, TFEA, and HFIA) and the initiator (I2959) used. Gels with high fluorine content (≥10 mol% TFEA) subject to reswelling in acetone prior to cutting and drying in ambient conditions formed small (roughly 3.25 mm diameter, 0.26 mm thickness), translucent disks, whereas lower fluorine feedstocks that were punched after swelling in water formed larger (about 5.64 mm diameter, 0.52 mm thickness for BG samples), opaque disks with varying diameters and thicknesses, which varied based upon the comonomer used (see Figure 5.3). For polymers generated with the pendent trifluoro group comonomer, characteristic vibrational bands at 1,639 cm^{-1} and 1,539 cm^{-1} (see Figure 5.4) mark the amide I (A1) and amide II peaks for PNIPAM,[154] and the downfield peak at 1,755 cm^{-1} represents the carbonyl signature from TFEA.[156, 177, 178] Shallow peaks at 1,281 cm^{-1} and 976 cm^{-1} correspond to C-F stretching[178] and CF_3 absorption or C-H bending, respectively.[178, 179] The latter band could also be due to $CH{=}CH_2$ wagging,[156] an artifact from water washing highly fluorinated copolymers, but the transmittance relative to the baseline adjacent to the peak at 1,003 cm^{-1} forms a linear relationship ($r^2 = 0.987$) throughout the TFEA molar feed ratios applied. Were the peak due to residual comonomer, significant accrual would be expected at the higher extreme of TFEA feeds in a, perhaps, logarithmic rather than linear fashion. The CF_x absorption from 1,173 cm^{-1} to 1,153 cm^{-1} is readily apparent in each TFEA polymer,[177, 179] and the ratio of this peak to the A1 band from NIPAM (see Figure 5.5) forms a fairly linear relation ($r^2 = 0.943$) across the range of TFEA feed ratios employed.

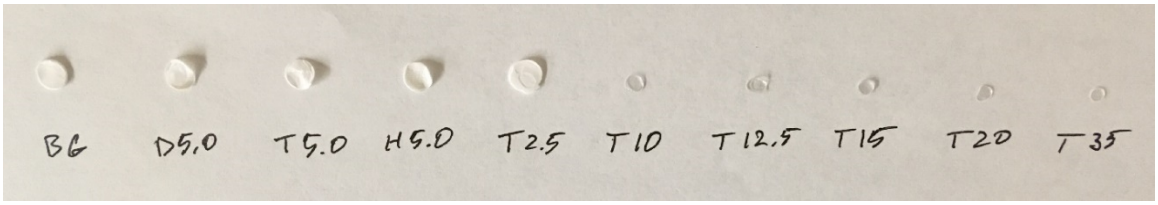

Figure 5.3. Photograph of hydrogels ranging in comonomer type and feed ratio. Acronyms are detailed in Table 5.1.

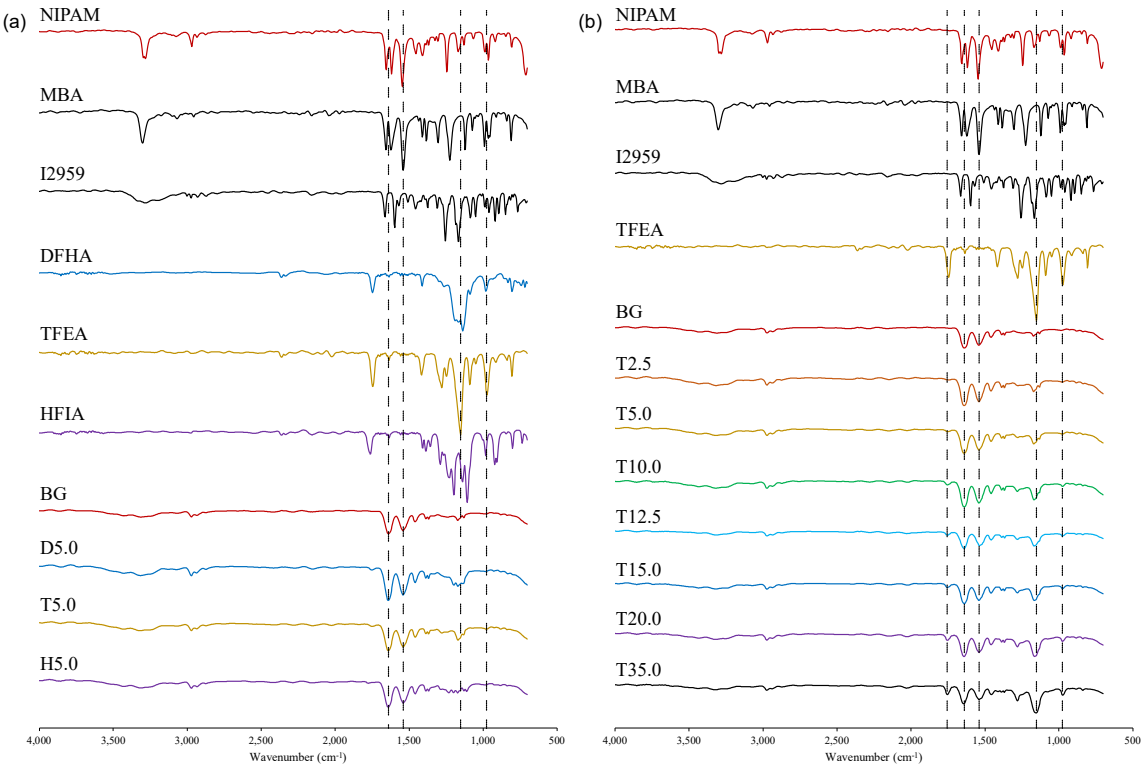

Figure 5.4. Fourier-transform infrared (FTIR) spectra for all monomers and gels used throughout the study. Initial comonomer survey for DFHA, TFEA, and HFIA with their respective hydrogels are provided in (a). Feed ratio incrementation of TFEA is shown in (b). Guidelines correspond to 1,639 cm^{-1}, 1,539 cm^{-1}, 1,153 cm^{-1}, and 976 cm^{-1} in (a) and 1,755 cm^{-1}, 1,639 cm^{-1}, 1,539 cm^{-1}, 1,153 cm^{-1}, and 976 cm^{-1} in (b).

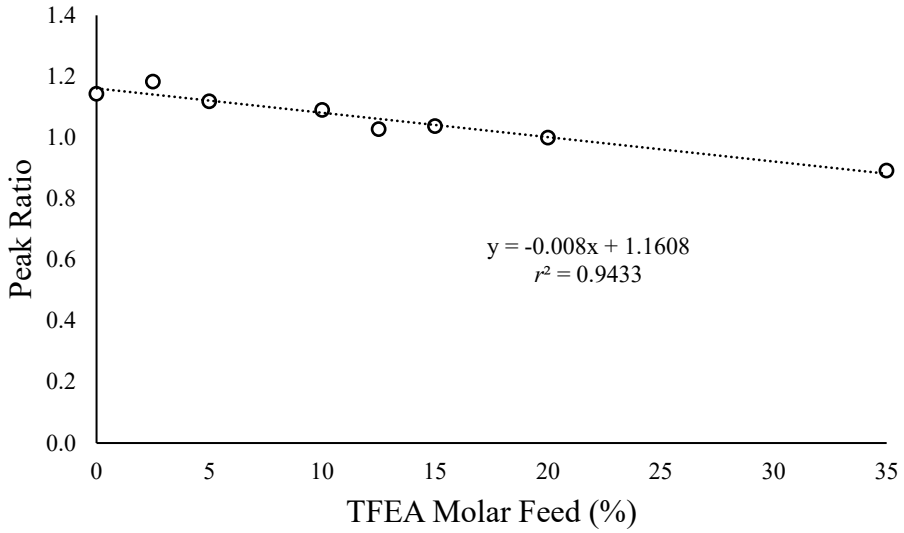

Figure 5.5. Ratio of the CF_x peak transmittance from 1,173cm^{-1} to 1,153 cm^{-1} to the amide I peak at 1,639 cm^{-1} for gels synthesized with varying feed ratios of 2,2,2-trifluoroethyl acrylate (TFEA).

Gels synthesized with DFHA have markedly similar peak distributions to those with TFEA, but with branching of the CF_x absorption band from 1,173 cm^{-1} to 1,153 cm^{-1} into three nearby peaks at 1,200 cm^{-1}, 1,169 cm^{-1}, and 1,134 cm^{-1} assigned to CF_2H, CF_2, and CH_2CF_2 absorptions, respectively. Those with HFIA show even more convoluted fingerprint regions with absorptions at 1,234 cm^{-1}, 1,200 cm^{-1}, 1,173 cm^{-1}, 1,130 cm^{-1}, and 1,111 cm^{-1} due to symmetric (upfield) and asymmetric (downfield) stretching of the branched CF_3 groups. The individuality of each spectrum combined with consistent amide signatures indicates successful copolymerization of NIPAM and each fluorinated comonomer.

Surface elemental analysis from XPS shown in Figure 5.6 (a) confirmed fluorine addition to the networks but with substantial variations from their anticipated theoretical outcomes. Gels synthesized with a 10 mol% TFEA feed displayed the highest surface fluorine deviation (55.1 ± 12.3%) while those with 35 mol% TFEA fell below their anticipated value (-43.2 ± 31.3%). Standard polymers with 5 mol% feeds of DFHA (0.0 ± 24.5%), TFEA (0.0 ± 24.1%), and HFIA (0.0 ± 41.7%) all held closely to their average projected fluorine content but with notably high error. To test whether the relatively

polar, hydrophilic SiO_2 surface of glass caused internalization of TFEA at higher feed concentrations, the depth profile for gels synthesized with a 35 mol% feed was scanned and presented in Figure 5.6 (b). Compared to the low (6.8 ± 3.7%) fluorine composition of their surface, the high TFEA feed gels demonstrated increased fluorine content throughout their depth (from 12.1 ± 1.8% to 13.2 ± 1.6%). Variability along the depth profile remains within error between individual points, but the rise in fluorine content at the gel surface potentially indicates a shallow TFEA concentration gradient at high comonomer feed extremes.

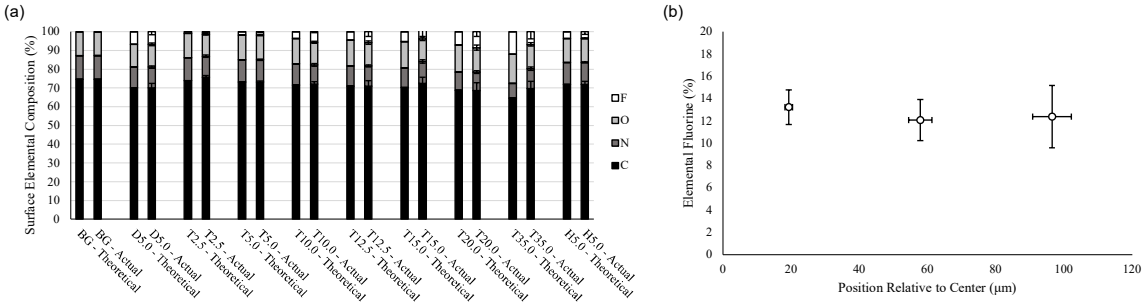

Figure 5.6. Surface elemental analysis for all gels studied (a) and atomic fluorine depth profile for gels synthesized with a 35 mol% TFEA feed (b). Disks examined in (b) had approximate thicknesses of 220 μm. Survey results in (a) show the compositional average and standard deviation for two points of one gel from three batches. Line scans in (b) likewise result from two points scanned across the thickness of a single gel taken from three separate batches.

5.3.2 Swelling Analysis

Building from the high sensitivity of PNIPAM gels toward TPFOS relative to other surfactants and hydrotropes at comparable concentrations explored previously, gels copolymerized with 5 mol% feed DFHA, TFEA, and HFIA were exposed to the same chemical survey to identify whether the addition of fluorinated comonomers to the network would exploit fluorine-fluorine attraction to enhance the network's responsiveness toward fluorinated analytes. Complementing prior observations of augmented swelling in solutions of 1 mM TPFOS, each fluorinated gel exhibited significantly higher swelling in the presence of TPFOS compared to 1 mM solutions of

OA, SDS, Ph, and SOS, a 10 mM solution of MeOH, and a 1 mM solution of PFOA with 10 mM MeOH (see Figure 5.7). Viewing swelling ratios in terms of their difference to a DI water control for each gel (shown in Figure 5.8 (a)), the systems demonstrate maximal swelling differences of 3,201 ± 466%, 3,100 ± 197%, 3,378 ± 173%, and 2,426 ± 284% at 35 °C for BG, D5.0, T5.0, and H5.0, respectively, with TPFOS. Maximal differences are, at best, two orders of magnitude lower for all other analytes tested (see Figure 5.9 for magnification of Figure 5.8 (a)) with T5.0 exposed to SDS showing the highest difference (80 ± 15%) at 25 °C and BG mixed with OA holding the lowest difference (-37 ± 8%) at 32.5 °C. The location of the maximal swelling difference for TPFOS occurs at the temperature step just prior to rapid deswelling, or the onset of swelling change acceleration (see Figure 5.10). Flattening of the water swelling ratio curve for each gel at approximately 32.5 °C is met by relative quiescence of their TPFOS curves, and the abrupt change in TPFOS trajectory thereafter marks the maximum difference for each system. From the four gels tested, T5.0 presents the highest maximum swelling difference of 3,378 ± 173% with an AUC (1.272 ± 0.072) across the temperature range examined bested by only D5.0 (1.491 ± 0.092). Prioritizing maximal sensitivity to the analyte of interest over potential improvement in linearity reflected by a larger AUC, TFEA was selected as the comonomer for further examination.

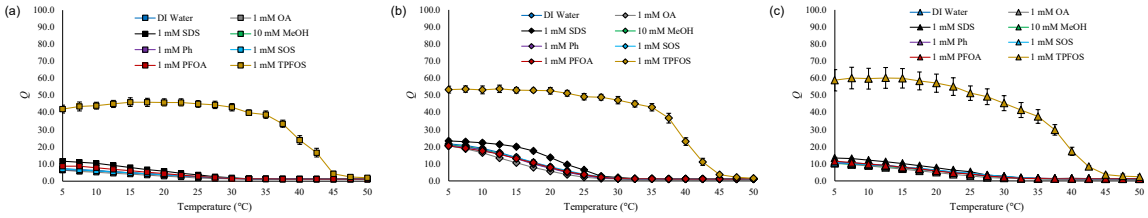

Figure 5.7. Swelling ratios for gels synthesized with 5 mol% feeds of (a) DFHA, (b) TFEA, and (c) HFIA exposed to DI water (dark blue), 1 mM OA (gray), 1 mM SDS (black), 10 mM MeOH (green), 1 mM Ph (purple), 1 mM SOS (light blue), 1 mM PFOA with 10 mM methanol (red), and 1 TPFOS (gold). Error bars represent a single standard deviation for $n = 3$ gels.

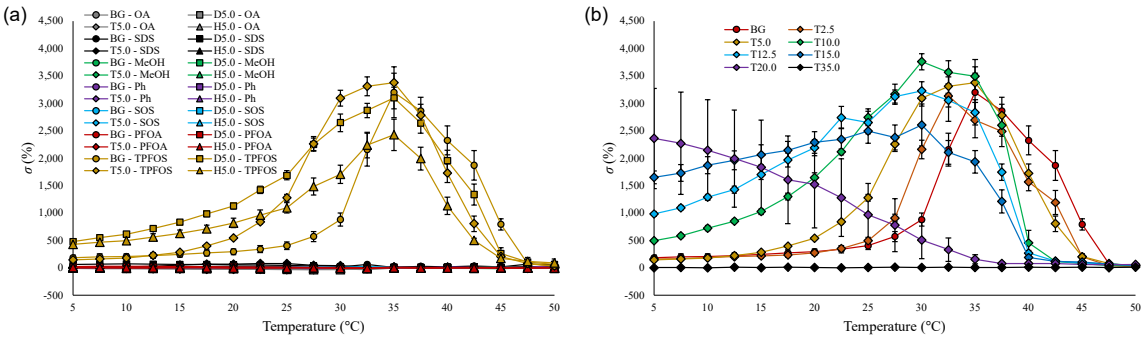

Figure 5.8. Water-analyte swelling differences for (a) gels without a comonomer (BG) and those with 5 mol% comonomer feeds exposed to 1 mM OA (gray), 1 mM SDS (black), 10 mM MeOH (green), 1 mM Ph (purple), 1 mM SOS (light blue), 1 mM PFOA with 10 mM methanol (red), and 1 mM TPFOS (gold) and (b) gels synthesized with varying TFEA feeds soaked in solutions of 1 mM TPFOS. Error bars represent a single standard deviation for $n = 3$ gels.

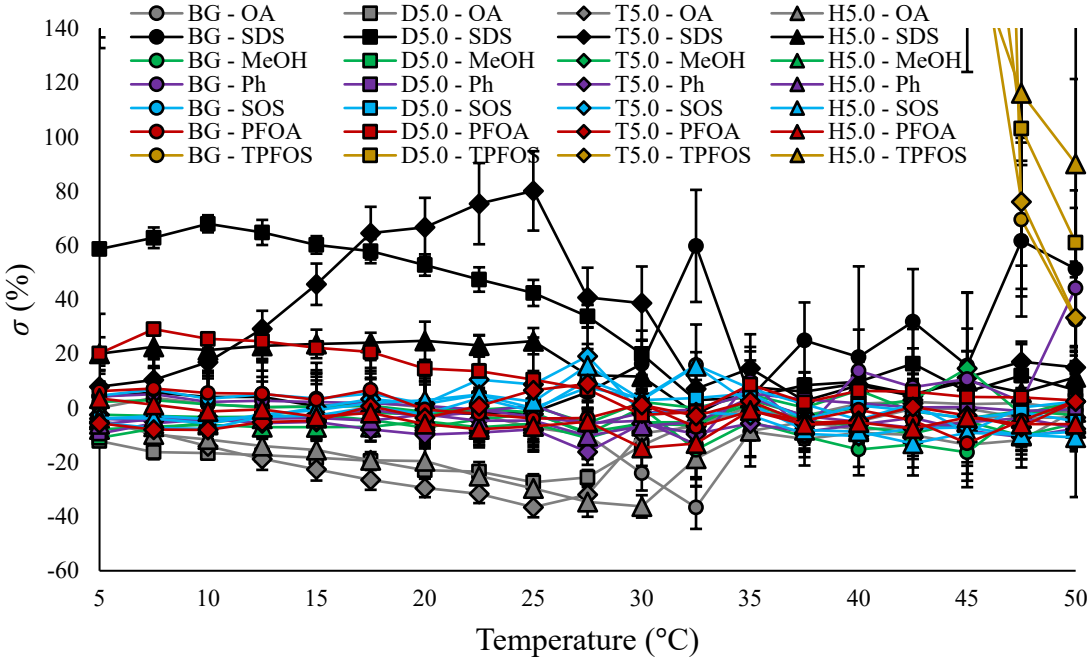

Figure 5.9. Zoomed view of the water-analyte swelling differences for chemicals examined in Figure 5.8 (a). Error bars represent a single standard deviation for $n = 3$ gels.

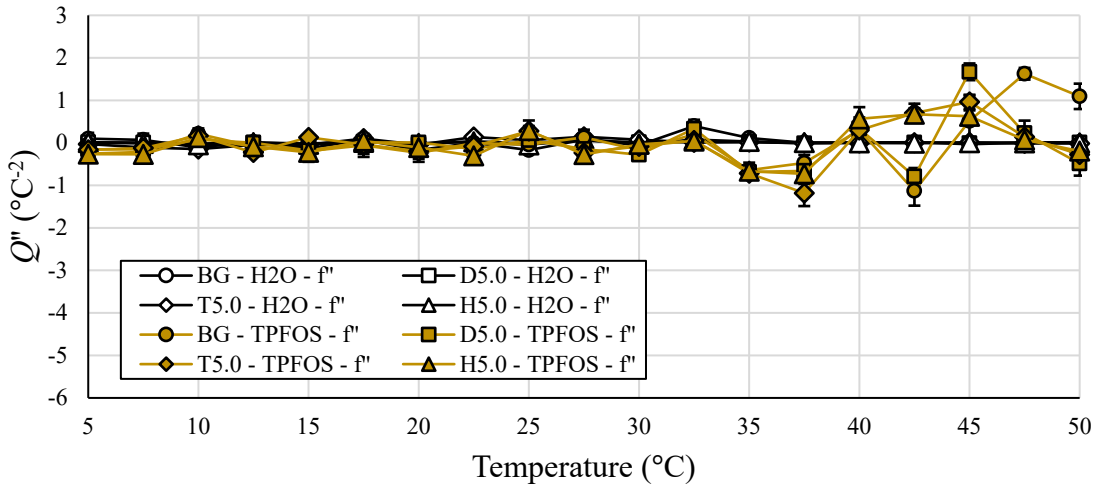

Figure 5.10. Second derivative of the swelling ratio as a function of temperature for gels without (BG, circles) or with 5 mol% feeds of DFHA (D5.0, squares), TFEA (T5.0, diamonds), or HFIA (H5.0, triangles) in DI water (H2O, white) or 1 mM TPFOS (gold). Error bars represent a single standard deviation for $n = 3$ gels.

Testing the influence of TPFOS specifically, gels with TFEA feeds ranging from 2.5 mol% to 35 mol% were subject to 1 mM concentrations of the analyte and the resulting differences (derived from the swelling ratios in Figure 5.11) are reported in Figure 5.8 (b). Slight alterations in the feed ratio of TFEA caused significant changes in both the maximum swelling difference of the gel, the position of maximal difference, and the TPFOS-induced AUC from 5 °C to 50 °C, all of which are recorded in Table 5.2. Increasing the TFEA feed composition from 5 mol% to 10 mol% raised the maximum difference to 3,761 ± 147% with a 5 °C drop in its temperature location, and the AUC accompanying the change (1.679 ± 0.094) was outcompeted only by furthering the feed to 12.5 mol% (1.772 ± 0.094). Fitting and normalizing trends for the maximum swelling ratio difference and the AUC across the composition range used, optima between the two parameters were found at TFEA feed concentrations of 10.7 mol% and 16.2 mol% (see Figure 5.12). The latter of the two compositions has lower extremes for both parameters, leading the former as the optimum TFEA composition for TPFOS sensitivity.

Table 5.2. List of the THM swelling ratios (LCST) in water and in 1 mM TPFOS, their corresponding difference, and the AUC, maximum, and temperature at which the maximum occurs for the water-analyte swelling difference of each gel used in this study. Error represents a single standard deviation for $n = 3$ samples where applicable.

	H_2O LCST (°C)	TPFOS LCST (°C)	LCST Rise (°C)	Normalized AUC	Max σ (%)	Max σ Temp. (°C)
BG	24.9 ± 0.2	40.2 ± 0.8	15.3 ± 0.7	1.000 ± 0.123	3,201 ± 466	35.0
D5.0	17.6 ± 0.2	40.0 ± 0.4	22.4 ± 0.4	1.491 ± 0.092	3,100 ± 197	35.0
T2.5	22.6 ± 0.1	39.7 ± 0.5	17.2 ± 0.4	0.977 ± 0.110	3,137 ± 466	32.5
T5.0	16.9 ± 0.1	39.1 ± 0.2	22.2 ± 0.2	1.272 ± 0.072	3,378 ± 173	35.0
T10.0	14.4 ± 0.1	37.6 ± 0.1	23.2 ± 0.1	1.679 ± 0.094	3,761 ± 147	30.0
T12.5	15.6 ± 0.4	35.9 ± 0.2	20.3 ± 0.4	1.772 ± 0.094	3,227 ± 166	30.0
T15.0	21.7 ± 0.9	32.4 ± 0.3	10.7 ± 0.8	1.674 ± 0.159	2,605 ± 381	30.0
T20.0	N/A	21.5 ± 3.2	N/A	0.997 ± 0.478	2,360 ± 916	5.0
T35.0	N/A	N/A	N/A	0.007 ± 0.008	12 ± 12	12.5
H5.0	20.0 ± 0.7	37.0 ± 0.3	17.0 ± 0.7	1.044 ± 0.095	2,426 ± 284	35.0

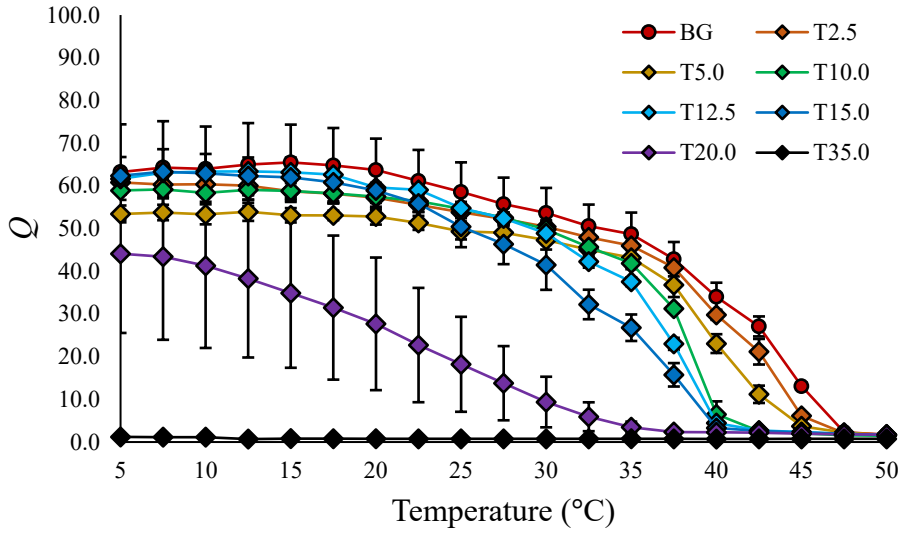

Figure 5.11. Swelling ratios for gels formed without (BG) or with varying concentrations of TFEA exposed to 1 mM TPFOS. Error bars represent a single standard deviation for $n = 3$ gels.

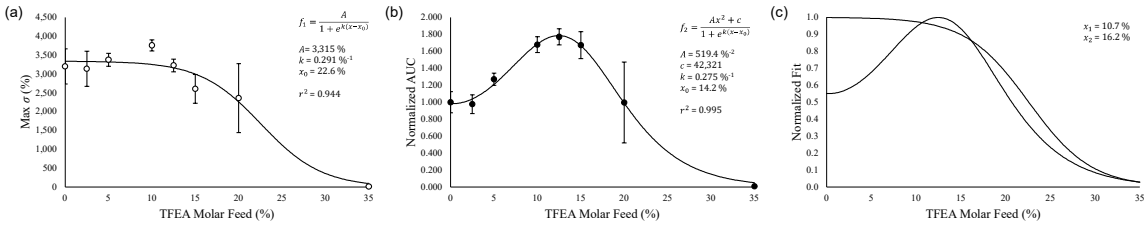

Figure 5.12. Plotted (a) maximum water-analyte swelling differences and (b) AUC for gels synthesized with varying feed ratios of TFEA soaked in 1 mM TPFOS. Data in (a) was fit logistically; data in (b) was fit with an empirical adaptation of the logistic fit in (a). Normalized fits were compared in (c) to award intersections at 10.7 mol% and 16.2 mol% TFEA feeds. Error bars in (a) and (b) represent a single standard deviation for n = 3 gels.

5.3.3 TPFOS Swelling Kinetics

Albeit useful for enhancing the polymer's responsiveness toward PFOS, raising the fluorine composition of gels could introduce unwanted diffusion limitations by increasing the innate hydrophobicity of the gels or restricting binding to surface adsorption rather than thorough absorption. To monitor potential restriction of analyte perfusion through the network, swelling kinetics of gels synthesized with 5 mol% to 15 mol% TFEA feeds were collected up to a sequential deviation of less than 1%. Equilibration times in 1 mM TPFOS solutions, marked in Figure 5.13 (a), display elongation from 48 h for T5.0 up to 244 h for T15.0. Fluorine-fluorine attraction and complementary hydrophobicity brought on by heightened TFEA content initially compress the network, impeding uptake of bulky PFOS molecules. Fluorosurfactant binding to the periphery of the gel in the manner detailed by Kokufuta et al.[180] accompanied by multilayered repulsion in the same region hypothesized in our previous study lends to progressive network expansion that lengthens the equilibration time as the fluorine content of the gel increases. The curvature of the T15.0 gels expresses this phenomenon the most clearly: initially, water penetrates the network with little resistance. As PFOS binds to the rim of the gel and complexes, swelling facilitates further fluorosurfactant penetration towards the interior. The inflection between 72 h and 96 h likely indicates complete network saturation bolstered by subsequent multilayering. Increasing the TFEA feed concentration beyond 15 mol% serves to extend the time to

1,320 h for a 20 mol% gel (see Figure 5.2), following a logarithmic trend (r^2 = 0.993) across the feed compositions tested.

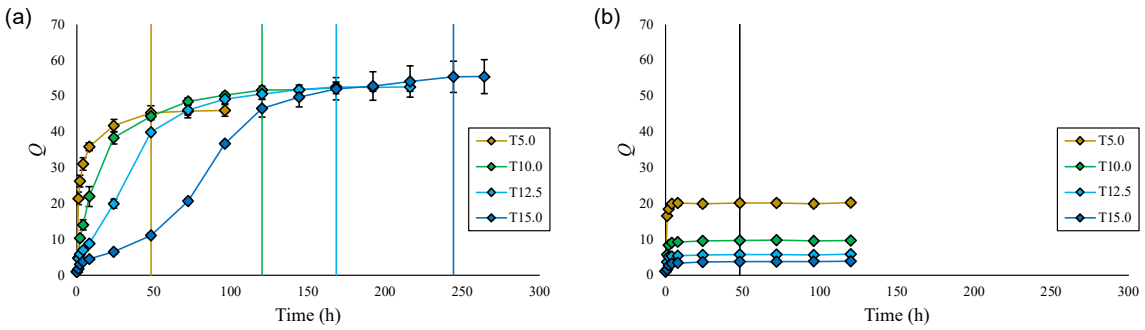

Figure 5.13. Swelling ratios for TFEA copolymers soaked in (a) 1 mM TPFOS and (b) 1 mM PFBS solutions at 5 °C. Dashed lines are meant to guide the eye to the equilibrium time (<1% deviation) for each system. Error bars represent the standard deviation for n = 3 gels.

If the diffusivity reduction was caused by initial network compression from fluorinated comonomers, analytes with lower molecular volume might breach the matrix more easily and accelerate swelling. Investigating this hypothesis, kinetics for PFBS, the four-carbon analog to PFOS currently used as an industry alternative, under the same concentration as TPFOS were monitored as shown in Figure 5.13 (b). Interestingly, the equilibrium swelling ratio for each gel after 48 h (20.2 ± 0.8 for T5.0, 9.6 ± 0.2 for T10.0, 5.8 ± 0.2 for T12.5, and 3.8 ± 0.2 for T15.0) is negligibly different from their swelling in water alone (21.7 ± 0.5 for T5.0, 9.9 ± 0.2 for T10.0, 5.7 ± 0.2 for T12.5, and 3.6 ± 0.1 for T15.0), suggesting that PFBS does not have an appreciable effect on the swelling or LCST of the gels. The relatively short tail length for PFBS raises its CMC significantly to 0.148 M[181] relative to 1.1-7.5 mM for TPFOS[129, 158] which, by raising its suitability for an aqueous environment, reflects lowered association to PNIPAM chains. Following the general rule for fluorosurfactants holding aggregation properties similar to hydrocarbon surfactants with 1.5 times longer carbon tails,[129] the four-carbon PFBS would be expected to mirror C_6 alkyl surfactants that have no discernable effect on the transition temperature of PNIPAM at concentrations two orders of magnitude larger than those used here.[150] Shortening the tail length enhances the contribution of the hydrophilic head group to the surfactant, placing PFBS as a relatively hydrophilic molecule that presents lower

partitioning to the gel than PFOS. These results agree with the attenuation of LCST perturbation at lowered tail lengths reported for non-fluorinated anionic surfactants,[148, 150] but they do little to reconcile the mechanism behind elongated swelling kinetics for these gels.

5.3.4 TPFOS Titration Assessment

Assessing the influence of TFEA composition over the polymer dose-response behavior to TPFOS, T12.5 gels in Figure 5.14 demonstrate only slight normalized swelling loss between 1.0 mM TPFOS (1.00 ± 0.02) and 0.5 mM (0.67 ± 0.06) at 20 °C while stagnating below 0.5 mM. The trend is maintained at 35 °C (1.00 ± 0.06 to 0.69 ± 0.06) and eliminated by 45 °C (0.98 ± 0.06 to 0.91 ± 0.07), probably due to the short initial equilibration time (16 h) employed. Response attrition between temperatures below (20 °C) and above (45 °C) the polymer's undisturbed LCST could indicate binding inhibition or a transition to adsorption rather than perfused absorption.[152] T2.5 and T5.0 gels, by contrast, have a linear response between 1.0 mM (1.00 ± 0.07 for T2.5 and T5.0) and 0.25 mM (0.51 ± 0.04 for T2.5, 0.46 ± 0.05 for T5.0) at 20 °C with attenuation below 0.25 mM. BG at the same temperature instead show a sharp decline in normalized swelling from 1.0 mM (1.00 ± 0.09) to 0.5 mM (0.32 ± 0.00) which levels thereafter. At elevated temperatures (i.e., 35 °C and 45 °C), all gels fed with ≤5 mol% TFEA display rapid decay in their response below 0.5 mM, likely due to their collapse at these temperatures which, again, alters uptake from thorough analyte penetration to limited adsorption. Given longer equilibration times, progressive expansion from complexation at the edges of the gel might eventually breach the diffusion barrier set at higher temperatures and allow for absorption into the network's confines, but the conditional variations necessary to explore uptake kinetics as a function of TFEA feed ratio and TPFOS concentration were not investigated here. Overall, relatively small additions of TFEA appear to enhance fluorinated analyte absorption while mitigating diminishing returns from innate polymer collapse and diffusion limitations at higher feed ratios (i.e., >5 mol%).

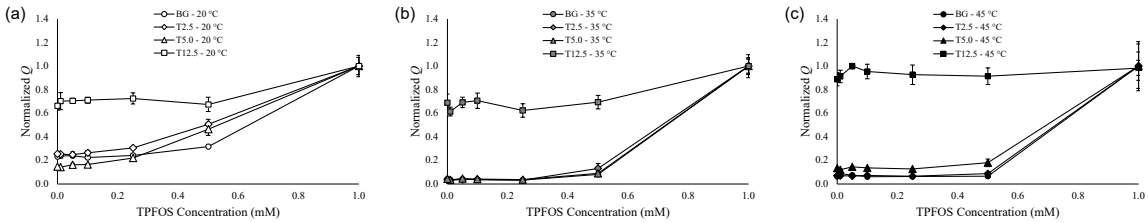

Figure 5.14. Normalized swelling ratios for gels fed with zero (circles), 2.5 mol% (diamonds), 5.0 mol% (triangles), and 12.5 mol% (squares) TFEA exposed to varying concentrations of TPFOS for 16 h at (a) 20 °C, (b) 35 °C, and (c) 45 °C. Error bars represent a single standard deviation from $n = 3$ gels.

5.4 Discussion

Fluorosurfactant-induced polymer swelling is a function of multiple competing weak molecular associations.

Despite showing tunable swelling responses via inclusion of fluorinated comonomers, the mechanisms involved in promoting the interaction of PFAAs to PNIPAM hydrogels remain unclear. Surveying the literature reveals that adsorption strategies for removing PFAS from aqueous samples have previously seen improved retrieval of longer chained fluorinated species (approaching and above C_8) using fluorinated polymers as adsorbents,[182-185] likely due to fluorinated compounds simultaneous hydrophobicity and oleophobicity. Repulsion from water together with weak intermolecular F-F interactions drives association between fluorous analytes and substrates,[186] and tight packing between fluorinated chains stabilizes their attraction despite the electron withdrawing effect of fluorocarbons heightening their electron density.[186, 187] When mixed with hydrocarbon constituents, additional hydrogen bonding and interfacial mechanisms owing to the fluorine groups oleophobicity also become apparent.[129, 186] The same phenomena are likely at play here, but their individual contributions are not easily discerned from the complex fluorocarbon-hydrocarbon copolymers employed in this study. Association discrepancies are likely the result of several disjointed phenomena such as the structure of the fluorine moieties (i.e., pendent CF_3 versus chained CF_2), individual monomer interactions effecting either the void

volume or diffusion resistance within the polymer matrix, the overall maximal swelling capacity and interchain separation of the gel, and the polymer's thermodynamics following lowered NIPAM content in exchange for hydro- and oleophobic comonomers working in unison to attract fluorinated species to the gel. The influence of each potential contributing factor and their relative weight toward the overall observed swelling behavior is convoluted; geometric and chemical properties in the form of molecular weight, composite and individual Van der Waals volume, surface area, solvent-accessible surface area, and component fluorine content for each comonomer did not show strong association (i.e., $r^2 > 0.900$) with the TPFOS-induced maximal swelling difference, swelling ratio, LCST, or LCST shift (data not shown). Suppositions regarding principle contributing factors are surmisable, such as fluorinated moieties stimulating binding or initially compressing the network to accentuate the resultant expansion by TPFOS, but the discrete contributions of each matrix component is complicated by the system's tandem fluorine and thermodynamic responses. Further investigation is necessary to elucidate the affinity of each polymer for fluorosurfactants across the scope of operational temperatures to verify whether the enhanced swelling response is attributable to binding stimulated by fluorinated comonomers or the innate swelling differential between fluorinated and non-fluorinated gels.

The structure of fluorinated pendant chains heavily influence the swelling behavior of their corresponding gels.

Although TFEA was chosen as the primary comonomer for study, the set feed composition (5 mol%) used for initial swelling analyses might have masked optimal feed ratios for DFHA and HFIA. T5.0, in this case, was the only gel that surpassed the maximal swelling difference of BG, but the difference for TFEA gels was further improved by raising the comonomer feed ratio to 10 mol%. Were the trend similar for DFHA and HFIA gels, slight alterations in their feed ratio could potentially improve their sensitivity. Should the limits for both comonomers hide outside of their tested composition, the high AUC for D5.0 in particular could indicate broadening of the response range that could further improve linearity at lower TPFOS concentrations. If the attractiveness of fluorinated comonomers to fluorinated contaminants is a consequence of the gel's atomic composition, DFHA ratios comparable to the TFEA gels

tested would show reasonably higher residues of absorption in the metrics examined. This phenomena would be offset by heightened hydrophobicity and premature gel collapse at the temperature issued, leaving the optimal compositions for alternative comonomers, as for TFEA, a question of balance between maximizing attractiveness in the form of favorable F-F association while minimizing the copolymer's intrinsic repulsion for aqueous environments.

Briefly assuming that comonomers are equally incorporated into their networks, the swelling ratio curves for H5.0 and T10.0 are remarkably similar when exposed to 1.0 mM TPFOS with only slight deviations between 40 °C and 42.5 °C (see Figure 5.7 and Figure 5.11). Comparison of D5.0 and T20.0 curves does, however, reveal considerable difference. Though both curves have similar initial swelling ratios at 5 °C, T20.0 linearly deswells across the temperature sweep, reaching a swelling ratio of 3.47 ± 1.31 by 35 °C while D5.0 demonstrates a rapid decay initiated at 37.5 °C resulting in a deswollen ratio of 4.26 ± 1.44 at 45 °C. If the assumption of equal comonomer incorporation remains serviceable, the TPFOS-induced swelling behavior of the gels would consequently be independent of the gels' total fluorine content. Rather, the structure of the comonomers appears to play a key role in defining their swelling response to TPFOS. Fluctuations in surface fluorine content from XPS in Figure 5.6 show TFEA-copolymerized gels holding higher total fluorine content than their theoretical loading would suggest and higher relative fluorine content than comparable non-TFEA gels. The similarity of the H5.0 and T10.0 curves despite potential deviations in their fluorine content reinforce the importance of the comonomer morphology in determining the influence of TPFOS on the gels' swelling.

Interestingly, the LCST in Table 5.2 for each gel fed with 5 mol% comonomer remains near that of BG (40.2 ± 0.8 °C). For T5.0 (39.1 ± 0.2 °C) and H5.0 (37.0 ± 0.3 °C), their values remain outside a single standard deviation, but still above their LCST in water (22.2 ± 0.2 °C for T5.0, 17.0 ± 0.7 °C for H5.0) by more than that of BG (15.3 ± 0.7 °C). The changes in LCST from 1 mM TPFOS relative to BG are less drastic than swelling differences for D5.0 and T5.0, whereby the TPFOS-induced LCST shift for D5.0 (-0.4 ± 1.9%) pales in comparison to its maximum swelling (-28.8 ± 9.3%) against BG. T5.0 likewise displays a much lower LCST change (-2.6 ± 1.7%) compared to its

swelling ratio (-16.8 ± 10.6%), but H5.0 shows similar deviation between its LCST (-8.0 ± 1.7%) and swelling (-7.0 ± 14.0%). The non-branched systems (i.e., D5.0 and T5.0) appear to have decoupled physical and thermodynamic cues in response to TPFOS, indicating that TFEA and DFHA must exclude a greater amount of water than HFIA without disrupting surfactant binding pathways. The linear structure of DFHA, which is expectedly rigid owing to the shell of fluorine surrounding the carbon chain, mimics the tail of PFOS sufficiently to facilitate compaction amongst adjacent fluorosurfactant molecules during saturation, potentially compressing the network to a greater degree than structurally dissimilar species like TFEA and HFIA. TFEA, with its single carbon atom populated by fluorines, marginally disrupts packing amongst fluorosurfactant tails to permit greater solvent penetration into the network. The ellipsoidal character of HFIA's branched fluorine shell spreads adjacent fluorosurfactants more than TFEA, furthering solvent penetration while encumbering TPFOS alignment. Assuming the surfactant association mechanisms to the matrix (e.g., electrostatics, interfacial separation) are uninterrupted by fluorinated comonomers, the packing of fluorosurfactants absorbed to the network determines the resulting volume available for solvent and, consequently, the resulting swelling ratio for the polymer-surfactant system. This proposal follows in-line with considerations for tightly packed perfluorosulfonates favoring solvent-penetrated cylindrical micelles at high concentrations.[129, 159, 166, 187] In this case, the driving forces behind fluorosurfactant reconfiguration and expulsion at higher temperatures allowing for collapse of the hydrogel would not differ significantly regardless of the comonomer used. The data for low comonomer feed ratios (i.e., ≤5 mol%) agree with this notion while larger fluorinated comonomer feeds become complicated by suppression of the copolymer's thermoresponsive portion, abundant fluorinated comonomer interplay, and innate polymer hydrophobicity that impedes overall swelling.

Detection of PFAAs using flourine-containing thermoresponsive copolymers hinges upon a delicate balance between favorable interactions and suppression of the polymers' temperature responsiveness.

Notably, several barriers remain for the use of fluorinated PNIPAM hydrogels to sense fluorinated analytes, namely: implementing fluorinated comonomers in the network, as discussed earlier, reduces the maximum swelling capacity of the polymer,

significantly prolongs equilibration times due to apparent diffusion limitations, and substitutes NIPAM binding domains for weak fluorine-fluorine attraction. The first two limitations have been detailed extensively thus far; the latter presents a tailorable tool for regulating the physiochemical response of the system. Although NIPAM moieties control the thermodynamic behavior of the gels, inclusion of fluorinated comonomers reduces the LCST for gels precipitously as the feed ratio of comonomer increases, possibly from nearby fluorine constituents disrupting the hydrophobic hydration or clathrate cage around the isopropyl groups of NIPAM. Preconditioned disorder in this domain would fuel entropy-driven demixing[188] and reduce the volume phase transition temperature of the system as this study's data illustrate. On the topic of analyte binding, the weak associations between fluorinated species,[186] likely from attractive van der Waals forces,[187] posts the advantage of reversibility should a hydrogel sensor be reusable but also the disadvantage of inefficacy for trace analysis. The relative strength of fluorine-fluorine association compared to the electrostatic association of fluorosurfactants with weakly polyelectrolytic PNIPAM alone is still unresolved.

From the swelling response of the gels tested, raising the fluorine content of the matrix did not appear to drastically alter the aggregation behavior of the fluorosurfactant to the gels. Employing swelling as a measure for the molecular association of fluorosurfactants to the polymer is, however, a course estimate of the phenomenon. In our previous study, association was found to occur at an order of magnitude lower concentration when monitored fluorimetrically. The initiation of swelling perturbations at 0.25 mM rather than 0.5 mM for T2.5 and T5.0 gels might consequently indicate slight lowering of the interpolated critical aggregation concentration. Additionally, implementing fluorinated comonomers did show changes in the response of gels at the highest TPFOS concentration used, whereby the maximum swelling difference and AUC were raised, granting the method usefulness for designing the breadth of the polymer's response to fluorosurfactants. Further improvements in the form of ionic comonomers could facilitate additional binding to the network via electrostatics that, together with fluorinated comonomers, may enhance the system's receptivity to the analyte of interest in future applications.

5.5 Conclusions

Incorporating fluorinated comonomers into the backbone of PNIPAM hydrogels served to provide a method for tailoring the responsiveness of the gels' swelling response toward fluorosurfactants through a delicate balance of comonomer selection and feed ratio optimization. As a sensing tool, a TFEA comonomer feed of 10.7 mol% was estimated to maximize the water-analyte swelling difference and AUC exhibited by the polymer in the presence of TPFOS from 5 °C to 50 °C. Raising feed ratios of TFEA was shown to broaden the swelling response range for the gels at the expense of reduced overall swelling ratios and exacerbated equilibrium times, opening a window for tuning the network's behavior with small (≤2.5 mol%) changes in comonomer feed ratio. Further, high feed concentrations of TFEA led to internalization of fluorinated monomers within the gel matrix, forwarding the symptoms of elongated equilibration as a consequence of a radially defined diffusion barrier synchronized with the penetration inhibition mechanisms described by Kokufuta et al.[180] Improvement to the system in the form of ionic comonomers used to capitalize on the electroactive head groups of fluorosurfactants in conjunction with fluorinated comonomers to exploit their fluorophilicity presents an avenue for continued honing of the polymer's physiochemical properties as a means to alert the presence of concerning fluorinated analytes.

CHAPTER 6. ASSESSING THE PERFLUOROALKYL ACID-INDUCED SWELLING OF FÖRSTER RESONANCE ENERGY TRANSFER-CAPABLE POLY(*N*-ISOPROPYLACRYLAMIDE) MICROGELS

6.1 Introduction

The previous two chapters have investigated functionalization of temperature responsive networks composed of PNIPAM with fluorinated comonomers to enhance association with fluorinated analytes, providing a platform for further improvement through miniaturization to augment sensitivity and shorten response times. The current study therefore attempts to build on previous attempts to tailor a polymeric matrix for PFAS by exploring microgel analogs to identify if raising the surface area-to-volume ratio might expand the detection limits capable for this simple polymeric approach to sensing.

Efforts to employ nanomaterials as sensing tools have yielded success for precise and selective determination of chemical species in solution, and polymeric agents acting as the recognition element or facilitating vehicle enable resolution unachievable by standalone materials. Microgels often act in the former capacity, exploiting their unique physiochemical properties, akin to the striking characteristics of inorganic nanomaterials, to enrich their response toward dilute contaminant concentrations. Earlier work utilizing colorimetric, luminescent, and electrochemical signaling motifs in conjunction with polymeric particles has shown promise for tracking biomolecules,[137, 189-194] metal ions,[125, 134, 195-198] and small molecule analytes.[141] Concurrently, extraction strategies have also used nanoparticles to improve PFAS separation; an example by Koda et al.[199] capitalized on favorable fluorous attraction with cationic comonomers to remove polyfluorinated chemicals with greater than 98% efficiency. A recent microscale adaptation of the same strategy by Kumarasamy et al.[200] demonstrated exceptional adsorption for both long- and short-chained PFAS from wastewater samples. Taken together, provisions for augmenting PFAS uptake combined with the proficiency of microgels to report molecular interactions give a basis for crafting a highly responsive sensor for the contaminants.

Expanding these methods, the approach herein first focuses on applying fluorinated comonomers in conjunction with PNIPAM microgels to heighten responsivity toward fluorinated analytes. Secondly, FRET-compatible dyes, cyanine 3 (Cy3) and

cyanine 5 (Cy5), are supplemented into the network to test if the fluorescent phenomenon is a suitable marker for the contaminants' concentration and if the signal reports the analytes' presence with greater fidelity than size estimates from light scattering alone. Packaging these characteristics into discrete gels with sub-micron dimensions serves to probe the system's standalone limits for detecting PFAS. Studying the effect of fluorosurfactants on PNIPAM gels in this manner will further understanding of their impact on the polymer's thermodynamics and the peculiar association behavior of fluorinated species with non- or semi-fluorinated hydrocarbons.

6.2 Methods

6.2.1 Materials

Reagents were used as received without further purification unless otherwise noted. *N*-isopropylacrylamide (NIPAM, Sigma, 97%), 2-aminoethyl methacrylate hydrochloride (AEMA, Sigma, 90%, stabilized with 500 ppm phenothiazine), and 2,2,2-trifluoroethylacrylate (TFEA, TCI, 98%, stabilized with 4-methoxyphenol) were used as monomers throughout the syntheses, and *N*,*N*'-methylenebis(acrylamide) (MBA, Sigma, 99%) was implemented as a crosslinker. Potassium peroxodisulfate (KPS, Fluka, 99%) was used to thermally initiate free radical polymerization. Cyanine 3 *N*-hydroxysuccinimide ester (Cy3-NHS, Lumiprobe, 95%) and cyanine 5 *N*-hydroxysuccinimide ester (Cy5-NHS, Lumiprobe, 95%) served as labels for amine-functionalized microgels. Octanoic acid (OA, Alfa, 98%), perfluorooctanoic acid (PFOA, TCI, 98%), sodium 1-octanesulfonate (SOS, TCI, 98%), tetraethylammonium perfluorooctane sulfonate (TPFOS, BeanTown Chemical, 98%), and phenol (Ph, Fluka, 99%) represented analytes for swelling and fluorimetric studies. Methanol (MeOH, Pharmco, HPLC-UV grade) was used as an analyte for swelling studies and a solvent for various stock solutions, and dimethyl sulfoxide (DMSO, Pharmco, reagent ACS grade) worked as a solvent for dye stocks. Deionized water (1 MΩ) was used for syntheses, buffer solutions, and analyte testing. Both MeOH and DMSO were kept over 3 Å sieves to mitigate residual water. Structures of reagents and analytes are included in Figure 6.1.

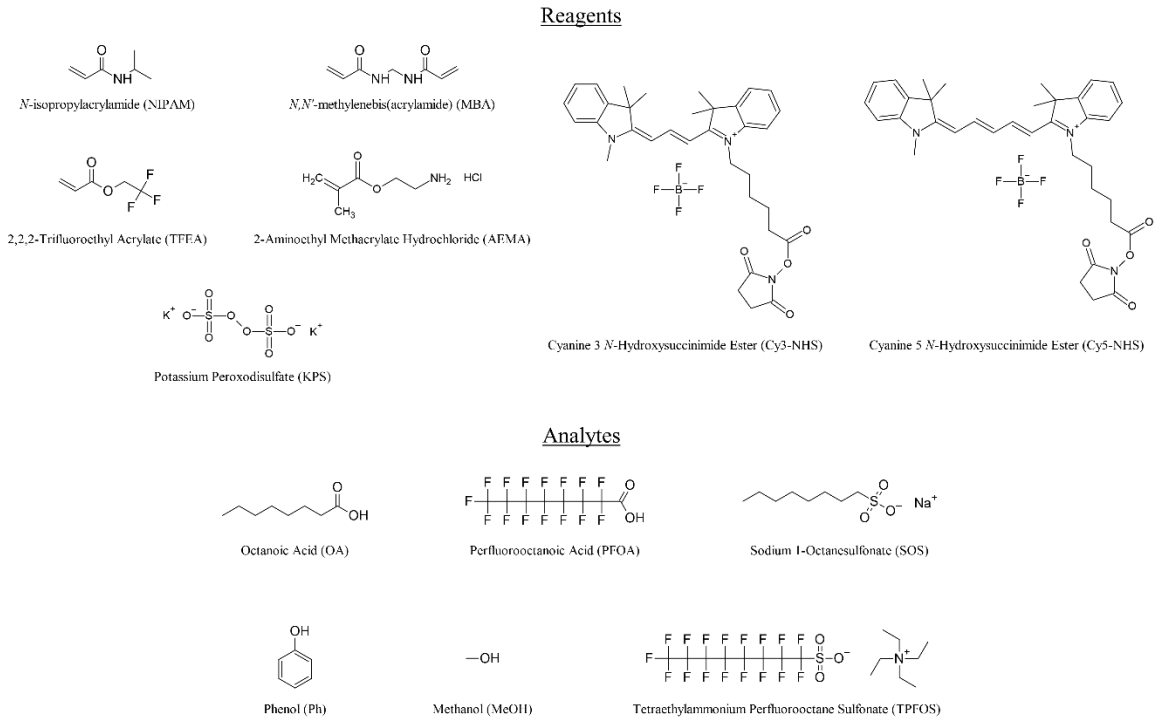

Figure 6.1. Chemical structures of synthesis reagents and analytes tested.

Sodium carbonate (Sigma, 99%), sodium bicarbonate (Mallinckrodt Chemicals, 99%), sodium phosphate monobasic dihydrate (Sigma, 99%), and sodium phosphate dibasic heptahydrate (VWR Chemicals, 98%) were used for generating buffer solutions. Briefly, for a 0.01 M ionic strength carbonate buffer system, 57.1 mg sodium carbonate and 38.8 mg sodium bicarbonate were mixed with 100 mL DI water (resulting in a measured pH between 10.12-10.18). Similarly, 0.01 M ionic strength phosphate buffers were produced with 65.9 mg sodium phosphate monobasic dihydrate and 154.9 mg sodium phosphate dibasic heptahydrate in 100 mL DI water (for a measured pH of 7.04-7.16).

6.2.2 Microgel Synthesis

The microgel synthesis method used for undyed particles was adapted from Chuang et al.[201] As an example for a non-fluorinated batch of microgels with a 97.5 mol% NIPAM feed complemented by 2.5 mol% MBA, 109.2 mg (0.965 mmol) of NIPAM was first added to a 20 mL scintillation vial and diluted with 9.178 mL DI water. Another 0.381 mL (0.025 mmol) from a 9.920 mg mL^{-1} MBA stock in DI water was then

added and mixed. The mixture was supplied with a stir bar and capped with a rubber septum before bubbling with ultra high purity compressed nitrogen (Scott-Gross, 99.999%) for 5 min. Thereafter, the purged mixture and a 39.364 mg mL^{-1} stock solution of KPS in DI water were warmed in a preheated 75 °C oil bath for 30 min. After heating, 0.334 mL (0.049 mmol) from the KPS stock was dripped into the reaction vessel with a glass syringe and left for 3 h. The solution turned milky approximately 5 min after adding the initiator. The reaction was then removed from the oil bath and quenched with cold water. The liquid was transferred to a 50 mL polypropylene centrifuge tube (VWR Ultra High Performance), and the scintillation vial was washed with DI water and the residual passed into the centrifuge tube until a total liquid volume of 45 mL was achieved. The solution was spun at 5,000 *g* for at least 6 h, decanted, refreshed with DI water and vortexed to disperse, and repeated for a total of 4 cycles. Upon decanting the final wash, the sediment was transferred to another 20 mL scintillation vial, flash frozen in liquid nitrogen, and lyophilized for 64 h. The resulting fluffy white powder was stored at 4 °C and subsequently used for characterization and analyte tests. Alterations for fluorinated microgels are shown in Table 6.1.

Table 6.1. Synthesis conditions for non-fluorinated and fluorinated microgels. Microgels synthesized with AEMA have similar conditions to T0, but 0.5 mol% of their NIPAM content is instead substituted for AEMA (maintaining a consistent TMC and initiator concentration (I)).

Acronym	NIPAM (mg)	MBA (mg)	TFEA (µL)	NIPAM (mol%)	MBA (mol%)	TFEA (mol%)	TMC (mM)	I (mM)
T0	109.2	3.8	0.0	97.5	2.5	0.0	98.9	4.9
T20	86.8	3.8	25.1	77.5	2.5	20.0	98.9	4.9
T40	64.4	3.8	50.1	57.5	2.5	40.0	98.9	4.9

The procedure for labeling amine-functionalized microgels was adapted from Jones et al.[202] For microgels dyed with Cy3, Cy5, or both, the initial reactants (NIPAM, MBA, KPS) were constituted in the 0.01 M carbonate buffer described earlier rather than DI water. AEMA was added from a 0.999 mg mL^{-1} stock in DI water prior to purging with nitrogen. The final solution used for the reaction consequently holds an ionic

strength of approximately 9.18 mM. After drying, the powder was constituted to 15 mg mL^{-1} in phosphate buffer. Aliquots from 4.975 mg mL^{-1} stock solutions of Cy3-NHS and Cy5-NHS were added according to the total mass of powder (assuming an average component molecular weight of 114.44 g mol^{-1} for the undyed microgels and a 0.5 mol% incorporation of AEMA) to create microgels dyed with 1 mol of Cy3, 1 mol of Cy5, or 1 mol of both Cy3 and Cy5 per mol of primary amine. The labeling reaction was covered with aluminum foil atop an orbital shaker rotating at 50 rpm for 24 h at room temperature. Once dyed, the microgels were washed under the same protocol detailed for undyed microgels and shielded from ambient light while drying. The resulting powders, colored with respect to their corresponding dye (i.e., pink for Cy3, cyan for Cy5, or dark blue for both dyes; see Figure 6.2), were used for testing analyte-induced FRET responses.

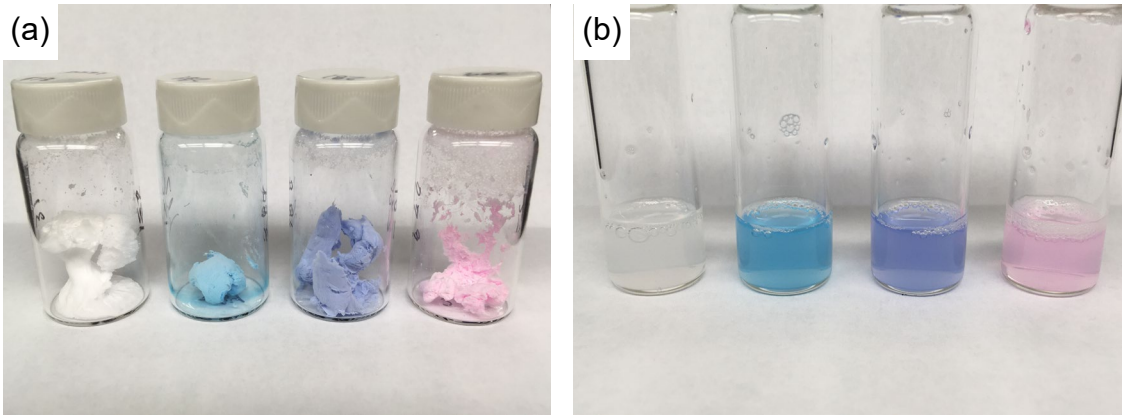

Figure 6.2. Pictures of microgels that are (a) dry and (b) dispersed in water at 2 mg mL^{-1}. From left to right: T0 microgels, microgels dyed with Cy5, Cy3 and Cy5, and Cy3.

6.2.3 Characterization

Dynamic light scattering (DLS) measurements were recorded on a Zetasizer Nano ZS90. Samples were scanned every 2 °C from 10 °C to 50 °C following 10 min equilibration at each temperature. The material was modeled using a refractive index of 1.480 and an absorption coefficient of 0.010, and the dispersant properties were held at those for water at a given temperature regardless of the analyte concentration. Three measurements were taken per scan with a 0 s delay. A 90° measurement angle accompanying 30 runs of 10 s each was selected under the general purpose (normal

resolution) analysis model. The software automatically searched for an optimum measurement position, and attenuation was left on automatic.

Fluorimetric studies were performed with a Varian Cary Eclipse Fluorescence Spectrophotometer equipped with a Cary Single Cell Peltier Accessory. All scans were conducted with 5 nm excitation and emission slits over 120 nm min^{-1}, and emission scans were excited at 510 nm. Smoothing was implemented with a moving average factor of 9, and the PMT detector voltage was set between 610 V and 750 V depending upon the microgel and analyte combination studied. Samples were held at their setpoint temperature for at least 10 min prior to scanning.

FTIR spectra were attained with a Varian 7000e FT-IR Spectrometer. Samples were scanned 32 times at a speed of 5 kHz and a resolution of 8 cm^{-1}, and the spectra shown represent the average of the scans.

6.2.4 Analyte Assessments

Samples for DLS were initially composed of 2 mg microgel in 2 mL DI water housed in a 3 mL quartz cuvette. A PTFE cap covered the cell throughout the temperature sweeps to mitigate evaporation. Following a baseline temperature sweep, analyte was added from 1,000.5 mM stocks for OA, PFOA, and Ph in MeOH. A MeOH stock was brought to the same concentration by dilution with DI water, and a SOS stock was fixed at 450.0 mM in DI water. As an example, adding 1.00 µL from an OA stock to a 2 mL sample of 1 mg mL^{-1} microgel results in a final analyte concentration of 0.5 mM, a MeOH concentration of 10.4 mM, a final microgel concentration of 0.9995 mg mL^{-1}, and a total volume of 2.001 mL. The minute change in microgel concentration between measurements was assumed to negligibly effect the recorded z-average diameter, and residual MeOH was not observed to impact sizing (described for fluorescence measurements below). A temperature sweep was subsequently performed in the Zetasizer before proceeding with successive analyte additions. In the case of OA, the cumulative analyte additions yielded an OA concentration of 5.0 mM, MeOH concentration of 103.9 mM, and a microgel concentration of 0.995 mg mL^{-1}. Microgels exposed to TPFOS were prepared individually at their appropriate TPFOS concentration

in DI water, leaving the total volume constant at 2 mL without residual MeOH throughout their evaluation.

Fluorescent microgels were first scanned from 700 μL of a 2 mg mL^{-1} solution in a quartz micro cuvette (Starna Cells). Like DLS, the cuvette was topped with a PTFE cap during temperature sweeps. After recording the baseline, 1.00 μL from a 175.25 mM stock of OA or PFOA in MeOH or SOS in DI water was added to result in an analyte concentration of 0.25 mM and a total volume of 701 μL. With the spectra thereafter scanned, the analyte addition procedure was repeated until a final analyte concentration of 3.00 mM and volume of 712 μL was met. Regardless of the analyte, the final microgel concentration fell to 1.966 mg mL^{-1}. Again, this small change in microgel concentration was considered negligible. Another 411.4 mM MeOH was present for OA and 406.1 mM MeOH for PFOA at the final analyte concentration of 3.00 mM, but the solvent did not significantly alter the z-average diameter of microgels at 450 mM MeOH in DLS (see Figure 6.3) and was not considered to impact the microgels' fluorescence. For TPFOS, 1.40 μL from a 50.0 mM stock in 50 v/v% MeOH was added to bring the post-baseline analyte concentration to 0.1 mM. Subsequent additions were conducted similarly to result in a final analyte concentration of 1.00 mM at a sample volume of 714 μL and microgel concentration of 1.960 mg mL^{-1} with a residual MeOH concentration of 247.2 mM. The FRET intensity, or sensitized emission, for fluorescent samples was calculated by subtracting the intensity at a given wavelength for Cy3- and Cy5-individually labeled microgels from that of a microgel containing both dyes. Each microgel-analyte combination was run in triplicate, and presented values represent the average and standard deviation for each possible combination of microgels.

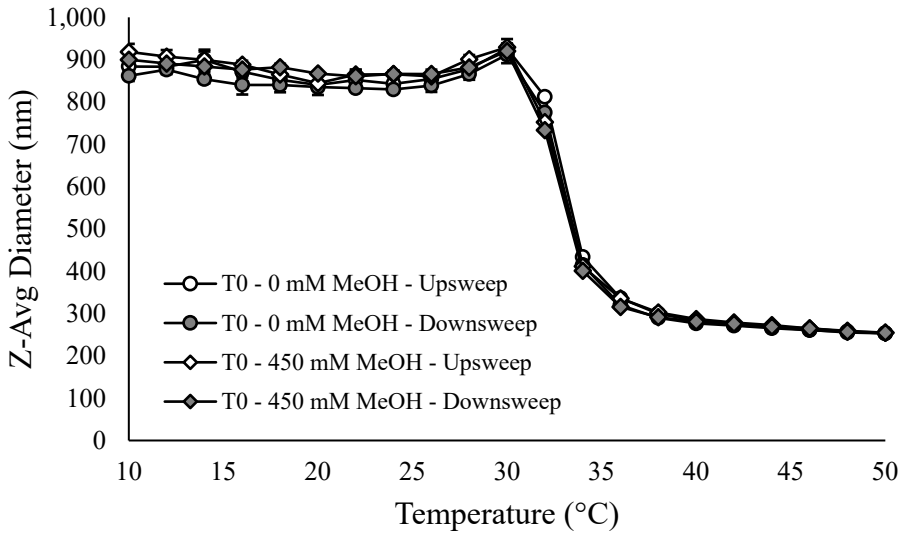

Figure 6.3. Temperature response of T0 microgels in water alone (circles) and exposed to 450 mM methanol (diamonds). Upsweeps progressing from 10 °C to 50 °C are colored white, and downsweeps from 50 °C to 10 °C are gray.

6.3 Results

6.3.1 Microgel Synthesis

Syntheses according to Table 6.1 yielded fluffy, static powders that dispersed easily into solution with vortexing after soaking. Characteristic FTIR absorption bands at 1,639 cm^{-1} representing the amide I peak for PNIPAM were present for each microgel (see Figure 6.4). Both the carbonyl and CF_x bands for TFEA at 1,748 cm^{-1} and 1,153 cm^{-1}, respectively, grow larger as the TFEA feed ratio is increased, and the baseline-corrected shifts for each band relative to the amide I band follows a linear increase with TFEA feed ratio (r^2 = 0.967; r^2 = 0.987). Non-fluorinated gels (T0), those fed with 20 mol% TFEA (T20), and those with 40 mol% TFEA (T40) display markedly different swelling curves in DI water as shown in Figure 6.5. Examining the temperature upswing curves for each microgel, or those progressing from 10 °C to 50 °C, the minimum and maximum z-average diameters for T0 gels span 246.4 ± 10.3 nm to 881.8 ± 18.6 nm, T20 range 214.8 ± 4.8 nm to 550.0 ± 17.1 nm, and T40 sit between 172.7 ± 2.1 nm to 254.9 ± 9.7 nm. The polydispersity index (PDI) for each particle group averaged across their

temperature sweeps labels them as monodisperse; the PDI registers 0.044 ± 0.039 for T0, 0.070 ± 0.052 for T20, and 0.025 ± 0.017 for T40. Estimating the LCST for each microgel as the linearly interpolated temperature corresponding to the average of their minimum and maximum z-average diameters, T0 holds the highest LCST of 33.2 ± 0.1 °C, followed by T40 at 25.4 ± 1.2 °C, and T20 at 23.2 ± 1.0 °C. The sharp transition region for non-fluorinated gels between 30 °C and 36 °C makes determination of their transition temperature relatively trivial; fluorinated gels, with their gradual transition from the start of the sweep at 10 °C to their eventual collapse, prove more difficult to accurately pinpoint the location defining their phase behavior. The derivative of their size as a function of temperature ($dS\ dT^{-1}$, see Figure 6.6) reinforces the LCST estimates for T0 and T20 gels but potentially suggests a LCST for T40 reaching 20 °C or below. The derivative approach is, however, obscured by sizable error for T40 samples, again making conclusive estimates of the microgels' LCST difficult.

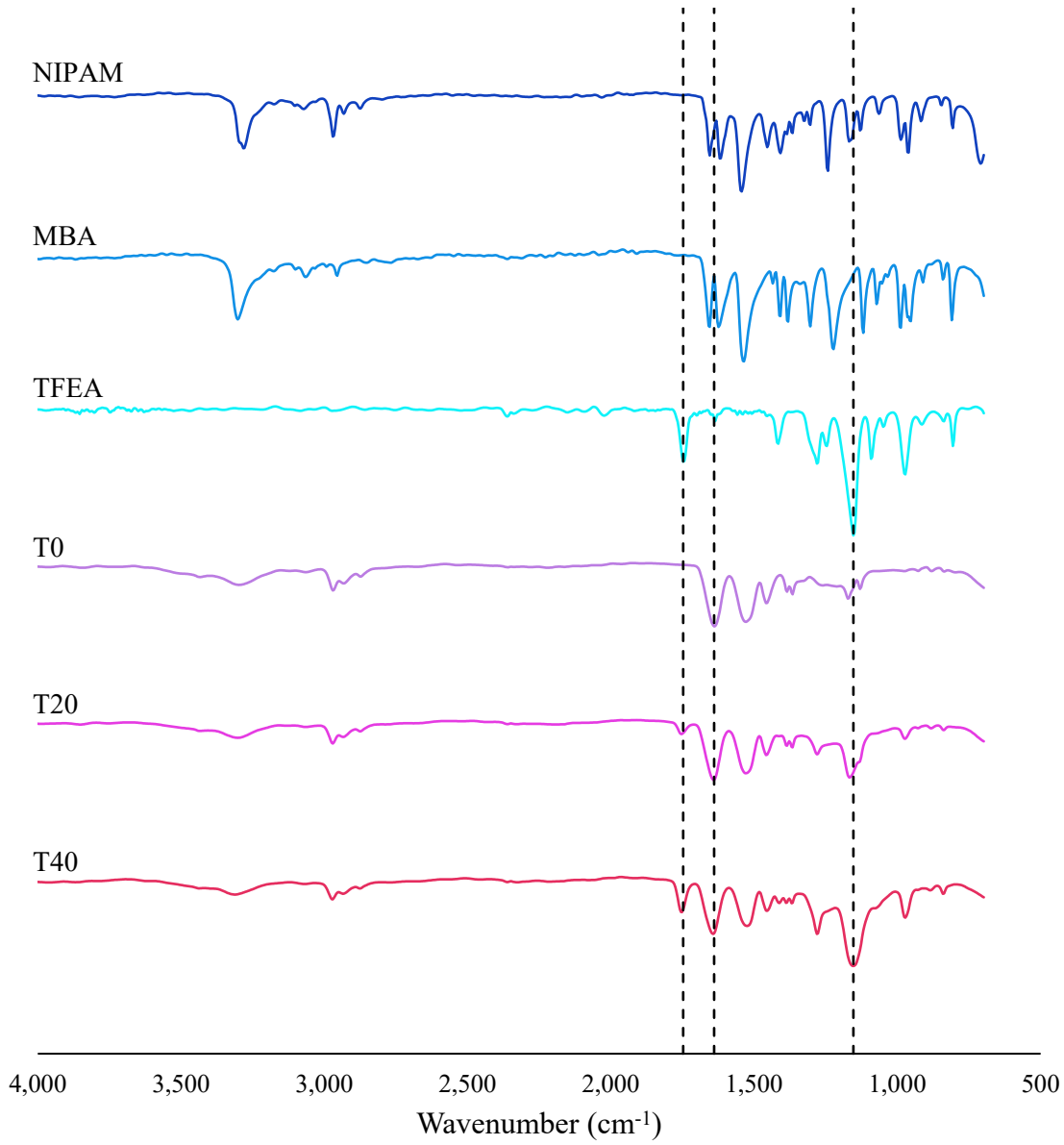

Figure 6.4. Fourier-transform infrared spectra for the monomers and resulting microgels synthesized. Dashed lines are guides representing 1,748 cm^{-1} (carbonyl), 1,639 cm^{-1} (amide I), and 1,153 cm^{-1} (CF_x) from left to right.

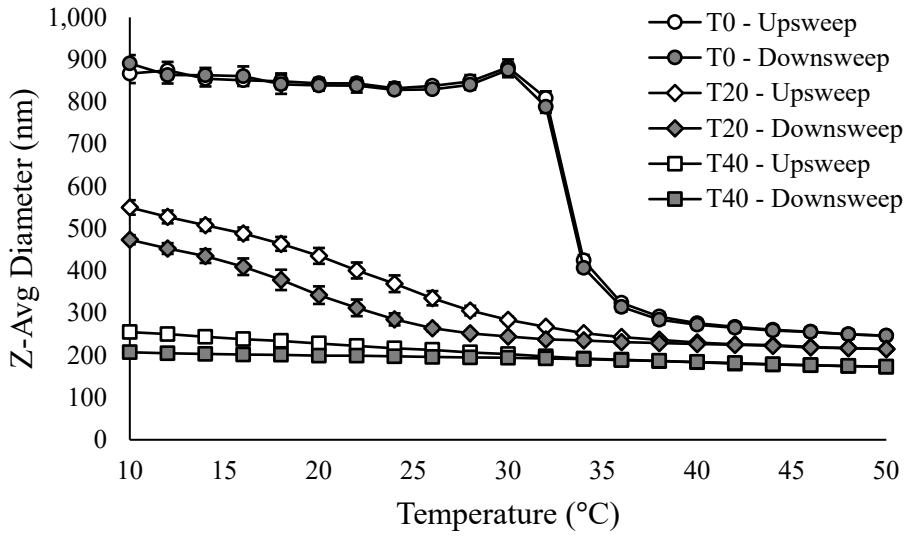

Figure 6.5. Temperature response curves for T0 (circle), T20 (diamond), and T40 (square) microgels during their upsweep from 10 °C to 50 °C (white) and downsweep from 50 °C to 10 °C (gray).

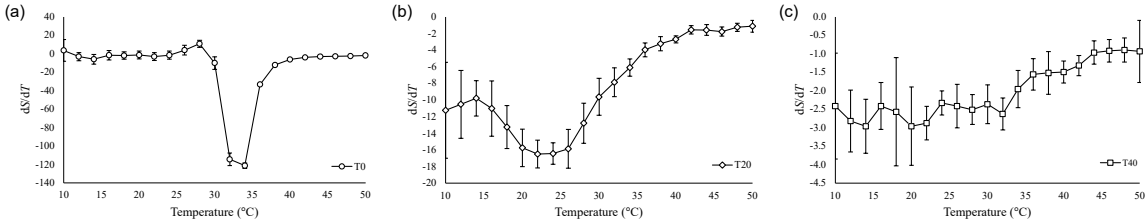

Figure 6.6. Derivative of the z-average diameter with respect to temperature for (a) T0, (b), T20, and (c) T40 microgels. Minima roughly indicate the position of the respective lower critical solution temperature for each microgel. Values were calculate using finite difference.

Both gels synthesized with TFEA demonstrate significant hysteresis on their temperature downsweeps from 50 °C to 10 °C, instead achieving a maximum z-average diameter of 473.5 ± 10.9 nm and 207.2 ± 2.3 nm for T20 and T40 gels, respectively, at 10 °C. These final diameters are 86.1% and 81.3% of their respective sizes at the same temperature from their upsweep curves. The addition of fluorine moieties into the networks entraps the gels in a solvent-excluded conformation that limits hydrogen bonding when collapsed. Reswelling is consequently impaired by the simultaneous

oleophobic and hydrophobic fluorine groups inhibiting hydration in favor of internal fluorophilicity.

Dye loading for the FRET-compatible microgels was controlled by regulating the addition of the coupling agent, AEMA, to the synthesis protocol. The effective load was estimated by modeling a sphere with known swollen and deswollen radii in-line with the dimensions for T0 gels and simulating dye positions within the sphere's swollen and collapsed states (see Figure 6.7). For each state, the volume of the sphere was divided by the volume occupied by a monomer subunit (126.9 $Å^3$, the average contribution of NIPAM and MBA) to yield the population of subunits within the microgel. The theoretical number of dye-anchoring subunits for a given AEMA load was then dispersed using uniformly distributed random variables positioned with cartesian normal random variables. The nearest neighbor distance for each point across the ensemble was then averaged to yield the dye separation for each state. To account for the gel volume influencing the total perceived number of subunits, a sham load was issued for the swollen state relative to the collapsed state to maintain the total population of dyes between each simulation. Tuning the dye loading according to this model approximated a 0.5 mol% AEMA load to afford an average spacing of 5.36 nm to 23.12 nm between dyes, both below and above the calculated Förster distance for the Cy3-Cy5 pair employed (approximately 5.49 nm). Gels synthesized with lower AEMA feeds showed little sensitized emission enhancement between 20 °C and 50 °C, and those with higher feeds experienced heightened swelling resulting from internal electrostatic repulsion accompanying the anchor's primary amines. A 0.5 mol% AEMA feed (siphoned from NIPAM, holding MBA constant) was consequently chosen as the loading for all FRET-related syntheses.

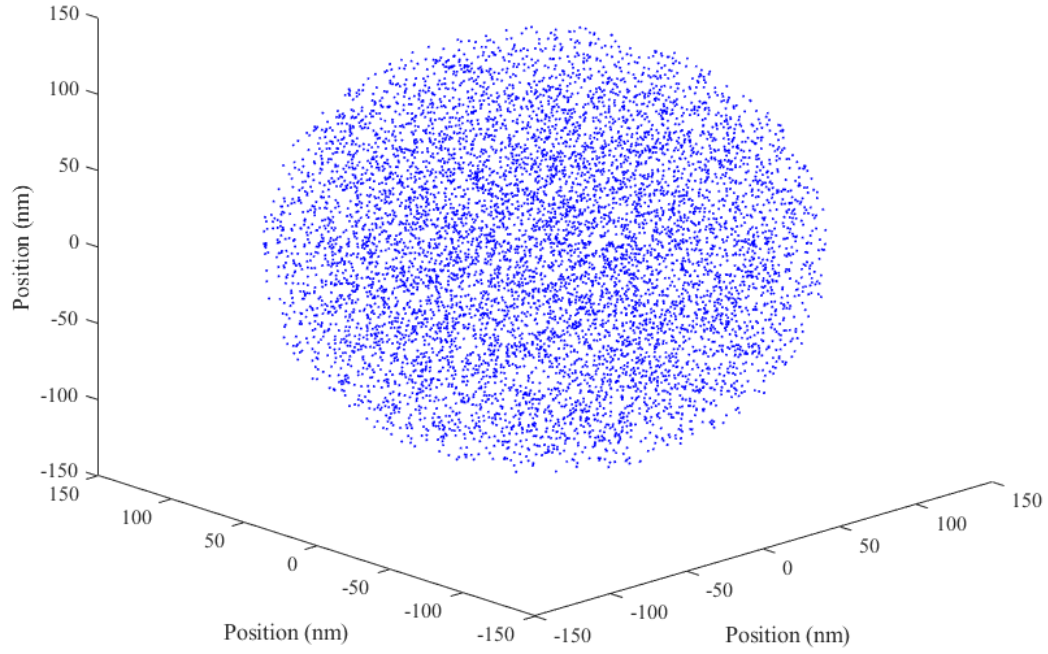

Figure 6.7. An example model of dye locations within a collapsed microgel holding a z-average diameter of 270.9 nm. The sphere shown contains a simulated 0.01 mol% theoretical load of AEMA. Each dye is randomly drawn; successive iterations of the same simulation will result in slightly different dye locations relative to this image.

6.3.2 Analyte-Induced Swelling Response

Initially surveying the impact of a suite of substances suspected to alter the swelling behavior of non-fluorinated microgels, dose-response curves for OA, PFOA, Ph, SOS, and MeOH concentrations up to 5.0 mM were collected near the gels' aqueous transition temperature (between 28 °C and 34 °C) to identify if a trend amongst the compounds might reveal the characteristics that fuel alterations to the phase transition of PNIPAM. From the analytes shown in Figure 6.8, MeOH did not significantly change the microgels' swelling as indicated by their normalized z-average diameter, likely due to its dilute concentration falling below the range anticipated for solvent-induced

perturbations to become apparent.[163] SOS demonstrated a perceptible decline in normalized z-average diameter at 0.5 mM regardless of temperature with a steeper slope at higher temperatures. The size reduction attenuates quickly, leveling within error by 2.0 mM for all temperatures, potentially signaling network saturation. The hydrotrope examined, Ph, follows a linear response across the concentration range for temperatures above 30 °C. At 32 °C, the gels experience their sharpest decline for Ph, reaching a normalized z-average diameter of 0.67 ± 0.01 by 5.0 mM, while at 34 °C the particles shrink to only 0.80 ± 0.04 for the same concentration. The latter temperature corresponds to the first temperature point collected beyond the gels' transition temperature in water alone, lowering the maximum shift for their size when compared to the temperature point acquired just prior to their collapse (32 °C). Both PFOA and OA, analogous fluorinated and non-fluorinated surfactants, show substantial reductions in microgel size as a function of concentration with the latter holding lower normalized minima. Interestingly, the thresholds for size disruption are heavily dependent upon temperature for both surfactants. For OA in particular, as the analyte concentration is increased, the size-temperature curve shifts toward lower temperatures in a nonlinear manner. Whereas the shift occurs linearly for Ph, small additions of C_8 carboxyl surfactants shrink the microgels precipitously near their transition temperature while requiring larger contributions to collapse the gels farther from their initial transition temperature. Though the trend is apparent for both surfactants, the gels deswell to a greater degree for OA than PFOA, falling to 0.31 ± 0.02 for a 5.0 mM concentration of OA at 30 °C compared to 0.41 ± 0.02 for PFOA at the same concentration and temperature. These normalized z-average diameters also mark the lowest extremes observed for the substances tested, placing far below the 0.82 ± 0.04 minima for SOS at 34 °C and the negligible contributions from MeOH.

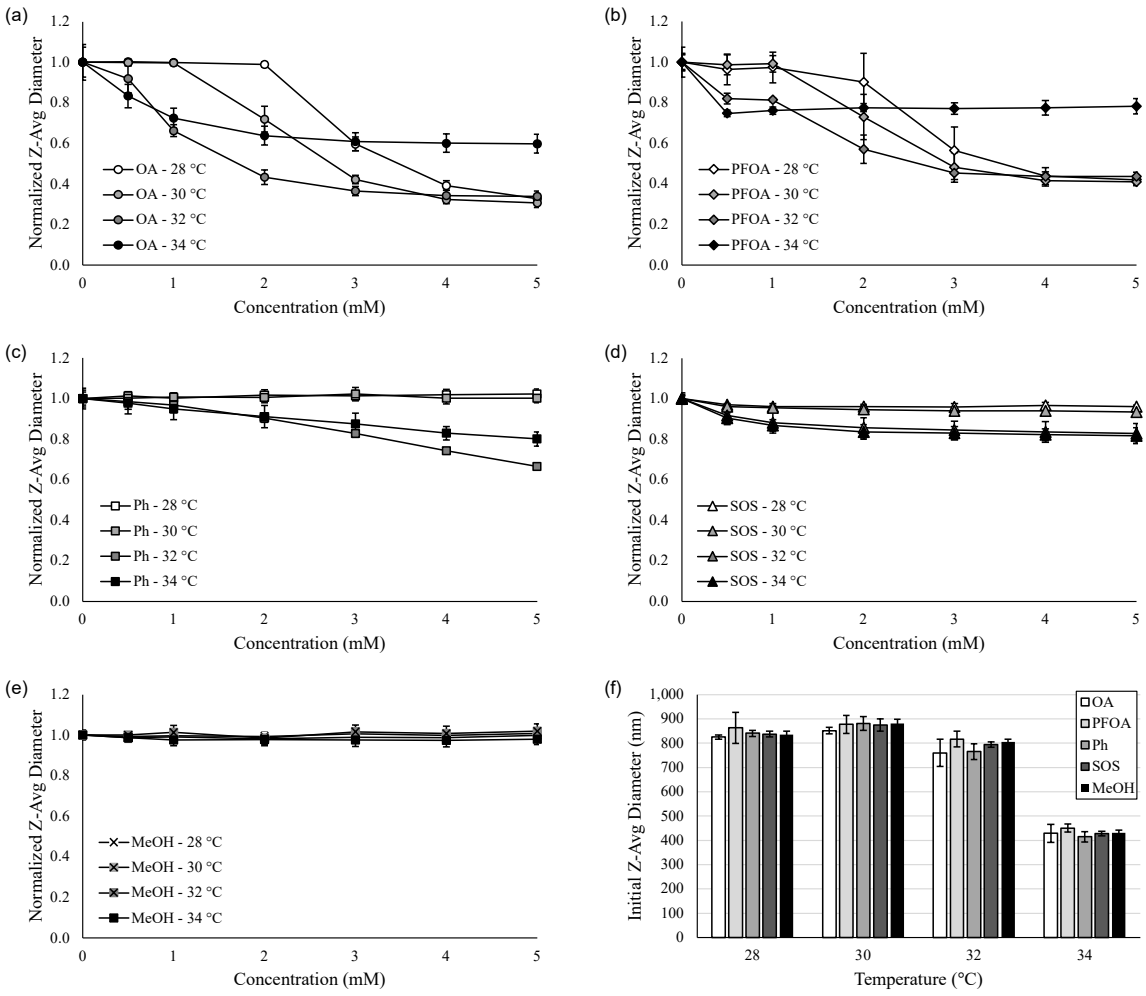

Figure 6.8. Normalized response curves of T0 microgels exposed to (a) OA, (b), PFOA, (c) Ph, (d) SOS, and (e) MeOH. Initial microgel z-average diameters are shown in (f).

Normalizing against the z-average diameter in water alone at each temperature for fluorinated particles with TPFOS, copolymerizing TFEA proved to alter the response characteristics of microgels to the fluorosurfactant by regulating both the linearity and maximum normalized shift across a concentration range up to 1.0 mM as shown in Figure 6.9. Inspecting upsweep curves, non-fluorinated microgels showed little receptivity toward TPFOS below 0.25 mM whereby their isotemperature line at 30 °C received the largest initial size increase of 23.8 ± 2.5%. Thereafter, the line corresponding to 40 °C, the first examined temperature beyond the gels' collapse in water, dramatically increased in size by 84.3 ± 2.0% at 0.5 mM and 167.2 ± 7.6% at 1.0 mM, indicating that the transition temperatures shifts higher as the concentration of TPFOS increases. Both

microgels synthesized with 20 mol% and 40 mol% TFEA showed similar trends, though disturbance of their sizing initiates at lower concentration thresholds and temperatures. With the fluorinated gels innately collapsing at lower temperatures due to incorporation of hydrophobic, fluorinated moieties in their networks, size disparities occurring as an extension of their heightened LCST in the presence of TPFOS consequently arise at lower temperatures than for non-fluorinated microgels. Additionally, both systems demonstrated heightened swelling at 0.1 mM TPFOS, possibly noting enhanced associated between the microgels and fluorosurfactant owing to the weakly attractive fluorinated groups incorporated in the polymers. The isotemperature line at 30 °C for T20 microgels displayed a markedly linear response ($r^2 = 0.996$), outperforming the 20 °C isotemperature line for T40 gels in terms of both linearity ($r^2 = 0.981$) and maximal size increase (118.3 ± 9.7% versus 88.4 ± 6.1%). Downsweep curves mainly replicate the general trends established by upsweep curves but at lower extremes. The hysteresis observed here is similar to that reported by Murase et al.[152] where ionic alkyl surfactants were shown to have significantly lower association to PNIPAM microgels in their collapsed state than in their swollen state. Applying their observations to this data, fluorosurfactant dissociation from the particles' collapsed state due to the resultant inaccessibility of the polymers' amide groups for electrostatic binding would inhibit reswelling to the same level afforded by the high degree of initial association acquired during the temperature upsweep. This condition is exacerbated by highly fluorinated copolymers whereby reswelling is impeded by the hydrophobicity of the networks' fluorine moieties which encumbers reassociation of TPFOS that would otherwise swell the microgels.

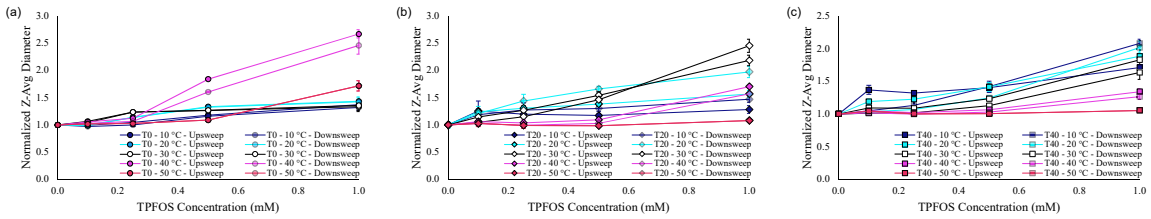

Figure 6.9. Normalized z-average diameters of (a) T0 (circles), (b) T20 (diamonds), and (c) T40 (squares) microgels exposed to a range of TPFOS concentrations. Upsweep responses at 10 °C (navy), 20 °C (teal), 30 °C (white), 40 °C (pink), and 50 °C (red) are fully colored, and downsweeps have slight transparency.

With PNIPAM microgels exhibiting significant responsiveness to both PFOA and TPFOS, the fluorosurfactants were coadded in Figure 6.10 to monitor their influence on the final size of the gels. Using the size data collected for T0 microgels in solution with 1.0 mM TPFOS as the norm, 1.0 mM of PFOA did not appear to reduce the swelling enhancement attributable to TPFOS and only served to potentially enlarge the particles further between 32 °C and 42 °C during their upsweep. Raising the concentration of PFOA to 10.0 mM, however, lowers the microgel z-average diameter significantly above 20 °C compared to those swollen with TPFOS alone, reducing the normalized size to 93.2 ± 5.4% of its normal value at 22 °C and further to 77.5 ± 4.5% at 50 °C. The upsweep z-average diameter at 10 °C (1,108.4 ± 73.3 nm) and 50 °C (327.0 ± 8.3 nm) in this cocontaminant mixture remains above the gels' size in water by 241.7 nm and 80.6 nm, respectively, on average, suggesting a significant association advantage for TPFOS over PFOA and the strong capability of TPFOS to stimulate swelling for these gels over size changes from other comparable contaminants.

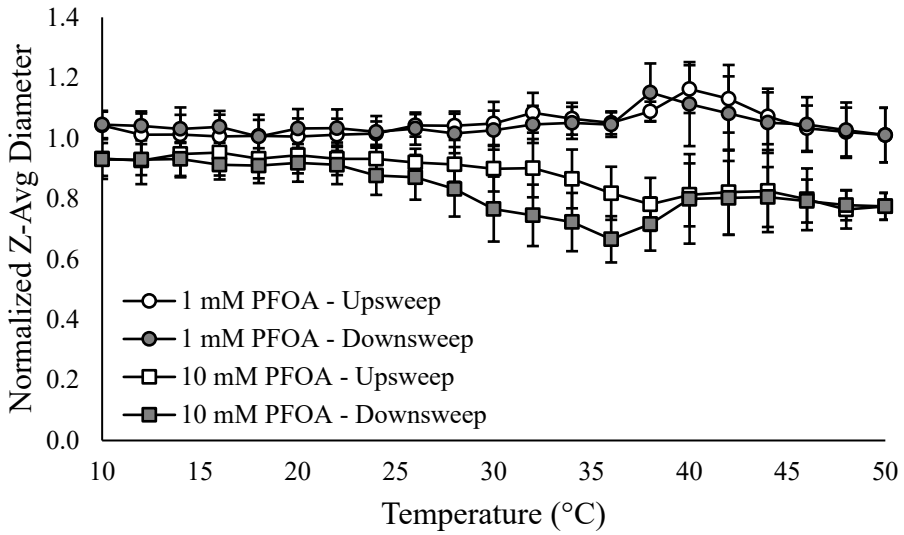

Figure 6.10. Relative z-average diameter of T0 microgels in solution with 1 mM TPFOS and 1 mM PFOA (circles) or 10 mM PFOA (squares) normalized against those in TPFOS alone. Upsweeps are colored white and downsweeps gray.

6.3.3 Förster Resonance Energy Transfer Analysis

Introducing FRET-compatible dyes to non-fluorinated microgels, four of the analytes evaluated for their impact on the gels' swelling were scanned for their respective effect on the gels' fluorescence behavior. Examining the FRET intensity at 670 nm shown in Figure 6.11, the concentration profiles for OA generally follow their anticipated trends, displaying an increase in intensity as temperature increases at low concentrations with attenuation at higher concentrations. This observation agrees with the sizing data from DLS whereby, at high OA concentrations, the microgels collapse at lower temperatures, indicative of a depressed LCST, which would encourage energy transfer between the dyes resulting in a larger FRET intensity. Clustering of the isotherms at 3.0 mM is surprising, however, considering the onset of collapse for gels under a 28 °C isotherm occurs at the same concentration by DLS. Extrapolation of the results from DLS would suggest higher swelling at 20 °C and, ultimately, a lower FRET intensity. Nonetheless, the concentration at which the FRET intensity initially begins to rise for a given isotherm increases as the temperature decreases, as would be expected for a falling LCST with OA concentration. PFOA shows a similar profile but with even higher

intensities and error than its hydrocarbon analog. From 1.0 mM to 2.0 mM, progressive intensity increases from 35 °C to 50 °C are replaced by intensity decrements, pointing to either reswelling of the gels or PFOA dissociation within this concentration range at higher temperatures. Lower temperatures again see increments in the concentrations at which the gels transition, but along narrower distributions of 0.5 mM than the 1.0 mM increments for OA. Though PFOA intensities increase toward the higher extreme of the concentration range tested, the points along the isotherms collected above 1.0 mM are marred by considerable error, preventing conclusive estimates of the phenomenon's trajectory. Compared to DLS, the intensity distribution did not noticeably fluctuate until 1.0 mM rather than 0.5 mM, denoting lower sensitivity to PFOA using FRET as the transducer.

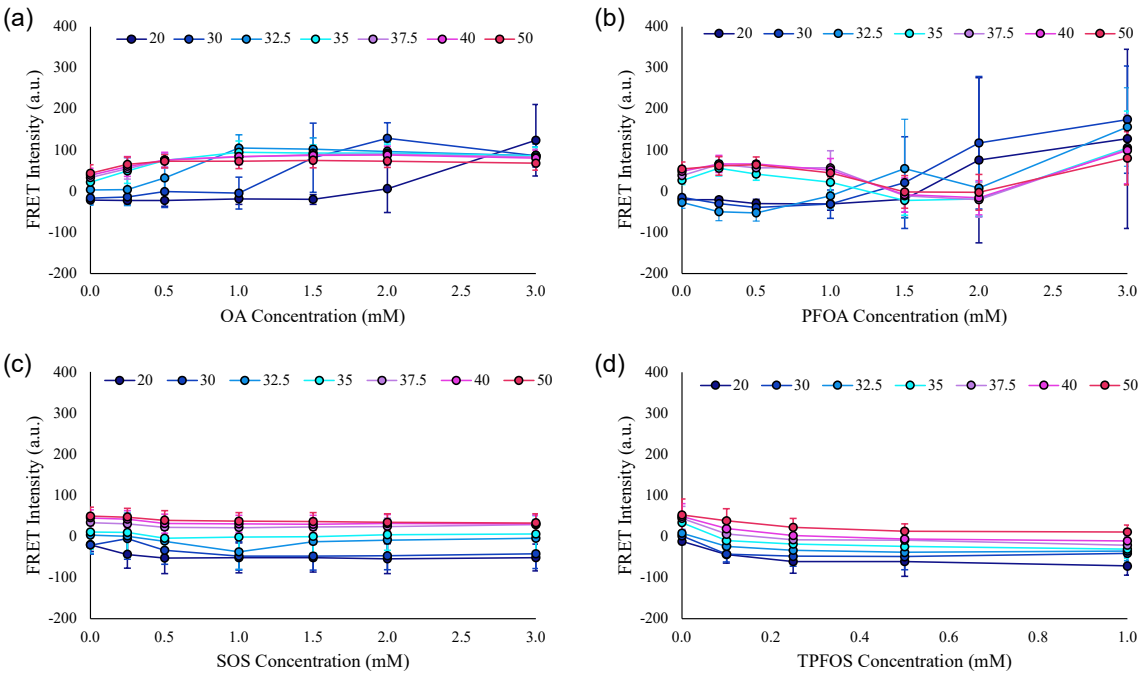

Figure 6.11. Sensitized emission (FRET intensity) for varying concentrations of (a) OA, (b) PFOA, (c) SOS, and (d) TPFOS. FRET intensities were calculated by subtracting the intensities of microgels labeled with Cy3 and Cy5 alone from that of a microgel containing both dyes at 670 nm. The PMT voltage was set to 750 V for (a), (b), and (c) and 725 V for (d). Temperature curves are colored from dark blue (20 °C) to red (50 °C) for each analyte.

Unlike the carboxylic derivatives examined, SOS contradicts its DLS trend by demonstrating lowered average sensitized emission with concentration. Reduced intensity implies swelling of the microgels and, consequently, separation of their dyes, but DLS instead showed a small size decrease approaching 1.0 mM. The absolute difference throughout the SOS concentration range has little fluctuation, ranging between 12.6 a.u. to 42.7 a.u. on average for 37.5 °C and 30 °C isotherms, respectively. The error accompanying each isotherm overlaps these shallow decrements in intensity, leaving the trend as insignificant. Regular intensity increments between 20 °C and 50 °C otherwise follow their anticipated trends. The gradual reduction in sensitized emission for TPFOS agrees with the swelling response measured by DLS, whereby, microgel swelling would raise the distance between donor-acceptor pairs beyond their Föster distance. Despite the differences between the maximum and minimum intensities for each isotherm again

appearing narrow relative to OA and PFOA, their values remain outside of a single standard deviation and imply significance for all but the 32.5 °C and 50 °C isotherms. Both exceptions show the lowest average absolute differences of the isotherms, potentially due to the initiation of deswelling at 32.5 °C regardless of TPFOS concentration and the attenuation of size changes for all concentrations but 1.0 mM at 50 °C providing insufficient size changes to significantly impact FRET. Applying the same significance criterion, FRET changes become significant at 0.1 mM at or below 35 °C while 37.5 °C and 40 °C do not deliver significance until 0.25 mM, exemplifying the temperature dependence of the system when calibrating its dose-response.

6.4 Discussion

The molecular composition and active functionality of analytes dictate their impact on the swelling response of PNIPAM microgels, and the effect of each constituent must be taken with respect to the overall structure of the molecule.

The microgel swelling behavior in response to the analytes tested herein differ significantly from the behavior seen for macrogels with similar compositions explored previously. Namely, the premature collapse caused by carboxylic surfactants, Ph, and SOS were absent for bulk polymers, attesting to the sensitivity granted by the microgels' relatively high surface area-to-volume ratio. The tendency to collapse rather than swell the networks as for TPFOS with macrogels does present a noteworthy deviation: referencing the perfluorosurfactants specifically, despite having similar tail groups (C_8F_{17} for TPFOS and C_7F_{15} for PFOA), the manner in which they influence microgel swelling properties are apparently dissimilar. This oddity follows for SOS relative to SDS whereby SDS has been reported to swell microgels similarly to TPFOS.[151] Head group differences are strictly apparent for the set of perfluorinated analogs; the highly electronegative sulfonate group of TPFOS provides the molecule greater acidity than the weakly acidic carboxyl group of PFOA.[169, 170] This factor does not represent the primary contributor to the difference in swelling, though, since SOS holds the same head group as TPFOS with a hydrocarbon tail. Drawing on the conclusions from our previous studies, multiple factors are at play when deducing how specific analytes direct the swelling of PNIPAM gels. Those influencing the distinctions between TPFOS and PFOA offer a

comparison that will illustrate the key considerations necessary to evaluate compounds for their effect on swelling. As prior tests for macrogels have shown, TPFOS multilayering following polymer charge neutralization orients the molecules within the network such that they electrostatically repel one another and increase swelling. PFOA, with its carboxylic head group, lacks the electronegativity of PFOS and, instead, lamellarizes in solution. This tendency results from either hydrogen bonding or the electron withdrawing behavior of its fluorinated tail rendering the molecule relatively neutral.[203] As such, when PFOA binds to the amide groups of PNIPAM via electrostatics or docks due to the interfacial tension arising from its fluorine groups, the substance serves to impair the hydrophobic hydration of PNIPAM that would otherwise maintain the polymer in its swollen state without contributing electrostatic repulsion that would swell the network. PFOA binding therefore induces the phase transition of PNIPAM to occur more readily at lower temperatures, as the data from Figure 6.8 substantiates.

SOS, by contrast, has a different set of factors affecting its inclination to collapse the network rather than swell. Two components are immediately apparent relative to SDS: SOS holds a sulfonate head group as opposed to sulfate, documented previously to significantly lower to propensity of a given surfactant to swell PNIPAM microgels,[150, 152] and it contains a C_8 tail group as opposed to a C_{12}. This latter factor influences two behavioral elements for the shorter-chained surfactant: the lesser contribution of the tail to the overall amphiphilicity of the molecule reduces its potential to separate from the solution and form micelles, ultimately raising its critical micelle concentration substantially (to 0.155 to 0.162 M from 8.18 mM for SDS),[157] and, in the same manner, its relatively high hydrophilicity owing to the proportion of its head group to its tail lowers its tendency to hydrophobically associated with the chains of PNIPAM. Together, these factors disfavor swelling for SOS at the concentrations tested here. Further, Uehara and Ogawa[204] previously reported the precipitation of linear PNIPAM in solution with SDS at 0.01 mM, roughly three orders of magnitude below its CMC. The concentration range employed for SOS lies within the same general magnitude, possibly indicating that, as with SDS, the relatively dilute concentration of the surfactant could impose disordered electrostatic binding to the polymer that disrupts its hydration barrier similarly to PFOA. Ph likely follows a similar interaction scheme, binding to the amide groups of PNIPAM

via hydrogen bonding while unsettling the network's hydration shell without achieving hydrotropy.[130]

From the analytes tested, TPFOS demonstrated the strongest association with PNIPAM.

Building on the discrepancies noted for TPFOS and PFOA, the capability of TPFOS to swell the microgels in the presence of an order of magnitude excess concentration of PFOA attests to the strength of the binding between the strongly acidic perfluorosurfactant relative to its weakly acidic counterpart. Though the addition of two fluorine atoms orbiting a carbon in TPFOS may enhance its hydrophobicity and improve its interfacial adsorption toward the alkyl chains and *N*-isopropyl groups of PNIPAM, the sulfonate head group of TPFOS appears to greatly improve its association with the network relative to PFOA as a consequence of greater electronegativity promoting electrostatics between the molecule's delocalized charge and the polymer's amide groups. Additionally, with the microgel diameter trending according to the swelling trajectory attributable to each fluorosurfactant individually, both molecules seem to independently influence the ultimate swelling behavior of the crosslinked polymer; the data does not support the formation of secondary complexes arising from the mixing of multiple fluorosurfactants that could complicate the microgel swelling response. Considering the current assumption of multilayering generating augmented swelling for TPFOS, PFOA in this regime must have a low degree of ionization when undergoing fluorophilic association with electrostatically bound TPFOS. Organization as such minimizes residual electrostatic repulsion from PFOA embedded within the TPFOS matrix, allowing PFOA to act as a hydration interferent similarly to its intrinsic behavior with PNIPAM while lowering the observed swelling as excess PFOA competes with TPFOS residence. Inferences for molecular structuring from sizing data could, however, disguise the formation of complexes. The occurrence of wormlike micelles[159, 166] and lamellar structures[205] for PFOS and PFOA, respectively, at their CMC imply differences in their packing parameters that, when mixed, might reasonably result in microstructure variations. These changes are undetectable from microgel sizing alone, possibly hiding cocontaminant interplay affecting the final z-average diameter of the gels.

Copolymerizing fluorinated moieties within the microgel matrix aided in signaling the presence of TPFOS.

Despite the head group heavily influencing both the associative strength and final swelling behavior of fluorosurfactants with PNIPAM microgels, their fluorocarbon tails also play a key role in determining their interaction with the polymer. The normalized z-average diameters of non-fluorinated microgels exposed to OA and PFOA and fluorinated microgels swept with TPFOS display this point effectively: in the former case, OA proves more potent for deswelling the microgels across the concentration range examined, resulting in a minimal size of 0.31 ± 0.02 compared to the 0.41 ± 0.02 of PFOA at 30 °C. The hydrocarbon tail of OA lacks both the bulky molecular volume occupied by the fluorines of PFOA and the electronegativity induced by electron withdrawal, together lowering the packing parameter for OA and mitigating its potential to electrostatically repel adjacent surfactant molecules when bound to microgels. Though PFOA also does not fully demonstrate the capacity to form multilayers and repulse nearby sheets in the manner hypothesized for TPFOS, the minor electrostatic contribution from its fluorinated tail must reduce its packing density relative to OA and lessen its observed deswelling capacity when introduced to the microgels. In the latter case, copolymerizing TFEA clearly enhanced the fluorinated microgels' sensitivity to TPFOS, lowering the minimal concentration at which fluorosurfactant-induced size changes become apparent to 0.1 mM compared to the 0.25 mM threshold for non-fluorinated gels. This improvement stems directly from the inclusion of fluorinated comonomers in the network, whereby the combination of the electrostatic and interfacial mechanisms harboring fluorosurfactant binding to non-fluorinated gels are aided by the addition of fluorophilicity. These three effects in tandem exploit the fluorinated tail group of TPFOS to the boost polymers' receptivity toward their target and facilitate size changes at lower fluorocontaminant concentrations.

Functionalization with transduction motifs indicating molecular-level associations is necessary to meet standard fluorocontaminant detection limits.

Overall, employing FRET as a transduction element for the microgels did little to alter their sensitivity to the analytes relative to sizing from DLS. With FRET acting as a primarily size-dependent transducer, these results were not unexpected; rather, equipping

the microgels with a fluorescent indicator served to demonstrate their robustness for signaling the presence of PFAAs beyond measurements from light scattering alone. Achieving a sensitivity of 0.1 mM to TPFOS does, however, leave the system's detection limit at six orders of magnitude beyond the non-regulatory lifetime health advisory limit for PFAS.[39] Consequently, further functionalization is necessary to prepare PNIPAM microgels for sensing fluorocontaminants at environmentally relevant concentrations. Exploiting minute changes in either the refractive index, as Serpe's group has demonstrated,[134, 193] or the dielectric properties of the gels near their transition temperature[206-208] to package a surface plasmon resonance, impedimetric, or fluorescent sensing system might yield higher resolution. With a complementing transducer, the combined effects of PNIPAM's temperature-induced collapse aside the temperature-dependent aggregation behavior of fluorosurfactants[205] grants the capacity to finely tune the system's dose-response, making the polymer an exciting candidate for sensing the emerging contaminants.

6.5 Conclusions

The temperature-responsive PNIPAM microgels examined here demonstrated exceptional swelling capacities varying with the ratio of copolymerized TFEA: the z-average diameter for those without TFEA ranged between 246.4 ± 10.3 nm and 890.8 ± 19.8 nm, a 20 mol% TFEA copolymer expanded between 214.8 ± 4.8 nm and 550.0 ± 17.1 nm, and a 40 mol% TFEA feed fell between 172.7 ± 2.1 nm and 254.9 ± 9.7 nm. When exposed to PFOA and its hydrocarbon analog, OA, non-fluorinated gels collapsed isothermally to 31 ± 2% and 41 ± 2% of their initial z-average diameters under a 5.0 mM concentration at 30 °C. Both Ph, the only hydrotrope tested, and SOS, the hydrocarbon analog of TPFOS, also deswelled the microgels to 67 ± 1% and 82 ± 4% of their original diameters at 32 °C and 34 °C, respectively, for 5.0 mM loads. This deswelling behavior is generally attributable to either electrostatic or hydrogen bonding of the analyte to the microgels accompanied by disruption of hydrophobic hydration around local *N*-isopropylacrylamide groups. A 1.0 mM solution of TPFOS, by contrast, swells both fluorinated and non-fluorinated microgels to 267 ± 8%, 245 ± 12%, and 208 ± 6% of their original z-average diameter for T0, T20, and T40 microgels, respectively, at 40 °C,

30 °C, and 10 °C of their upsweep, downsweep, and downsweep temperature curves. This enhancement coincides with previous observations of the same phenomenon for macrogels from earlier entries, following the behavior typically reported for SDS in the literature; the mechanism generating increased swelling is considered the same as that noted for macrogels whereby TPFOS multilayers repulse nearby sheets. Appreciable differences in swelling ratios for fluorinated gels exposed to TPFOS at 0.1 mM and the FRET intensity for non-fluorinated microgels at the same concentration are comparable to the sensitivity acquired for nile red-incubated macrogels at a similar level, indicating that the swelling response for microgels initiates at lower fluorocontaminant concentrations than for their bulk counterparts. Exploitation of this behavior with transducers relating chemical rather than physical cues might serve to sharpen the detection limit for the gels further in pursuit of the dilute extremes necessary for environmental applications.

CHAPTER 7. CONCLUSIONS

7.1 Recapitulation

Three predominant observations were recorded in this work: 1) using fluorinated comonomers with PNIPAM requires a delicate balance of comonomer type and feed ratio to maintain appreciable swelling in aqueous environments while maximizing fluorosurfactant association, 2) surfactants demonstrate multiple binding avenues with PNIPAM, differing between electrostatic association and fluorophilicity for fluorinated copolymers, resulting in disparate agglomeration regimes depending on the surfactant chemistry, and 3) the morphology of PNIPAM, whether synthesized as macrogels or microgels, heavily influences its swelling behavior when exposed to various analytes. Evaluating the performance of fluorinated macrogels containing DFHA, TFEA, and HFIA showed that the structure of their comonomer dominated their swelling ratios when exposed to TPFOS. Gels with TFEA and HFIA at theoretically equivalent fluorine contents held similar swelling ratios, but the same comparison between TFEA and DFHA showed marked deswelling departures. Whereas gels synthesized with 5.0 mol% DFHA followed curves similar to TFEA and HFIA with the same loading, having an LCST of 40.0 ± 0.4 °C, those with 20 mol% TFEA collapsed at lower temperatures and posted a LCST of 21.5 ± 3.2 °C. This difference was exacerbated by equilibration times for T20.0 gels reaching up to 1,320 h while D5.0 gels equilibrated significantly faster. As a function of relative molar ratios, higher fluorinated comonomer incorporation stimulates inbuilt fluorophilicity within the networks and occludes solvent penetration, extending equilibration times and lowering the overall swelling ratio of the system. Isolating an optimal copolymer feed ratio consequently requires careful consideration of the polymer's resultant swelling differential between its analyte-loaded and water-swollen states to design a polymer with a suitable swelling ratio, equilibration time, and fluorous attraction for the analyte of interest.

The binding motifs of the analytes tested varied considerably depending on their particular chemistry, varying even amongst fluorosurfactants. Monitoring the swelling of microgels revealed this principle clearly: binding to the amide groups of PNIPAM via hydrogen bonding or electrostatics for Ph and SOS replaced hydrogen bonding to

surrounding solvent molecules and disrupted hydrophobic hydration around PNIPAM's isopropyl group, reducing the gels' size near their transition temperature. TPFOS, by contrast, enlarged both the microgel and macrogel networks by multilayering and electrostatically repulsing nearby layers. Despite having a fluorous tail group similar to that of TPFOS, PFOA collapsed the microgels because of its lower dissociation and electronegativity. When mixed, TPFOS demonstrated stronger association to the networks relative to PFOA, potentially due to the strength of its electrostatic coupling and the addition of two fluorine atoms to its tail enhancing interfacial separation that favors deposition along the polymer's backbone. The deswelling capacity of PFOA was insignificant for macrogels, further showing its insubstantial association compared to TPFOS. Altogether, the binding pathway and resultant swelling behavior of the polymer exposed to differing analytes depends upon the individual molecule's structure, and the addition of fluorinated comonomers to the networks reinforces these disparities.

Finally, macrogels and microgels displayed different swelling responses due to their sizes. For macrogels, TPFOS and, to a lesser extent, SDS showed appreciable changes in size with concentration, in which exposure to TPFOS raised their swelling on a mass basis relative to water alone by up to 3,761 ± 147% for those synthesized with 10.0 mol% TFEA. Microgels instead saw a size change for each analyte, deswelling for Ph, SOS, OA, and PFOA while growing larger for TPFOS. The extent of this deviation was considerable for PFOA given a maximal deswelling of 76 ± 2% at 34 °C for 1.0 mM compared to an insignificant mass swelling ratio difference for the compound at the same concentration and similar temperatures with macrogels. Measurement parameters could, however, mask the macrogels' overall performance; the equilibrium mass swelling ratio for a 1.0 mM concentration of OA fell to 63 ± 8% for non-fluorinated macrogels at 32.5 °C, and the normalized z-average diameters of non-fluorinated microgels was 66 ± 3% at 32 °C. More pronounced were the substantial changes in equilibration times between microgels and macrogels. Where microgels required only 10 minutes to achieve equilibrium, macrogels needed, at minimum, 48 hours. The high surface area-to-volume ratio (SA:V) for microgels promotes their rapid swelling or deswelling in response to analytes, while macrogels with a SA:V roughly seven orders of magnitude below that of microgels must undergo gradual diffusion throughout their network to reach equilibrium.

The morphology of the polymer must therefore be carefully considered when designing the response rates of sensing systems utilizing PNIPAM.

7.2 Shortcomings and Caveats

Though the detection goal set at the outset of this research program was 70 ppt (approaching 0.1 nM), the minimum significant detectable observation was only as low as 0.05 mM for TPFOS as per the use of nile red with non-fluorinated macrogels shown in Figure 4.7. Other strategies for calibrating the gels' response showed varying detection limits at higher extremes, reaching 0.1 mM for the swelling of fluorinated microgels, 0.25 mM for non-fluorinated microgels, and 0.5 mM for fluorinated and non-fluorinated macrogels. As such, the system falls approximately six orders of magnitude short of the limit required for environmentally relevant detection with swelling posing as the output signal. With that in mind, a few approaches are available for improving bridging this gap: 1) despite avoided in the outset goals for the project to ease in-field execution, sample preconcentration in a manner similar to that used by EPA Method 537.1[40] could artificially increase the sample concentration by approximately two orders of magnitude (i.e., concentrating a sample from a 250 mL initial volume to 1 mL via solid phase extraction), 2) applying a secondary transduction motif, explored further in CHAPTER 8, could induce signaling upon molecular association before bulk physical parameters manifest, and, 3) albeit explicitly circumvented to mitigate downstream contamination, molecular imprinting might improve fluorosurfactant association with the network and, consequently, reduce the concentration at which registerable alterations to the polymer's physiochemical properties occur. Taking the first procedural alteration as a given, the latter two addendums must span at least another four orders of magnitude to reach environmentally relevant concentrations. As mentioned in CHAPTER 4, Serpe's group has seen success in using Fabry-Pérot and photonic crystal-based systems, mediated by the swelling of PNIPAM to induce colorimetric changes, as tools for detecting various chemical species in the micromolar to picomolar range,[134] but, with the efficacy of the systems dependent upon the strength of the analyte-receptor binding interaction, the configuration of the resonator or photonic crystals, and potential inhibitory effects generated by the analyte itself, improvements attributable to such

systems is difficult to pin. Imprinting brings similar concerns whereby the supposed associative enhancement owed to structural vacancies are not trivial to compare and may be impaired by the considerable swelling changes characterizing PNIPAM. From the work presented herein and with respect to the speculations provided here, a firm declaration of the potential for this system to meet the detection limits necessary for environmental samples cannot be made.

Aside, biologically relevant concentrations of PFAS found in human serum are common in the low parts per billion range,[209] approximately two orders of magnitude above those for aqueous detection. Still accounting for preconcentration, this lowers the detection level gap to only two orders of magnitude required for appended signal transducers which may serve as a more achievable goal in the short term. Notably, biological fluids are necessarily complex and will pose a host of additional concerns regarding possible false positives or negatives spawned from extraneous chemicals should they bypass preconcentration or sample purification procedures.

A final noteworthy caveat for the data presented follows their simulation in ideal solutions. Environmental matrices are not without a host of other complicating substances beyond PFAS, including but not limited to metal ions, chemical waste products, biological waste products, microorganisms, viruses, and other trace environmental pollutants. Each substance within a matrix has the potential to interfere with the thermoresponsive behavior of PNIPAM and must be considered before implementing any technology using the polymer as the primary signaling element. One class of substances in particular that was not studied here, natural organic matter (e.g., fulvic and humic acids), are bulky molecules with numerous hydroxyl and carboxylic functional groups present at parts per million concentrations in surface waters.[210] If these substances are not eliminated from the test solution, perturbations similar to those derived for hydrotropes or swelling corresponding to repulsive analyte ionization could occur. These effects will be conditioned by the molecular weight of the organic matter and their corresponding degree of association to the polymer, again making their ultimate impact on the polymer's swelling difficult to predict. Altogether, the occurrence of secondary analytes in environmental samples will inevitably affect the swelling behavior of PNIPAM and cannot be ignored when analyzing the polymer's performance.

CHAPTER 8. EXTENSIONS

The phenomena recorded herein serve as the basis for investigating the mechanisms underlying the association of fluorosurfactants, distinct in their pathways from their hydrocarbon analogs, to weak polyelectrolytes and the exploitation of their interactions as a means for constructing sensing systems using polymers in their design. The macroscale observations documented for the fluorosurfactant-induced swelling behavior of PNIPAM signal underlying chemical cues that manifest significant physiochemical changes. Equipping the polymer with appropriate transduction motifs may enhance the system's sensitivity by emphasizing minute alterations in PNIPAM's properties rather than relying solely on assessments of bulk swelling. Visiting electrochemical techniques exploiting the polymer's permittivity as a function of temperature would, with the interesting electrostatics surrounding fluorocarbon electron induction, presumably offer appreciable fluctuations representative of an analyte's concentration. Changes in the overall refractive index of the polymer near its transition temperature, taking in part the contribution from water and the polymer dependent on the polymer's hydration, could likewise present precise indications of association relatable with techniques like SPR. Other surface functionalization strategies utilizing quartz crystal microbalance or the deflection of microcantilevers might also expose minor deviations in mass attributable to fluorosurfactant deposition. In any case, circumventing reliance on swelling, which, from the results described herein, reaches an appreciable change primarily under sufficiently high analyte loading to induce surfactant aggregation and layering responsible for network collapse or swelling, should aid in capturing binding phenomena rather than macroscale perturbations.

Before investigating alternative transducers, further characterization is required to build on the fundamentals established here to achieve a sensor approaching the detection limits necessary to meet regulatory requirements for PFAS with PNIPAM. Though the mixed matrix results for microgels imply a higher association constant for TPFOS relative to PFOA, determining constant values for each analyte tested via isothermal titration calorimetry or adsorption modeling across the copolymer combinations explored would prove useful for tailoring the polymer's binding patterns toward specific analytes

of interest beyond the swelling protocols presented earlier for fluorinated macrogels. Additionally, the effectiveness of FRET-compatible microgels can be greatly improved with fluorescence correlation spectroscopy to estimate dye loading for gels containing donor-acceptor pairs or an individual dye. Altering the synthesis process for these gels to better correlate the dyes would help to calibrate their relative intensities and allow for more accurate determination of sensitized emission and FRET efficiencies. Albeit offering little insight beyond the information acquired from sensitized emission, calculating FRET efficiency would reveal whether the dye ensemble passes their Förster distance when the microgels transition from their swollen to collapsed states. If the dyes are inappropriately distanced under the total loading used currently, adjusting their concentration to suit would improve the sensitized emission of the system and potentially sharpen their response.

Copolymerizing association enhancers or response elements could accommodate both the binding optimization and signaling motifs mentioned earlier into a single polymeric unit. With the fluorosurfactants investigated here having acidic head groups, cationic comonomers in the form of primary or ternary amines may change the innate swelling behavior of the gels by providing inbuilt electrostatic repulsion and encourage electrostatic interactions with the highly electronegative sulfonate group of PFOS or the weakly acidic carboxyl of PFOA. In the case of PFOA, swelling brought on by the polymer's cations would be curtailed, possibly promoting the microgel's collapse. Heightened swelling by PFOS might be hidden by innate expansion, or electrostatic binding could facilitate deswelling at concentrations below those augmenting swelling. Regarding transducers, adding solvachromatic in place of FRET dyes might capture the response enhancement observed for macrogels to raise copolymerized microgels' sensitivity. Alternatively, employing dyes susceptible to quenching in the presence of fluorosurfactants could function as a turn-off approach for sensing the contaminants.

Lastly, though PFOA and PFOS represent the most widely studied fluorocontaminants in the literature, other fluorosurfactants like perfluorononanoic acid and perfluorodecanoic acid are also commonly found in contaminated water supplies at trace concentrations and, with their longer fluorocarbon tails, would presumably impact the swelling behavior of PNIPAM with greater potency than their shorter-chained

analogs. Should longer-chained molecules be effective in this manner, testing their affect in solution with PFOA and PFOS would provide a more holistic description of the polymer's anticipated performance in complex, substantive matrices. Also, though unexplored here, investigating the effect of partially fluorinated surfactants would serve as a useful tool for elucidating the aggregation phenomena involved in fluorocarbon association with non- and partially fluorinated PNIPAM further. Available hydrocarbon sectors within a partially fluorinated tail might capitalize on residual hydrophobicity to better associate with non-fluorinated polymer regions than oleophobic fluorocarbons, possibly generating perturbations in the polymer's physiochemical behavior at even lower concentrations.

APPENDIX 1. ACRONYMS

σ – water-analyte swelling difference

AEMA – 2-aminoethyl methacrylate

AgINP – silver iodide nanoparticle

APTES – aminopropyltriethoxysilane

APTMS – 3-aminopropyltrimethoxysilane

ATR – attenuated total reflectance

AUC – area under the curve

BCH – berberine chloride hydrate

BFC – biofuel cell

BG – base gel (i.e., macrogel – 97.5 mol% NIPAM, 2.5 mol% MBA)

BOD – bilirubin oxidase

BSA – bovine serum albumin

CAC – critical aggregation concentration

CMC – critical micelle concentration

CNC – charge neutralization concentration

CQD – carbon quantum dot

Cy3 – cyanine 3

Cy5 – cyanine 5

Cy3-NHS – cyanine 3 *N*-hydroxysuccinimide ester

Cy5-NHS – cyanine 5 *N*-hydroxysuccinimide ester

D5.0 – 5 mol% DFHA feed macrogel

DFHA – 1*H*,1*H*,7*H* - dodecafluoroheptyl acrylate

DI – deionized

DLS – dynamic light scattering

DMSO – dimethyl sulfoxide

DNA – deoxyribonucleic acids

ECL – electrochemiluminescence

EDS – energy dispersive X-ray spectroscopy

EGDMA – ethylene glycol dimethacrylate

EPA – United States Environmental Protection Agency

6:2FTS – 1*H*,1*H*,2*H*,2*H*-perfluorooctanesulfonic acid

F-53B – 6:2 chlorinated polyfluorinated ether sulfonate

FcCOOH – ferrocenecarboxylic acid

FITC – fluorescein 6-isothiocyanate

FRET – Förster resonance energy transfer

FTIR – Fourier-transform infrared spectroscopy

FTO – fluorine-doped tin oxide

GCE – glassy carbon electrode

GDH – glutamate dehydrogenase

H5.0 – 5 mol% HFIA feed macrogel

HFIA – 1,1,1,3,3,3-hexafluoroisopropyl acrylate

I – initiator

I2959 – 2-hydroxy-4'-(2-hydroxyethoxy)-2-methylpropiophenone; Irgacure 2959

IF – imprinting factor

IgA – immunoglobin A

IgD – immunoglobin D

IgE – immunoglobin E

IgG – immunoglobin G

IgM – immunoglobin M

KPS – potassium peroxodisulfate

K_{sv} – quenching constant

LC/MS/MS – liquid chromatography with tandem mass spectroscopy

LCST – lower critical solution temperature

LOD – limit of detection

MAA – methacrylic acid

MBA – *N*,*N'*-methylenebis(acrylamide)

MeOH – methanol

m_i – initial dry mass

MIP – molecularly imprinted polymer

MIT – molecularly imprinted technology

m_s – swollen mass

MWNH – multi-walled carbon nanohorn

NCD – nitrogen-doped carbon dot

NIPAM – *N*-isopropylacrylamide

NR – nile red

OA – octanoic acid

OPD – *o*-phenylenediamine

PCR – polymerase chain reaction

PDI – polydispersity index

PEI – polyethyleneimine

PFAA – perfluoroalkyl acid

PFAS – poly- and perfluoroalkyl substances

PFBS – perfluorobutane sulfonate

PFC – perfluorinated compound

PFCA – perfluorocarboxylic acid

PFHxA – perfluorohexanoic acid

PFHxS – perfluorohexane sulfonate

PFNA – perfluorononanoic acid

PFOA – perfluorooctanoic acid

PFOS – perfluorooctane sulfonate

PFOSF – perfluorooctane sulfonyl fluoride

Ph – phenol

PNIPAM – poly(*N*-isopropylacrylamide)

PPARα – peroxisomal proliferator-activated receptor-alpha

PTFE – polytetrafluoroethylene

PVDF – polyvinylidene fluoride

Q – swelling ratio

Q_A – analyte-induced swelling ratio

QCM – quartz crystal microbalance

QD – quantum dot

QD-SA – streptavidin-modified quantum dots

Q_W – water-induced swelling ratio

RLS – resonance light scattering

RNA – ribonucleic acids

RXRα – retinoid X receptor-alpha

SA:V – surface area-to-volume ratio

SAW – surface acoustic wave

SDBS – sodium dodecylbenzenesulphonate

SDS – sodium dodecyl sulfate

SELEX – systematic evolution of ligands by exponential enrichment

SEM – scanning electron microscopy

SILAR – successive ionic layer adsorption and reaction

SOS – sodium octyl sulfonate

SPE – screen-printed electrode

SPR – surface plasmon resonance

T0 – non-fluorinated microgel (i.e., 97.5 mol% NIPAM, 2.5 mol% MBA)

T2.5 – 2.5 mol% TFEA feed macrogel

T5.0 – 5 mol% TFEA feed macrogel

T10.0 – 10 mol% TFEA feed macrogel

T12.5 – 12.5 mol% TFEA feed macrogel

T15.0 – 15 mol% TFEA feed macrogel

T20 – 20 mol% TFEA feed microgel

T20.0 – 20 mol% TFEA feed macrogel

T35.0 – 35 mol% TFEA feed macrogel

T40 – 40 mol% TFEA feed microgel

TEA – triethanolamine

TFEA – 2,2,2-trifluoroethyl acrylate

THM – temperature at half maximum

TMC – total monomer concentration

TPFOS – tetraethylammonium perfluorooctane sulfonate

utg-C_3N_4 – ultrathin graphitic-based carbon nitride

UV – ultraviolet

V_{oc} – open circuit voltage

XPS – X-ray photoelectron spectroscopy

REFERENCES

1. Butt, C. M.; Muir, D. C. G.; Mabury, S. A., Biotransformation pathways of fluorotelomer-based polyfluoroalkyl substances: A review. *Environmental Toxicology and Chemistry* **2014,** *33* (2), 243-267.
2. Li, Y.; Fletcher, T.; Mucs, D.; Scott, K.; Lindh, C. H.; Tallving, P.; Jakobsson, K., Half-lives of PFOS, PFHxS and PFOA after end of exposure to contaminated drinking water. *Occupational and environmental medicine* **2018,** *75* (1), 46-51.
3. Russell, M. H.; Berti, W. R.; Szostek, B.; Buck, R. C., Investigation of the Biodegradation Potential of a Fluoroacrylate Polymer Product in Aerobic Soils. *Environmental Science & Technology* **2008,** *42* (3), 800-807.
4. Washington, J. W.; Ellington, J. J.; Jenkins, T. M.; Evans, J. J.; Yoo, H.; Hafner, S. C., Degradability of an Acrylate-Linked, Fluorotelomer Polymer in Soil. *Environmental Science & Technology* **2009,** *43* (17), 6617-6623.
5. Ghisi, R.; Vamerali, T.; Manzetti, S., Accumulation of perfluorinated alkyl substances (PFAS) in agricultural plants: A review. *Environmental Research* **2019,** *169*, 326-341.
6. Working Towards a Global Emission Inventory of PFASs: Focus On PFCAs - Status Quo and the Way Forward. State, U. S. D. o., Ed. Paris, 2015.
7. O'Hagan, D., Understanding organofluorine chemistry. An introduction to the C–F bond. *Chemical Society Reviews* **2008,** *37* (2), 308-319.
8. Wang, Z.; Cousins, I. T.; Scheringer, M.; Buck, R. C.; Hungerbühler, K., Global emission inventories for C4–C14 perfluoroalkyl carboxylic acid (PFCA) homologues from 1951 to 2030, Part I: production and emissions from quantifiable sources. *Environment International* **2014,** *70*, 62-75.
9. History and Use of Per- and Polyfluoroalkyl Substances (PFAS). 2017; p 8.
10. Giesy, J. P.; Kannan, K., Global Distribution of Perfluorooctane Sulfonate in Wildlife. *Environmental Science & Technology* **2001,** *35* (7), 1339-1342.
11. Houde, M.; De Silva, A. O.; Muir, D. C. G.; Letcher, R. J., Monitoring of Perfluorinated Compounds in Aquatic Biota: An Updated Review. *Environmental Science & Technology* **2011,** *45* (19), 7962-7973.
12. Chu, S.; Letcher, R. J.; McGoldrick, D. J.; Backus, S. M., A New Fluorinated Surfactant Contaminant in Biota: Perfluorobutane Sulfonamide in Several Fish Species. *Environmental Science & Technology* **2016,** *50* (2), 669-675.
13. Muir, D.; Bossi, R.; Carlsson, P.; Evans, M.; De Silva, A.; Halsall, C.; Rauert, C.; Herzke, D.; Hung, H.; Letcher, R.; Rigét, F.; Roos, A., Levels and trends of poly- and perfluoroalkyl substances in the Arctic environment – An update. *Emerging Contaminants* **2019,** *5*, 240-271.
14. Rankin, K.; Mabury, S. A.; Jenkins, T. M.; Washington, J. W., A North American and global survey of perfluoroalkyl substances in surface soils: Distribution patterns and mode of occurrence. *Chemosphere* **2016,** *161*, 333-341.
15. Xiao, F., Emerging poly- and perfluoroalkyl substances in the aquatic environment: A review of current literature. *Water Research* **2017,** *124*, 482-495.
16. Olsen, G. W.; Burris, J. M.; Ehresman, D. J.; Froehlich, J. W.; Seacat, A. M.; Butenhoff, J. L.; Zobel, L. R., Half-Life of Serum Elimination of Perfluorooctanesulfonate,

Perfluorohexanesulfonate, and Perfluorooctanoate in Retired Fluorochemical Production Workers. *Environmental Health Perspectives* **2007,** *115* (9), 1298-1305.
17. Buck, R. C.; Franklin, J.; Berger, U.; Conder, J. M.; Cousins, I. T.; de Voogt, P.; Jensen, A. A.; Kannan, K.; Mabury, S. A.; van Leeuwen, S. P., Perfluoroalkyl and polyfluoroalkyl substances in the environment: Terminology, classification, and origins. *Integrated Environmental Assessment and Management* **2011,** *7* (4), 513-541.
18. Jian, J.-M.; Guo, Y.; Zeng, L.; Liang-Ying, L.; Lu, X.; Wang, F.; Zeng, E. Y., Global distribution of perfluorochemicals (PFCs) in potential human exposure source–A review. *Environment International* **2017,** *108*, 51-62.
19. Guidance for the inventory of perfluorooctane sulfonic acid (PFOS) and related chemicals listed under the Stockholm Convention on Persistent Organic Pollutants. Stockholm Convention on Persistent Organic Pollutants: Switzerland, 2017.
20. TOWARD A NEW COMPREHENSIVE GLOBAL DATABASE OF PER- AND POLYFLUOROALKYL SUBSTANCES (PFASs): SUMMARY REPORT ON UPDATING THE OECD 2007 LIST OF PER- AND POLYFLUOROALKYL SUBSTANCES (PFASs). OECD Environment, Health and Safety Publications: Paris, France, 2018.
21. Wallington, T. J.; Hurley, M. D.; Xia, J.; Wuebbles, D. J.; Sillman, S.; Ito, A.; Penner, J. E.; Ellis, D. A.; Martin, J.; Mabury, S. A.; Nielsen, O. J.; Sulbaek Andersen, M. P., Formation of C7F15COOH (PFOA) and Other Perfluorocarboxylic Acids during the Atmospheric Oxidation of 8:2 Fluorotelomer Alcohol. *Environmental Science & Technology* **2006,** *40* (3), 924-930.
22. Ellis, D. A.; Martin, J. W.; De Silva, A. O.; Mabury, S. A.; Hurley, M. D.; Sulbaek Andersen, M. P.; Wallington, T. J., Degradation of Fluorotelomer Alcohols: A Likely Atmospheric Source of Perfluorinated Carboxylic Acids. *Environmental Science & Technology* **2004,** *38* (12), 3316-3321.
23. Prevedouros, K.; Cousins, I. T.; Buck, R. C.; Korzeniowski, S. H., Sources, Fate and Transport of Perfluorocarboxylates. *Environmental Science & Technology* **2006,** *40* (1), 32-44.
24. Jian, J.-M.; Chen, D.; Han, F.-J.; Guo, Y.; Zeng, L.; Lu, X.; Wang, F., A short review on human exposure to and tissue distribution of per- and polyfluoroalkyl substances (PFASs). *Science of The Total Environment* **2018,** *636*, 1058-1069.
25. Sunderland, E. M.; Hu, X. C.; Dassuncao, C.; Tokranov, A. K.; Wagner, C. C.; Allen, J. G., A review of the pathways of human exposure to poly- and perfluoroalkyl substances (PFASs) and present understanding of health effects. *Journal of Exposure Science & Environmental Epidemiology* **2019,** *29* (2), 131-147.
26. Boone, J. S.; Vigo, C.; Boone, T.; Byrne, C.; Ferrario, J.; Benson, R.; Donohue, J.; Simmons, J. E.; Kolpin, D. W.; Furlong, E. T.; Glassmeyer, S. T., Per- and polyfluoroalkyl substances in source and treated drinking waters of the United States. *Science of The Total Environment* **2019,** *653*, 359-369.
27. Susmann, H. P.; Schaider, L. A.; Rodgers, K. M.; Rudel, R. A., Dietary Habits Related to Food Packaging and Population Exposure to PFASs. *Environmental Health Perspectives* **2019,** *127* (10), 107003.
28. Domingo, J. L.; Nadal, M., Per- and Polyfluoroalkyl Substances (PFASs) in Food and Human Dietary Intake: A Review of the Recent Scientific Literature. *Journal of Agricultural and Food Chemistry* **2017,** *65* (3), 533-543.

29. Haug, L. S.; Thomsen, C.; Brantsæter, A. L.; Kvalem, H. E.; Haugen, M.; Becher, G.; Alexander, J.; Meltzer, H. M.; Knutsen, H. K., Diet and particularly seafood are major sources of perfluorinated compounds in humans. *Environment International* **2010,** *36* (7), 772-778.
30. Toxicological Profile for Perfluoroalkyls (Draft for Public Comment). Services, U. S. D. o. H. a. H., Ed. 2018.
31. Barry, V.; Winquist, A.; Steenland, K., Perfluorooctanoic Acid (PFOA) Exposures and Incident Cancers among Adults Living Near a Chemical Plant. *Environmental Health Perspectives* **2013,** *121* (11-12), 1313-1318.
32. Kim, M. J.; Moon, S.; Oh, B.-C.; Jung, D.; Ji, K.; Choi, K.; Park, Y. J., Association between perfluoroalkyl substances exposure and thyroid function in adults: A meta-analysis. *PLOS ONE* **2018,** *13* (5), e0197244.
33. Joensen, U. N.; Veyrand, B.; Antignac, J.-P.; Blomberg Jensen, M.; Petersen, J. H.; Marchand, P.; Skakkebæk, N. E.; Andersson, A.-M.; Le Bizec, B.; Jørgensen, N., PFOS (perfluorooctanesulfonate) in serum is negatively associated with testosterone levels, but not with semen quality, in healthy men. *Human Reproduction* **2012,** *28* (3), 599-608.
34. Di Nisio, A.; Sabovic, I.; Valente, U.; Tescari, S.; Rocca, M. S.; Guidolin, D.; Dall'Acqua, S.; Acquasaliente, L.; Pozzi, N.; Plebani, M.; Garolla, A.; Foresta, C., Endocrine Disruption of Androgenic Activity by Perfluoroalkyl Substances: Clinical and Experimental Evidence. *The Journal of Clinical Endocrinology & Metabolism* **2018,** *104* (4), 1259-1271.
35. Darrow, L. A.; Groth, A. C.; Winquist, A.; Shin, H.-M.; Bartell, S. M.; Steenland, K., Modeled Perfluorooctanoic Acid (PFOA) Exposure and Liver Function in a Mid-Ohio Valley Community. *Environmental Health Perspectives* **2016,** *124* (8), 1227-1233.
36. DeWitt, J. C.; Blossom, S. J.; Schaider, L. A., Exposure to per-fluoroalkyl and polyfluoroalkyl substances leads to immunotoxicity: epidemiological and toxicological evidence. *Journal of Exposure Science & Environmental Epidemiology* **2019,** *29* (2), 148-156.
37. Drinking Water Health Advisory for Perfluorooctane Sulfonate (PFOS). Agency, U. S. E. P., Ed. Office of Water: 2016.
38. Drinking Water Health Advisory for Perfluorooctanoic Acid (PFOA). Agency, U. S. E. P., Ed. Office of Water: 2016.
39. EPA's Per- and Polyfluoroalkyl Substances (PFAS) Action Plan. Interior, U. S. D. o. t., Ed. 2019.
40. Shoemaker, J. A.; Tettenhorst, D. R., Method 537.1 Determination of Selected Per- and Polyfluorinated Alkyl Substances in Drinking Water by Solid Phase Extraction and Liquid Chromatography/Tandem Mass Spectrometry (LC/MS/MS). Interior, U. S. D. o. t., Ed. National Exposure Research Laboratory, Office of Research and Development: Cincinnati, OH, 2018; p 50.
41. Nakayama, S. F.; Yoshikane, M.; Onoda, Y.; Nishihama, Y.; Iwai-Shimada, M.; Takagi, M.; Kobayashi, Y.; Isobe, T., Worldwide trends in tracing poly- and perfluoroalkyl substances (PFAS) in the environment. *TrAC Trends in Analytical Chemistry* **2019**.
42. Trojanowicz, M.; Koc, M., Recent developments in methods for analysis of perfluorinated persistent pollutants. *Mikrochimica acta* **2013,** *180* (11-12), 957-971.

43. Ruan, T.; Jiang, G., Analytical methodology for identification of novel per- and polyfluoroalkyl substances in the environment. *TrAC Trends in Analytical Chemistry* **2017,** *95*, 122-131.
44. Lorenzo, M.; Campo, J.; Picó, Y., Analytical challenges to determine emerging persistent organic pollutants in aquatic ecosystems. *TrAC Trends in Analytical Chemistry* **2018,** *103*, 137-155.
45. Justino, C. I. L.; Duarte, A. C.; Rocha-Santos, T. A. P., Recent Progress in Biosensors for Environmental Monitoring: A Review. **2017,** *17* (12), 2918.
46. Gu, M. B.; Mitchell, R. J.; Kim, B. C., Whole-Cell-Based Biosensors for Environmental Biomonitoring and Application. In *Biomanufacturing*, Zhong, J.-J., Ed. Springer Berlin Heidelberg: Berlin, Heidelberg, 2004; pp 269-305.
47. Gui, Q.; Lawson, T.; Shan, S.; Yan, L.; Liu, Y., The Application of Whole Cell-Based Biosensors for Use in Environmental Analysis and in Medical Diagnostics. **2017,** *17* (7), 1623.
48. Singh, A.; Poshtiban, S.; Evoy, S., Recent Advances in Bacteriophage Based Biosensors for Food-Borne Pathogen Detection. **2013,** *13* (2), 1763-1786.
49. Zhang, W.; Liu, Q. X.; Guo, Z. H.; Lin, J. S., Practical Application of Aptamer-Based Biosensors in Detection of Low Molecular Weight Pollutants in Water Sources. **2018,** *23* (2), 344.
50. Dai, Y.; Furst, A.; Liu, C. C., Strand Displacement Strategies for Biosensor Applications. *Trends in Biotechnology* **2019,** *37* (12), 1367-1382.
51. Fan, Y.; Evans, C. R.; Ling, J., Rewiring protein synthesis: From natural to synthetic amino acids. *Biochimica et Biophysica Acta (BBA) - General Subjects* **2017,** *1861* (11, Part B), 3024-3029.
52. Hoyos-Nogués, M.; Gil, F. J.; Mas-Moruno, C., Antimicrobial Peptides: Powerful Biorecognition Elements to Detect Bacteria in Biosensing Technologies. **2018,** *23* (7), 1683.
53. Barbosa, A. J. M.; Oliveira, A. R.; Roque, A. C. A., Protein- and Peptide-Based Biosensors in Artificial Olfaction. *Trends in Biotechnology* **2018,** *36* (12), 1244-1258.
54. Xiao, X.; Kuang, Z.; Slocik, J. M.; Tadepalli, S.; Brothers, M.; Kim, S.; Mirau, P. A.; Butkus, C.; Farmer, B. L.; Singamaneni, S.; Hall, C. K.; Naik, R. R., Advancing Peptide-Based Biorecognition Elements for Biosensors Using in-Silico Evolution. *ACS Sensors* **2018,** *3* (5), 1024-1031.
55. Pacholski, C.; Perelman, L. A.; VanNieuwenhze, M. S.; Sailor, M. J., Small molecule detection by reflective interferometric Fourier transform spectroscopy (RIFTS). **2009,** *206* (6), 1318-1321.
56. Dover, J. E.; Hwang, G. M.; Mullen, E. H.; Prorok, B. C.; Suh, S.-J., Recent advances in peptide probe-based biosensors for detection of infectious agents. *Journal of Microbiological Methods* **2009,** *78* (1), 10-19.
57. Conroy, P. J.; Hearty, S.; Leonard, P.; O'Kennedy, R. J., Antibody production, design and use for biosensor-based applications. *Seminars in Cell & Developmental Biology* **2009,** *20* (1), 10-26.
58. Sharma, S.; Byrne, H.; O'Kennedy, Richard J., Antibodies and antibody-derived analytical biosensors. *Essays in Biochemistry* **2016,** *60* (1), 9-18.

59. Reynoso, E. C.; Torres, E.; Bettazzi, F.; Palchetti, I., Trends and Perspectives in Immunosensors for Determination of Currently-Used Pesticides: The Case of Glyphosate, Organophosphates, and Neonicotinoids. **2019,** *9* (1), 20.
60. Badihi-Mossberg, M.; Buchner, V.; Rishpon, J., Electrochemical Biosensors for Pollutants in the Environment. **2007,** *19* (19-20), 2015-2028.
61. Fránek, M.; Hruska, K., Antibody based methods for environmental and food analysis: A review. *Veterinarni Medicina* **2005,** *50*.
62. Kang, J.; Kim, S.; Kwon, Y., Antibody-based biosensors for environmental monitoring. *Toxicology and Environmental Health Sciences* **2009,** *1* (3), 145-150.
63. Peltomaa, R.; Glahn-Martínez, B.; Benito-Peña, E.; Moreno-Bondi, M. C., Optical Biosensors for Label-Free Detection of Small Molecules. **2018,** *18* (12), 4126.
64. Bojorge Ramírez, N.; Salgado, A. M.; Valdman, B., The evolution and developments of immunosensors for health and environmental monitoring: problems and perspectives %J Brazilian Journal of Chemical Engineering. **2009,** *26*, 227-249.
65. Robinson, P. K., Enzymes: principles and biotechnological applications. *Essays in Biochemistry* **2015,** *59*, 1-41.
66. Pinyou, P.; Blay, V.; Muresan, L. M.; Noguer, T., Enzyme-modified electrodes for biosensors and biofuel cells. *Materials Horizons* **2019,** *6* (7), 1336-1358.
67. Clark Jr., L. C.; Lyons, C., ELECTRODE SYSTEMS FOR CONTINUOUS MONITORING IN CARDIOVASCULAR SURGERY. **1962,** *102* (1), 29-45.
68. Dhar, D.; Roy, S.; Nigam, V. K., Chapter 10 - Advances in protein/enzyme-based biosensors for the detection of pharmaceutical contaminants in the environment. In *Tools, Techniques and Protocols for Monitoring Environmental Contaminants*, Kaur Brar, S.; Hegde, K.; Pachapur, V. L., Eds. Elsevier: 2019; pp 207-229.
69. Karunakaran, C.; Madasamy, T.; Sethy, N. K., Chapter 3 - Enzymatic Biosensors. In *Biosensors and Bioelectronics*, Karunakaran, C.; Bhargava, K.; Benjamin, R., Eds. Elsevier: 2015; pp 133-204.
70. Nigam, V.; Shukla, P., Enzyme Based Biosensors for Detection of Environmental Pollutants- A Review. *Journal of microbiology and biotechnology* **2015,** *25*.
71. Lyagin, I. V.; Efremenko, E. N.; Varfolomeev, S. D., Enzymatic biosensors for determination of pesticides. *Russian Chemical Reviews* **2017,** *86* (4), 339-355.
72. Serna Cock, L.; Zetty Arenas, A. M.; Ayala Aponte, A., Use of Enzymatic Biosensors as Quality Indices: A Synopsis of Present and Future Trends in The Food Industry %J Chilean journal of agricultural research. **2009,** *69*, 270-280.
73. Sonawane, A.; Manickam, P.; Bhansali, S., Stability of Enzymatic Biosensors for Wearable Applications. *IEEE Reviews in Biomedical Engineering* **2017,** *PP*, 1-1.
74. Rocchitta, G.; Spanu, A.; Babudieri, S.; Latte, G.; Madeddu, G.; Galleri, G.; Nuvoli, S.; Bagella, P.; Demartis, M. I.; Fiore, V.; Manetti, R.; Serra, P. A., Enzyme Biosensors for Biomedical Applications: Strategies for Safeguarding Analytical Performances in Biological Fluids. **2016,** *16* (6), 780.
75. Reyes-De-Corcuera, J. I.; Olstad, H. E.; García-Torres, R., Stability and Stabilization of Enzyme Biosensors: The Key to Successful Application and Commercialization. **2018,** *9* (1), 293-322.
76. Song, S.; Wang, L.; Li, J.; Fan, C.; Zhao, J., Aptamer-based biosensors. *TrAC Trends in Analytical Chemistry* **2008,** *27* (2), 108-117.

77. Munzar, J. D.; Ng, A.; Juncker, D., Duplexed aptamers: history, design, theory, and application to biosensing. *Chemical Society Reviews* **2019,** *48* (5), 1390-1419.
78. Blind, M.; Blank, M., Aptamer Selection Technology and Recent Advances. *Molecular Therapy - Nucleic Acids* **2015,** *4*, e223.
79. Kalra, P.; Dhiman, A.; Cho, W. C.; Bruno, J. G.; Sharma, T. K., Simple Methods and Rational Design for Enhancing Aptamer Sensitivity and Specificity. **2018,** *5* (41).
80. Zhang, Y.; Lai, B. S.; Juhas, M., Recent Advances in Aptamer Discovery and Applications. **2019,** *24* (5), 941.
81. Odeh, F.; Nsairat, H.; Alshaer, W.; Ismail, M. A.; Esawi, E.; Qaqish, B.; Bawab, A. A.; Ismail, S. I., Aptamers Chemistry: Chemical Modifications and Conjugation Strategies. **2020,** *25* (1), 3.
82. Song, K.-M.; Lee, S.; Ban, C., Aptamers and Their Biological Applications. **2012,** *12* (1), 612-631.
83. Meek, K. N.; Rangel, A. E.; Heemstra, J. M., Enhancing aptamer function and stability via in vitro selection using modified nucleic acids. *Methods* **2016,** *106*, 29-36.
84. Wang, R. E.; Zhang, Y.; Cai, J.; Cai, W.; Gao, T., Aptamer-based fluorescent biosensors. *Curr Med Chem* **2011,** *18* (27), 4175-4184.
85. Mehlhorn, A.; Rahimi, P.; Joseph, Y., Aptamer-Based Biosensors for Antibiotic Detection: A Review. **2018,** *8* (2), 54.
86. Ndunda, E. N.; Mizaikoff, B., Molecularly imprinted polymers for the analysis and removal of polychlorinated aromatic compounds in the environment: a review. *Analyst* **2016,** *141* (11), 3141-3156.
87. Shen, F.; Ren, X., Covalent molecular imprinting made easy: a case study of mannose imprinted polymer. *RSC Advances* **2014,** *4* (25), 13123-13125.
88. Hashim, S. N. N. S.; Boysen, R. I.; Schwarz, L. J.; Danylec, B.; Hearn, M. T. W., A comparison of covalent and non-covalent imprinting strategies for the synthesis of stigmasterol imprinted polymers. *Journal of Chromatography A* **2014,** *1359*, 35-43.
89. Chen, L.; Wang, X.; Lu, W.; Wu, X.; Li, J., Molecular imprinting: perspectives and applications. *Chemical Society Reviews* **2016,** *45* (8), 2137-2211.
90. Speltini, A.; Scalabrini, A.; Maraschi, F.; Sturini, M.; Profumo, A., Newest applications of molecularly imprinted polymers for extraction of contaminants from environmental and food matrices: A review. *Analytica Chimica Acta* **2017,** *974*, 1-26.
91. Pichon, V.; Chapuis-Hugon, F., Role of molecularly imprinted polymers for selective determination of environmental pollutants—A review. *Analytica Chimica Acta* **2008,** *622* (1), 48-61.
92. Inanan, T.; Tüzmen, N.; Akgöl, S.; Denizli, A., Selective cholesterol adsorption by molecular imprinted polymeric nanospheres and application to GIMS. *International Journal of Biological Macromolecules* **2016,** *92*, 451-460.
93. Yang, L.; Yu, W.; Yan, X.; Deng, C., Decyl-perfluorinated magnetic mesoporous microspheres for extraction and analysis perfluorinated compounds in water using ultrahigh-performance liquid chromatography–mass spectrometry. *Journal of Separation Science* **2012,** *35* (19), 2629-2636.
94. Song, X.; Wang, J.; Zhu, J., Effect of porogenic solvent on selective performance of molecularly imprinted polymer for quercetin. *Materials Research* **2009,** *12*, 299-304.

95. Saloni, J.; Walker, K.; Hill, G., Theoretical Investigation on Monomer and Solvent Selection for Molecular Imprinting of Nitrocompounds. *The Journal of Physical Chemistry A* **2013,** *117* (7), 1531-1534.
96. Bird, L.; Herdes, C., The porogen effect on the complexation step of trinitrotoluene–methacrylic acid: towards efficient imprinted polymer sensors. *Molecular Systems Design & Engineering* **2018,** *3* (1), 89-95.
97. Song, X.; Xu, S.; Chen, L.; Wei, Y.; Xiong, H., Recent advances in molecularly imprinted polymers in food analysis. *Journal of Applied Polymer Science* **2014,** *131* (16).
98. Ertürk, G.; Mattiasson, B., Molecular Imprinting Techniques Used for the Preparation of Biosensors. *Sensors (Basel, Switzerland)* **2017,** *17* (2), 288.
99. Luliński, P., Molecularly imprinted polymers based drug delivery devices: a way to application in modern pharmacotherapy. A review. *Materials Science and Engineering: C* **2017,** *76*, 1344-1353.
100. Yoon, H., Current Trends in Sensors Based on Conducting Polymer Nanomaterials. **2013,** *3* (3), 524-549.
101. Wong, Y. C.; Ang, B. C.; Haseeb, A. S. M. A.; Baharuddin, A. A.; Wong, Y. H., Review—Conducting Polymers as Chemiresistive Gas Sensing Materials: A Review. *Journal of The Electrochemical Society* **2019,** *167* (3), 037503.
102. Song, E.; Choi, J.-W., Multi-analyte detection of chemical species using a conducting polymer nanowire-based sensor array platform. *Sensors and Actuators B: Chemical* **2015,** *215*, 99-106.
103. Zhang, D. Q.; Zhang, W. L.; Liang, Y. N., Adsorption of perfluoroalkyl and polyfluoroalkyl substances (PFASs) from aqueous solution - A review. *Science of The Total Environment* **2019,** *694*, 133606.
104. Basabe-Desmonts, L.; Reinhoudt, D. N.; Crego-Calama, M., Design of fluorescent materials for chemical sensing. *Chemical Society Reviews* **2007,** *36* (6), 993-1017.
105. Zhang, J.; Wan, Y.; Li, Y.; Zhang, Q.; Xu, S.; Zhu, H.; Shu, B., A rapid and high-throughput quantum dots bioassay for monitoring of perfluorooctane sulfonate in environmental water samples. *Environmental Pollution* **2011,** *159* (5), 1348-1353.
106. Zhang, T.; Zhao, H.; Lei, A.; Quan, X., Electrochemical Biosensor for Detection of Perfluorooctane Sulfonate Based on Inhibition Biocatalysis of Enzymatic Fuel Cell. *Electrochemistry* **2014,** *82* (2), 94-99.
107. Cennamo, N.; Zeni, L.; Tortora, P.; Regonesi, M. E.; Giusti, A.; Staiano, M.; D'Auria, S.; Varriale, A., A High Sensitivity Biosensor to detect the presence of perfluorinated compounds in environment. *Talanta* **2018,** *178*, 955-961.
108. Cennamo, N.; Zeni, L.; Agostino, G. D.; Porto, G.; Biasiolo, A. In *Optical chemical fiber sensor for the detection of perfluorinated compounds in water*, 2018 IEEE International Instrumentation and Measurement Technology Conference (I2MTC), 14-17 May 2018; 2018; pp 1-5.
109. Cennamo, N.; D'Agostino, G.; Porto, G.; Biasiolo, A.; Perri, C.; Arcadio, F.; Zeni, L., A Molecularly Imprinted Polymer on a Plasmonic Plastic Optical Fiber to Detect Perfluorinated Compounds in Water. **2018,** *18* (6), 1836.
110. Cennamo, N.; D'Agostino, G.; Sequeira, F.; Mattiello, F.; Porto, G.; Biasiolo, A.; Nogueira, R.; Bilro, L.; Zeni, L., A Simple and Low-Cost Optical Fiber Intensity-Based Configuration for Perfluorinated Compounds in Water Solution. **2018,** *18* (9), 3009.

111. Feng, H.; Wang, N.; Tran.T, T.; Yuan, L.; Li, J.; Cai, Q., Surface molecular imprinting on dye–(NH2)–SiO2 NPs for specific recognition and direct fluorescent quantification of perfluorooctane sulfonate. *Sensors and Actuators B: Chemical* **2014,** *195*, 266-273.
112. Jiao, Z.; Li, J.; Mo, L.; Liang, J.; Fan, H., A molecularly imprinted chitosan doped with carbon quantum dots for fluorometric determination of perfluorooctane sulfonate. *Microchimica Acta* **2018,** *185* (10), 473.
113. Zheng, L.; Zheng, Y.; Liu, Y.; Long, S.; Du, L.; Liang, J.; Huang, C.; Swihart, M. T.; Tan, K., Core-shell quantum dots coated with molecularly imprinted polymer for selective photoluminescence sensing of perfluorooctanoic acid. *Talanta* **2019,** *194*, 1-6.
114. Chen, S.; Li, A.; Zhang, L.; Gong, J., Molecularly imprinted ultrathin graphitic carbon nitride nanosheets–Based electrochemiluminescence sensing probe for sensitive detection of perfluorooctanoic acid. *Analytica Chimica Acta* **2015,** *896*, 68-77.
115. Karimian, N.; Stortini, A. M.; Moretto, L. M.; Costantino, C.; Bogialli, S.; Ugo, P., Electrochemosensor for Trace Analysis of Perfluorooctanesulfonate in Water Based on a Molecularly Imprinted Poly(o-phenylenediamine) Polymer. *ACS Sensors* **2018,** *3* (7), 1291-1298.
116. Moro, G.; Cristofori, D.; Bottari, F.; Cattaruzza, E.; De Wael, K.; Moretto, L. M., Redesigning an Electrochemical MIP Sensor for PFOS: Practicalities and Pitfalls. **2019,** *19* (20), 4433.
117. Kazemi, R.; Potts, E. I.; Dick, J. E., Quantifying Interferent Effects on Molecularly Imprinted Polymer Sensors for Per- and Polyfluoroalkyl Substances (PFAS). *Analytical Chemistry* **2020,** *92* (15), 10597-10605.
118. Fang, C.; Chen, Z.; Megharaj, M.; Naidu, R., Potentiometric detection of AFFFs based on MIP. *Environmental Technology & Innovation* **2016,** *5*, 52-59.
119. Gong, J.; Fang, T.; Peng, D.; Li, A.; Zhang, L., A highly sensitive photoelectrochemical detection of perfluorooctanic acid with molecularly imprined polymer-functionalized nanoarchitectured hybrid of AgI–BiOI composite. *Biosensors and Bioelectronics* **2015,** *73*, 256-263.
120. Li, X.; Wang, X.; Fang, T.; Zhang, L.; Gong, J., Disposable photoelectrochemical sensing strip for highly sensitive determination of perfluorooctane sulfonyl fluoride on functionalized screen-printed carbon electrode. *Talanta* **2018,** *181*, 147-153.
121. Tran.T, T.; Li, J.; Feng, H.; Cai, J.; Yuan, L.; Wang, N.; Cai, Q., Molecularly imprinted polymer modified TiO2 nanotube arrays for photoelectrochemical determination of perfluorooctane sulfonate (PFOS). *Sensors and Actuators B: Chemical* **2014,** *190*, 745-751.
122. Liang, J.; Deng, X.; Tan, K., An eosin Y-based "turn-on" fluorescent sensor for detection of perfluorooctane sulfonate. *Spectrochimica Acta Part A: Molecular and Biomolecular Spectroscopy* **2015,** *150*, 772-777.
123. Chen, Q.; Zhu, P.; Xiong, J.; Gao, L.; Tan, K., A sensitive and selective triple-channel optical assay based on red-emissive carbon dots for the determination of PFOS. *Microchemical Journal* **2019,** *145*, 388-396.
124. Cheng, Z.; Dong, H.; Liang, J.; Zhang, F.; Chen, X.; Du, L.; Tan, K., Highly selective fluorescent visual detection of perfluorooctane sulfonate via blue fluorescent carbon dots and berberine chloride hydrate. *Spectrochimica Acta Part A: Molecular and Biomolecular Spectroscopy* **2019,** *207*, 262-269.

125. Lin, L.; Zhou, S.; Guo, H.; Chen, Y.; Lin, S.; Yan, L.; Li, K.; Li, J., Nitrogen-doped carbon dots as an effective fluorescence enhancing system for the determination of perfluorooctyl sulfonate. *Microchimica Acta* **2019,** *186* (6), 380.
126. Faiz, F.; Baxter, G.; Collins, S.; Sidiroglou, F.; Cran, M., Polyvinylidene fluoride coated optical fibre for detecting perfluorinated chemicals. *Sensors and Actuators B: Chemical* **2020,** *312*, 128006.
127. Boswell, P. G.; Anfang, A. C.; Bühlmann, P., Preparation of a highly fluorophilic phosphonium salt and its use in a fluorous anion-exchanger membrane with high selectivity for perfluorinated acids. *Journal of Fluorine Chemistry* **2008,** *129* (10), 961-967.
128. Chen, L. D.; Lai, C.-Z.; Granda, L. P.; Fierke, M. A.; Mandal, D.; Stein, A.; Gladysz, J. A.; Bühlmann, P., Fluorous Membrane Ion-Selective Electrodes for Perfluorinated Surfactants: Trace-Level Detection and in Situ Monitoring of Adsorption. *Analytical Chemistry* **2013,** *85* (15), 7471-7477.
129. Kissa, E., *Fluorinated Surfactants and Repellents, Second Edition*. Taylor & Francis: 2001.
130. Dhara, D.; Chatterji, P. R., Phase Transition in Linear and Cross-Linked Poly(N-Isopropylacrylamide) in Water: Effect of Various Types of Additives. *Journal of Macromolecular Science, Part C* **2000,** *40* (1), 51-68.
131. Khan, N.; Brettmann, B., Intermolecular Interactions in Polyelectrolyte and Surfactant Complexes in Solution. *Polymers* **2019,** *11* (1), 51.
132. Islam, M. R.; Ahiabu, A.; Li, X.; Serpe, M. J., Poly (N-isopropylacrylamide) Microgel-Based Optical Devices for Sensing and Biosensing. *Sensors* **2014,** *14* (5), 8984-8995.
133. Gao, Y.; Li, X.; Serpe, M. J., Stimuli-responsive microgel-based etalons for optical sensing. *RSC Advances* **2015,** *5* (55), 44074-44087.
134. Li, X.; Gao, Y.; Serpe, M. J., Stimuli-Responsive Assemblies for Sensing Applications. *Gels* **2016,** *2* (1), 8.
135. Jiang, Y.; Colazo, M. G.; Serpe, M. J., Poly(N-isopropylacrylamide) microgel-based sensor for progesterone in aqueous samples. *Colloid and Polymer Science* **2016,** *294* (11), 1733-1741.
136. Jiang, Y.; Colazo, M. G.; Serpe, M. J., Poly(N-isopropylacrylamide) microgel-based etalons for the label-free quantitation of estradiol-17β in aqueous solutions and milk samples. *Analytical and Bioanalytical Chemistry* **2018,** *410* (18), 4397-4407.
137. Mugo, S. M.; Dhanjai; Alberkant, J., A Biomimetric Lactate Imprinted Smart Polymers as Capacitive Sweat Sensors. *IEEE Sensors Journal* **2020**, 1-1.
138. Kim, J.; Nayak, S.; Lyon, L. A., Bioresponsive Hydrogel Microlenses. *Journal of the American Chemical Society* **2005,** *127* (26), 9588-9592.
139. Islam, M. R.; Serpe, M. J., Label-free detection of low protein concentration in solution using a novel colorimetric assay. *Biosensors and Bioelectronics* **2013,** *49*, 133-138.
140. Islam, M. R.; Serpe, M. J., Polymer-based devices for the label-free detection of DNA in solution: low DNA concentrations yield large signals. *Analytical and Bioanalytical Chemistry* **2014,** *406* (19), 4777-4783.
141. Mutharani, B.; Ranganathan, P.; Chen, S.-M.; K, D. V. S., Stimuli-enabled reversible switched aclonifen electrochemical sensor based on smart PNIPAM/PANI-Cu hybrid conducting microgel. *Sensors and Actuators B: Chemical* **2020,** *304*, 127232.

142. Hoare, T.; Pelton, R., Engineering Glucose Swelling Responses in Poly(N-isopropylacrylamide)-Based Microgels. *Macromolecules* **2007,** *40* (3), 670-678.
143. Sorrell, C. D.; Serpe, M. J., Glucose sensitive poly (N-isopropylacrylamide) microgel based etalons. *Analytical and Bioanalytical Chemistry* **2012,** *402* (7), 2385-2393.
144. Zhang, Q. M.; Xu, W.; Serpe, M. J., Optical Devices Constructed from Multiresponsive Microgels. *Angewandte Chemie International Edition* **2014,** *53* (19), 4827-4831.
145. Shu, T.; Shen, Q.; Wan, Y.; Zhang, W.; Su, L.; Zhang, X.; Serpe, M. J., Silver nanoparticle-loaded microgel-based etalons for H2O2 sensing. *RSC Advances* **2018,** *8* (28), 15567-15574.
146. Jung, S.; MacConaghy, K. I.; Kaar, J. L.; Stoykovich, M. P., Enhanced Optical Sensitivity in Thermoresponsive Photonic Crystal Hydrogels by Operating Near the Phase Transition. *ACS Applied Materials & Interfaces* **2017,** *9* (33), 27927-27935.
147. Zhang, J.-T.; Smith, N.; Asher, S. A., Two-Dimensional Photonic Crystal Surfactant Detection. *Analytical Chemistry* **2012,** *84* (15), 6416-6420.
148. Schild, H. G.; Tirrell, D. A., Interaction of poly(N-isopropylacrylamide) with sodium n-alkyl sulfates in aqueous solution. *Langmuir* **1991,** *7* (4), 665-671.
149. Kokufuta, E.; Zhang, Y. Q.; Tanaka, T.; Mamada, A., Effects of surfactants on the phase transition of poly(N-isopropylacrylamide) gel. *Macromolecules* **1993,** *26* (5), 1053-1059.
150. Sakai, M.; Satoh, N.; Tsujii, K.; Zhang, Y.-Q.; Tanaka, T., Effects of Surfactants on the Phase Transition of a Hydrophobic Polymer Gel. *Langmuir* **1995,** *11* (7), 2493-2495.
151. Wu, C.; Zhou, S., Effects of surfactants on the phase transition of poly(N-isopropylacrylamide) in water. *Journal of Polymer Science Part B: Polymer Physics* **1996,** *34* (9), 1597-1604.
152. Murase, Y.; Onda, T.; Tsujii, K.; Tanaka, T., Discontinuous Binding of Surfactants to a Polymer Gel Resulting from a Volume Phase Transition. *Macromolecules* **1999,** *32* (25), 8589-8594.
153. Miyagishi, S.; Takagi, M.; Kadono, S.; Ohta, A.; Asakawa, T., Effect of amino acid surfactants on phase transition of poly(N-isopropylacrylamide) gel. *Journal of Colloid and Interface Science* **2003,** *261* (1), 191-196.
154. Futscher, M. H.; Philipp, M.; Müller-Buschbaum, P.; Schulte, A., The Role of Backbone Hydration of Poly(N-isopropyl acrylamide) Across the Volume Phase Transition Compared to its Monomer. *Scientific Reports* **2017,** *7* (1), 17012.
155. Evanghelidis, A.; Beregoi, M.; Diculescu, V. C.; Galatanu, A.; Ganea, P.; Enculescu, I., Flexible Delivery Patch Systems based on Thermoresponsive Hydrogels and Submicronic Fiber Heaters. *Scientific Reports* **2018,** *8* (1), 17555.
156. Nyquist, R. A.; Fiedler, S.; Streck, R., Infrared study of vinyl acetate, methyl acrylate and methyl methacrylate in various solvents. *Vibrational Spectroscopy* **1994,** *6* (3), 285-291.
157. Mukerjee, P.; Mysels, K. J., Critical Micelle Concentrations of Aqueous Surfactant Systems. Commerce, U. S. D. o., Ed. NBS Publications: 1970.
158. Gente, G.; La Mesa, C.; Muzzalupo, R.; Ranieri, G. A., Micelle Formation and Phase Equilibria in a Water−Trifluoroethanol−Fluorocarbon Surfactant System. *Langmuir* **2000,** *16* (21), 7914-7919.

159. Knoblich, A.; Matsumoto, M.; Murata, K.; Fujiyoshi, Y., Cryogenic Transmission Electron Microscopic Studies of Micellar Structure Correlated with Solution Viscosity on Perfluorooctyl Sufonates and Their Mixtures with a Nonionic Surfactant. *Langmuir* **1995,** *11* (7), 2361-2366.
160. Greenspan, P.; Fowler, S. D., Spectrofluorometric studies of the lipid probe, nile red. *Journal of Lipid Research* **1985,** *26* (7), 781-9.
161. Garada, M. B.; Kabagambe, B.; Kim, Y.; Amemiya, S., Ion-Transfer Voltammetry of Perfluoroalkanesulfonates and Perfluoroalkanecarboxylates: Picomolar Detection Limit and High Lipophilicity. *Analytical Chemistry* **2014,** *86* (22), 11230-11237.
162. Torres-Vega, J. J.; Vásquez-Espinal, A.; Ruiz, L.; Fernández-Herrera, M. A.; Alvarez-Thon, L.; Merino, G.; Tiznado, W., Revisiting Aromaticity and Chemical Bonding of Fluorinated Benzene Derivatives. *ChemistryOpen* **2015,** *4* (3), 302-307.
163. Bischofberger, I.; Calzolari, D. C. E.; De Los Rios, P.; Jelezarov, I.; Trappe, V., Hydrophobic hydration of poly-N-isopropyl acrylamide: a matter of the mean energetic state of water. *Scientific Reports* **2014,** *4* (1), 4377.
164. Zhu, P.-W.; Chen, L., Conformational collapse of spherical poly(N-isopropylacrylamide) brushes under the constraint of bound micelles. *Physical Chemistry Chemical Physics* **2017,** *19* (46), 31362-31376.
165. Zhu, P. W., Effects of Sodium Dodecyl Sulfate on Structures of Poly(N-isopropylacrylamide) at the Particle Surface. *The Journal of Physical Chemistry B* **2015,** *119* (1), 359-371.
166. Wang, X.; Chen, J.; Wang, D.; Dong, S.; Hao, J.; Hoffmann, H., Monitoring the different micelle species and the slow kinetics of tetraethylammonium perfluorooctane-sulfonate by 19F NMR spectroscopy. *Advances in Colloid and Interface Science* **2017,** *246*, 153-164.
167. Bossev, D. P.; Matsumoto, M.; Nakahara, M., H and 19F NMR Study of the Counterion Effect on the Micellar Structures Formed by Tetraethylammonium and Lithium Perfluorooctylsulfonates. 1. Neat Systems. *The Journal of Physical Chemistry B* **1999,** *103* (39), 8251-8258.
168. Gerry, H. E.; Jacobs, P. T.; Anacker, E. W., The effect of fluorination on surfactant aggregation number and dye solubilization efficiency. *Journal of Colloid and Interface Science* **1977,** *62* (3), 556-561.
169. Goss, K.-U., The pKa Values of PFOA and Other Highly Fluorinated Carboxylic Acids. *Environmental Science & Technology* **2008,** *42* (2), 456-458.
170. Brooke, D.; Footitt, A.; Nwaogu, T., *Environmental Risk Evaluation Report: Perflurooctanesulphonate (PFOS)*. 2004.
171. Hoffmann, H.; Würtz, J., Unusual phenomena in perfluorosurfactants. *Journal of Molecular Liquids* **1997,** *72* (1), 191-230.
172. Shima, M.; Yohdoh, K.; Yamaguchi, M.; Kimura, Y.; Adachi, S.; Matsuno, R., Effects of Medium-chain Fatty Acids and Their Acylglycerols on the Transport of Penicillin V across Caco-2 Cell Monolayers. *Bioscience, Biotechnology, and Biochemistry* **1997,** *61* (7), 1150-1155.
173. Li, G.; Liu, Y.; Xu, W.; Song, A.; Hao, J., Transition of Phase Structures in Mixtures of Lysine and Fatty Acids. *The Journal of Physical Chemistry B* **2014,** *118* (51), 14843-14851.

174. Wellen, B. A.; Lach, E. A.; Allen, H. C., Surface pKa of octanoic, nonanoic, and decanoic fatty acids at the air–water interface: applications to atmospheric aerosol chemistry. *Physical Chemistry Chemical Physics* **2017,** *19* (39), 26551-26558.
175. Koga, S.; Sasaki, S.; Maeda, H., Effect of Hydrophobic Substances on the Volume-Phase Transition of N-Isopropylacrylamide Gels. *The Journal of Physical Chemistry B* **2001,** *105* (19), 4105-4110.
176. Chen, S.; Wang, K.; Zhang, W., A new thermoresponsive polymer of poly(N-acryloylsarcosine methyl ester) with a tunable LCST. *Polymer Chemistry* **2017,** *8* (20), 3090-3101.
177. Le, D. V.; Kendrick, M. M.; O'Rear, E. A., Admicellar Polymerization and Characterization of Thin Poly(2,2,2-trifluoroethyl acrylate) Film on Aluminum Alloys for In-Crevice Corrosion Control. *Langmuir* **2004,** *20* (18), 7802-7810.
178. Kadimi, A.; Kaddami, H.; Ounaies, Z.; Habibi, Y.; Dieden, R.; Ameduri, B.; Raihane, M., Preparation and dielectric properties of poly(acrylonitrile-co-2,2,2-trifluoroethyl methacrylate) materials via radical emulsion copolymerization. *Polymer Chemistry* **2019,** *10* (40), 5507-5521.
179. Huang, K. P.; Lin, P.; Shih, H. C., Structures and properties of fluorinated amorphous carbon films. *Journal of Applied Physics* **2004,** *96* (1), 354-360.
180. Kokufuta, E.; Suzuki, H.; Sakamoto, D., On the Local Binding of Ionic Surfactants to Poly(N-isopropylacrylamide) Gels. *Langmuir* **1997,** *13* (10), 2627-2632.
181. *ECOTOXICOLOGY AND ENVIRONMENTAL FATE TESTING OF SHORT CHAIN PERFLUOROALKYL COMPOUNDS RELATED TO 3M CHEMISTRIES*; Exhibit 2231; Hennepin County District Court: 2008.
182. Takayose, M.; Nishimoto, K.; Matsui, J., A fluorous synthetic receptor that recognizes perfluorooctanoic acid (PFOA) via fluorous interaction obtained by molecular imprinting. *Analyst* **2012,** *137* (12), 2762-2765.
183. Yan, Z.; Cai, Y.; Zhu, G.; Yuan, J.; Tu, L.; Chen, C.; Yao, S., Synthesis of 3-fluorobenzoyl chloride functionalized magnetic sorbent for highly efficient enrichment of perfluorinated compounds from river water samples. *Journal of Chromatography A* **2013,** *1321*, 21-29.
184. Yan, Z.; Zhu, G.; Cai, Y.; Yuan, J.; Yao, S., Preparation of fluorine functionalized magnetic nanoparticles for fast extraction and analysis of perfluorinated compounds from traditional Chinese medicine samples. *Analytical Methods* **2015,** *7* (21), 9054-9063.
185. Xiao, L.; Ling, Y.; Alsbaiee, A.; Li, C.; Helbling, D. E.; Dichtel, W. R., β-Cyclodextrin Polymer Network Sequesters Perfluorooctanoic Acid at Environmentally Relevant Concentrations. *Journal of the American Chemical Society* **2017,** *139* (23), 7689-7692.
186. Baker, R. J.; Colavita, P. E.; Murphy, D. M.; Platts, J. A.; Wallis, J. D., Fluorine–Fluorine Interactions in the Solid State: An Experimental and Theoretical Study. *The Journal of Physical Chemistry A* **2012,** *116* (5), 1435-1444.
187. Giulieri, F.; Krafft, M.-P., Can the formation of vesicles from single-chain perfluoroalkylated amphiphiles be predicted? *Colloids and Surfaces A: Physicochemical and Engineering Aspects* **1994,** *84* (1), 121-127.
188. Bischofberger, I.; Calzolari, D. C. E.; Trappe, V., Co-nonsolvency of PNiPAM at the transition between solvation mechanisms. *Soft Matter* **2014,** *10* (41), 8288-8295.

189. Zhou, X.; Zhou, J., Improving the Signal Sensitivity and Photostability of DNA Hybridizations on Microarrays by Using Dye-Doped Core−Shell Silica Nanoparticles. *Analytical Chemistry* **2004,** *76* (18), 5302-5312.
190. Wu, W.; Mitra, N.; Yan, E. C. Y.; Zhou, S., Multifunctional Hybrid Nanogel for Integration of Optical Glucose Sensing and Self-Regulated Insulin Release at Physiological pH. *ACS Nano* **2010,** *4* (8), 4831-4839.
191. Wu, W.; Chen, S.; Hu, Y.; Zhou, S., A fluorescent responsive hybrid nanogel for closed-loop control of glucose. *J Diabetes Sci Technol* **2012,** *6* (4), 892-901.
192. Cenci, L.; Andreetto, E.; Vestri, A.; Bovi, M.; Barozzi, M.; Iacob, E.; Busato, M.; Castagna, A.; Girelli, D.; Bossi, A. M., Surface plasmon resonance based on molecularly imprinted nanoparticles for the picomolar detection of the iron regulating hormone Hepcidin-25. *Journal of Nanobiotechnology* **2015,** *13* (1), 51.
193. Li, X.; Gao, Y.; Serpe, M. J., Responsive Polymer-Based Assemblies for Sensing Applications. **2015,** *36* (15), 1382-1392.
194. Cennamo, N.; Maniglio, D.; Tatti, R.; Zeni, L.; Bossi, A. M., Deformable molecularly imprinted nanogels permit sensitivity-gain in plasmonic sensing. *Biosensors and Bioelectronics* **2020,** *156*, 112126.
195. Liu, T.; Hu, J.; Yin, J.; Zhang, Y.; Li, C.; Liu, S., Enhancing Detection Sensitivity of Responsive Microgel-Based Cu(II) Chemosensors via Thermo-Induced Volume Phase Transitions. *Chemistry of Materials* **2009,** *21* (14), 3439-3446.
196. Lin, S.; Wang, W.; Ju, X.-J.; Xie, R.; Liu, Z.; Yu, H.-R.; Zhang, C.; Chu, L.-Y., Ultrasensitive microchip based on smart microgel for real-time online detection of trace threat analytes. *Proceedings of the National Academy of Sciences* **2016**, 201518442.
197. Qiao, J.; Ding, H.; Liu, Q.; Zhang, R.; Qi, L., Preparation of Polymer@AuNPs with Droplets Approach for Sensing Serum Copper Ions. *Analytical Chemistry* **2017,** *89* (3), 2080-2085.
198. Cao, Z.; Chen, Y.; Zhang, Q.; Xia, Y.; Liu, G.; Wu, D.; Ma, W.; Cheng, J.; Liu, C., Preparation and ion sensing property of the self-assembled microgels by QCM %J Nanofabrication. **2017,** *3* (1), 16.
199. Koda, Y.; Terashima, T.; Sawamoto, M., Fluorous Microgel Star Polymers: Selective Recognition and Separation of Polyfluorinated Surfactants and Compounds in Water. *Journal of the American Chemical Society* **2014,** *136* (44), 15742-15748.
200. Kumarasamy, E.; Manning, I. M.; Collins, L. B.; Coronell, O.; Leibfarth, F. A., Ionic Fluorogels for Remediation of Per- and Polyfluorinated Alkyl Substances from Water. *ACS Central Science* **2020,** *6* (4), 487-492.
201. Chuang, C.-Y.; Don, T.-M.; Chiu, W.-Y., Synthesis and properties of chitosan-based thermo- and pH-responsive nanoparticles and application in drug release. **2009,** *47* (11), 2798-2810.
202. Jones, C. D.; McGrath, J. G.; Lyon, L. A., Characterization of Cyanine Dye-Labeled Poly(N-isopropylacrylamide) Core/Shell Microgels Using Fluorescence Resonance Energy Transfer. *The Journal of Physical Chemistry B* **2004,** *108* (34), 12652-12657.
203. Fontell, K.; Lindman, B., Fluorocarbon surfactants. Phase equilibriums and phase structures in aqueous systems of a totally fluorinated fatty acid and some of its salts. *The Journal of Physical Chemistry* **1983,** *87* (17), 3289-3297.

204. Uehara, N.; Ogawa, M., Interaction of Poly(N-isopropylacrylamide) with Sodium Dodecyl Sulfate below the Critical Aggregation Concentration. *Langmuir* **2014,** *30* (22), 6367-6372.
205. Weber, R.; Hoffmann, H., Order parameters of dye molecules in lyotropic nematic mesophases. *Liquid Crystals* **1988,** *3* (2), 203-216.
206. Yang, M.; Liu, C.; Lian, Y.; Zhao, K.; Zhu, D.; Zhou, J., Relaxations and phase transitions during the collapse of a dense PNIPAM microgel suspension—thorough insight using dielectric spectroscopy. *Soft Matter* **2017,** *13* (14), 2663-2676.
207. Yang, M.; Liu, C.; Zhao, K., Concentration dependent phase behavior and collapse dynamics of PNIPAM microgel by dielectric relaxation. *Physical Chemistry Chemical Physics* **2017,** *19* (23), 15433-15443.
208. Su, W.; Zhao, K.; Wei, J.; Ngai, T., Dielectric relaxations of poly(N-isopropylacrylamide) microgels near the volume phase transition temperature: impact of cross-linking density distribution on the volume phase transition. *Soft Matter* **2014,** *10* (43), 8711-8723.
209. Fourth National Report on Human Exposure to Environmental Chemicals. Services, U. S. D. o. H. a. H., Ed. 2019; Vol. 1.
210. Boggs, S.; Livermore, D.; Seitz, M. G., Humic substances in natural waters and their complexation with trace metals and radionuclides: a review.[129 references]. **1985**.

VITA

Dustin graduated from Louisiana Tech University with bachelor's degrees in Chemical Engineering and Nanosystems Engineering in May 2016. He then moved to Lexington in August and began his doctoral studies under the coadvisement of Dr. Thomas Dziubla and Dr. Zach Hilt later that semester.

Honors & Awards:

- Recipient of Dr. and Mrs. P. K. Smith Endowed Scholarship
- 2016 Senior Design Competition, AIChE Spring Meeting & 12th Global Congress on Process Safety, 1st Place
- 2018 Poster Competition, 5th Annual Materials and Chemical Engineering Graduate Student Association Spring Symposium, 1st Place

Presentations & Posters:

- D. T. Savage, J. Z. Hilt, T. D. Dziubla. Synthesis and Characterization of Fluorescent Polymers for the Detection of Polychlorinated Biphenyls. 2017 AIChE Annual Meeting, Minneapolis, MN, November 1, 2017.
- I. Ahmad, D. T. Savage, J. Z. Hilt, T. D. Dziubla. Fluorescence Based Detection of Polychlorinated Biphenyls in Water. 2017 AIChE Annual Meeting, Minneapolis, MN, November 1, 2017.
- D. T. Savage, J. Z. Hilt, T. D. Dziubla. Analyte-Responsive Nanoparticles for the Detection of Polychlorinated Biphenyls. DioXin 2018 & 10th International PCB Workshop, Kraków, Poland, August 28, 2018.
- D. T. Savage, J. Z. Hilt, T. D. Dziubla. Synthesis and Characterization of Analyte-Responsive Nanoparticles for the Detection of Polychlorinated Biphenyls. 2018 AIChE Annual Meeting, Pittsburgh, PA, October 30, 2018.

- D. T. Savage, J. Z. Hilt, T. D. Dziubla. Progression Toward a Poly(*N*-Isopropylacrylamide)-Based Sensor for Perfluorooctane Sulfonate. SRP 2019, Seattle, WA, November 19, 2019. Poster.

Publications:

- D. T. Savage, J. Z. Hilt, T. D. Dziubla. In Vitro Methods for Assessing Nanoparticle Toxicity. In *Nanotoxicity;* Q. Zhang, Ed.; Humana Press, New York, 2019; Vol. 1894, pp 1-29.
- D. T. Savage et al. On the Swelling Behavior of Poly(*N*-Isopropylacrylamide) Hydrogels Exposed to Perfluoroalkyl Acids. Manuscript submitted.
- D. T. Savage, J. Z. Hilt, T. D. Dziubla. Leveraging the Thermoresponsiveness of Fluorinated Poly(*N*-Isopropylacrylamide) Copolymers as a Sensing Tool for Perfluorooctane Sulfonate. Manuscript in preparation.
- D. T. Savage, J. Z. Hilt, T. D. Dziubla. Assessing the Perfluoroalkyl Acid-Induced Swelling of Förster Resonance Energy Transfer-Capable Poly(*N*-Isopropylacrylamide) Microgels. Manuscript in preparation.
- D. T. Savage, J. Z. Hilt, T. D. Dziubla. Polymeric Approaches for Sensing Per- and Polyfluoroalkyl Substances. Manuscript in preparation.